ABSTRACT

ANALYSIS OF CIRULAR DICHROISM AND LINEAR DICHROISM SPECTROSCOPY

Julie M. DiNitto

April 10, 2012

Director: John M. Kenney

DEPARTMENT OF PHYSICS

Circular Dichroism (CD) and Linear Dichroism (LD) spectroscopies measure the difference in absorption between left and right circularly polarized light and parallel and perpendicular linearly polarized light as a function of wavelength respectively. CD and LD are popular biomedical physics techniques used to determine structural changes in biomolecules. This dissertation addresses improvements made to the measurement of CD and LD signals by characterizing the transfer function of the spectrometer. Shot noise, stray light and dark current were characterized. A new model for the measurement of the CD signal involving the presence of static birefringence was derived and tested by implementation of novel techniques used to measure the phase-difference amplitude and static birefringence in the photoelastic modulator (PEM) crystal. The model was tested by measuring the fractional change in the signal on Camphorsulfonic Acid (for CD) and Chrysazin (for LD). It is hoped that this study will impact how CD and LD are measured and analyzed in the future.

ANALYSIS OF CIRCULAR DICHROISM AND LINEAR DICHROISM SPECTROSCOPY

A Dissertation

Presented to

The Faculty of the Department of Physics

East Carolina University

In Partial Fulfillment of the Requirements for the Degree

Doctor of Philosophy in Biomedical Physics

By

Julie M. DiNitto

April 2012

ANALYSIS OF CIRULAR DICHROISM AND LINEAR DICHROISM SPECTROSCOPY

By

Julie M. DiNitto

APPROVED BY:

DIRECTOR OF DISSERTATION _____

John M. Kenney, Ph.D.

COMMITTEE MEMBER_____

Michael Dingfelder, Ph.D.

COMMITTEE MEMBER_____

Yong-Qing Li, Ph.D.

COMMITTEE MEMBER_____

Anthony Kennedy, Ph.D.

COMMITTEE MEMBER_____

John C. Sutherland, Ph.D.

CHAIR OF THE DEPARTMENT OF PHYSICS _____

John C. Sutherland, Ph.D.

DEAN OF THE GRADUATE SCHOOL_____

Paul J. Gemperline, PhD

DEDICATION

To my parents Louis and Betsy DiNitto for all encouragement.

ACKNOWLDEGMENTS

First and foremost I would like to thank my dissertation advisor Dr. John M. Kenney for all the help and encouragement through these last few years. I have learned a great deal and would not have been able to complete this dissertation without his help.

My thanks goes to Chris Bonnerup (ECU physics electronics shop) for designing and building the electronics for the voltage converter on the photoelastic modulator and all his help dealing with the electronics section in this dissertation. I would like to thank Gene Oakley (ECU Physics machine shop) for helping in the design of the Stokes parameter optical device holder, polymer stretcher, and educating myself on CAT drawings. Thanks to Jens Spanget-Larsen in the Spanget-Larsen Lab in Denmark for providing us with the same LDPE used in their measurements of Chrysazin. I would also like to thank Dr. Xin-Hua Hu for allowing me to borrow an adjustable compensator.

Lastly, I would like to thank Dr. Anthony Kennedy for help in the dissertation writing process and Dr. John C. Sutherland for sharing his wisdom in the world of CD with me.

TABLE OF CONTENTS

LIST OF FIGURES

LIST OF TABLES

LIST OF ABBREVIATIONS, SYMBOLS, UNITS, AND CONSTANTS

0.1 ABBREVIATIONS

AC	Alternating current
C	Capacitor
CD	Circular Dichroism
DC	Direct current
G	Gain
I	Intensity
IC	Integrated Circuit
L	Inductor
LC	Inductor Capacitor Circuit
LD	Linear Dichroism
M_H	Horizontal polarization Muller matrix
M_{LP}	Linear polarization Muller matrix
M_{PEM}	Photoelastic modulator Muller matrix
M_V	Vertical polarization Muller matrix
PEM	Photoelastic modulator
PMT	Photomultiplier tube
RV	Variable resistor

S	Stokes parameters
SW1	Switch 1
V_0	High Tension
VDC	Direct current applied to the photoelastic modulator

0.2 SYMBOLS

δ_0	amplitude phase difference of photoelastic modulator
δ_s	static birefringence of photoelastic modulator
δ	phase difference of photoelastic modulator
f	frequency
λ	wavelength
σ	standard deviation
θ_1	polarization axis for linear polarizer 1
θ_2	polarization axis for linear polarizer 2
θ_p	polarization axis for photoelastic modulator
ψ	phase difference of waveplate
φ	linear polarizer transmission axis angle
ϕ	rotation angle of the circular polarizer analyzer

0.3 UNITS

dOD	difference in optical density
kHz	kilohertz
mdeg	millidegrees
V	volts

CHAPTER 1: CIRCULAR DICHROISM AND LINEAR DICHROISM

The discovery of the α-helix and β-sheet structure in 1951 launched interest in the study of bimolecular structures and initiated the interest in the development of new types of absorption spectroscopy[1,2]. With the major advancements in computers (software) and industrial (hardware) development, absorption spectroscopy continues to improve and be used as one of the main sources for determining the structure of biomolecules[2]. One unique class of absorption spectroscopy that includes circular dichroism (CD) and linear dichroism (LD), deals with differential absorption detection in the electromagnetic spectrum (near infrared, visible, and ultraviolet range). It is used in biomedical fields such as *in vitro* disease research[3], pharmaceutical testing, and analytical chemistry[4]. This dissertation addresses advances in the theory and practice of data collection of CD and LD.

This dissertation will mainly concentrate on noise characterization, modeling and measuring the polarization states induced by the photoelastic modulator, and new developments to calibrate and model the signal of the instrument. These are three different but related issues to improve upon the detection and measurement of both circular dichroism and linear dichroism; noise characterization, signal modeling, and measurement techniques. Chapter 2 discusses types and characteristics of noise for the CD spectrometer[5,6]. Specifically, the signal-to-noise ratio is determined as a function of different parameters, the detection of stray light and dark current in the photomultiplier tube, and the relationship between noise and high tension. Chapter 3 discusses an extension of the existing model of phase difference and measurements of phase-difference amplitude and static birefringence in a photoelastic modulator crystal. Phase-difference amplitude is detected using a new technique developed to improve previous

measurements[7]. The detection of static birefringence has been observed and measured in a photoelastic modulator, but not explained and applied to CD and LD measurements. Chapter 4 discusses the development and implementation of a novel technique to measure the Stokes parameters of the photoelastic modulator[8]. Chapter 5 characterizes the model of the CD and LD signal using camphorsulfonic acid and chrysazin[9]. Overall the work complete here is expected to have an impact in many fields including biomedical physics and chemistry by improving upon the detection of CD and LD.

1.1 ABSORPTION OF BIOMOLECULES

A protein is a series of amino acids (defined as the primary structure) that are connected by carbonyl bonds that form a polypeptide[10]. Each bond has phi-psi angles that specify the angular orientation of the connection between the two joined amino acids and hence determine a three dimensional arrangement (secondary structure)[10]. The phi-psi angles indicate how tight or flexible the arrangements of the amino acids are in the structure.

Secondary structures, such as α-helix, β-sheet, and random coil, are of interest in understanding information about how proteins fold and unfold. Electronic transitions can occur when light is incident on a biological molecule where absorption occurs. Proteins absorb light as described by Beer's law[11],

$$I = I_0 e^{-a} \tag{1.1.1}$$

where I_0 is the initial intensity incidental on the protein and a is the absorption of the light which depends on the molar extinction coefficient, path length, and concentration

$$a = \varepsilon l c \tag{1.1.2}$$

where ε (L mol^{-1} cm^{-1}) is the molar extinction coefficient, l (cm) is the path length the light travels through the medium and c (mol L^{-1}) is the concentration[11]. When light is absorbed, it causes electrons in the molecules to be excited and transition to a higher energy state. The absorption of the light depends on the orientation of the electromagnetic wave's electric vector and the electric dipole transition in the bond. These transitions depend on the secondary structure of the molecule.

Circular Dichroism (CD) and Linear Dichroism (LD) are differential absorption techniques that were developed in the 1950's to determine information about the secondary structure and the orientation of biological molecules. CD is best known for its ability to investigate changes in molecular secondary structures in their natural environment at low concentration[11].

Circular Dichroism (CD) is the difference in left and right circularly polarized light,

$$\Delta a_{CD} = a_L(\lambda) - a_R(\lambda) \qquad (1.1.3)$$

where $a_L(\lambda)$ is the eulerian absorption of left circularly polarized light and $a_R(\lambda)$ is the eulerian absorption of right circularly polarized light[12]. This spectroscopic technique investigates secondary structures of chiral biological molecules. Absorption due to the carbonyl bonds is in the UV wavelength range (amide region; 170-260 nm)[13,14], the side chains of proteins in the near UV (aromatic region), and the metal-ion binding of proteins in the visible range[15].

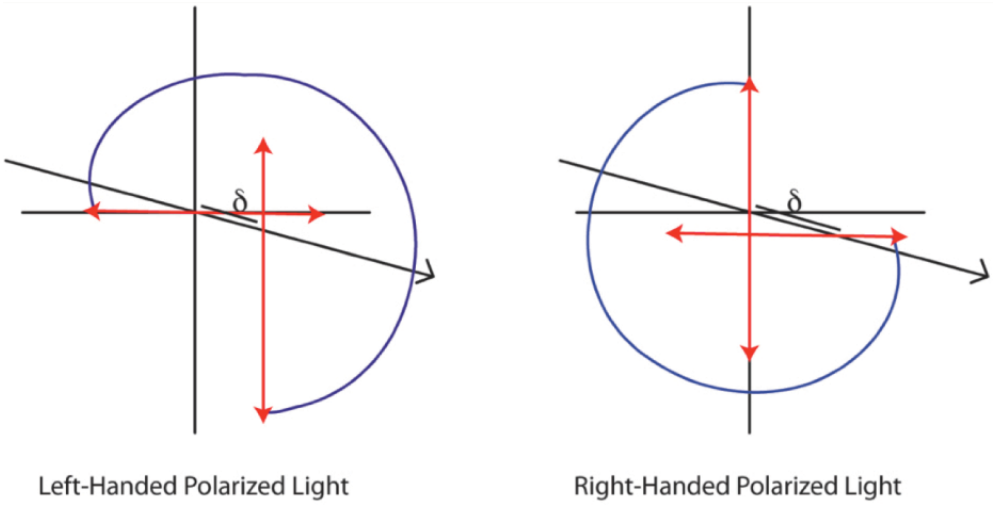

Figure 1: Circularly polarized light is formed by delaying either the horizontal electric field or the vertical electric field with respect to the other.

Linear Dichroism (LD) is the difference in absorption of parallel and perpendicular linearly polarized light[16],

$$\Delta a_{LD} = a_{\parallel}(\lambda) - a_{\perp}(\lambda) \qquad (1.1.4)$$

where $a_{\parallel}(\lambda)$ is the eulerian absorption of parallel linearly polarized light and $a_{\perp}(\lambda)$ is the eulerian absorption of perpendicular linearly polarized light with respect to initial polarization state of the light exiting the monochromator[12]. LD is used to measure the orientation of the molecule's electric dipoles relative to the polarization state of the light. If equation (1.1.4) is positive, the molecules electric dipoles are parallel to the orientation of the initial polarized light. If (1.1.4) is negative, the molecules electric dipoles are perpendicular to the orientation of the initial polarized light or optical axis of the instrument.

1.2 CD SPECTROMETER

The CD spectrometer contains several different types of optical components[17]. The light is produced by a xenon lamp and prisms which disperse the light by refraction allow for selection of wavelength. The light is then passed through a horizontal linear polarizer to polarize it for the photoelastic modulator. The photoelastic modulator is rotated at 45° with respect to the initial polarized light, allowing horizontally polarized light to be separated into +45° linearly polarized light and –45° linearly polarized light. One component is delayed with respect to the other (phase difference) and oscillated at a 50 kHz voltage that is applied to the photoelastic modulator (PEM) (discussed more in section 1.3) (See figure 1). This creates the desired polarization state to pass through the sample. The total intensity passing through the sample is then detected by a photomultiplier tube (PMT). Then the PMT signal is passed through a lock-in amplifier tuned to the resonant frequency, *f*, and phase at which the photoelastic modulator is oscillating. For CD the lock-in amplifier collects data at *f* and for LD the lock-in amplifier collects data at 2*f*. The phase is determined by referencing back to the photoelastic modulator 50kHz signal. The output signal has DC and AC components that can be used to determine Δa for CD or LD. This is discussed in section 1.3.

1.3 THE CD AND LD DETECTED SIGNAL

The creation of the polarization states needed to determine CD and LD is done by implementing a photoelastic modulator (PEM) that will oscillate between right and left circularly polarized light (for CD) and parallel and perpendicular (to the optical axis) linearly polarized light (for LD). The PEM oscillates inducing a phase difference

$$\delta(t) = \delta_0 \sin(\omega_0 t) \qquad (1.3.1)^{18}$$

where δ_0 is the phase-difference amplitude between the +45° and -45° linear polarization state amplitudes, ω_0 is the angular frequency of the voltage applied to the PEM, and t is time. CD is the difference in absorption between left and right circularly polarized light, but what is actually being detected is the transmitted intensity. The signal leaving the sample can be defined as

$$I[t] = I_L e^{-a_L} + I_R e^{-a_R} \tag{1.3.2}$$

where I_L, I_R, a_L, and a_R are the intensities and absorption for the left and right circularly polarized light respectively and are defined as

$$I_{L/R} = \frac{I_0}{2}(1 \pm \sin(\delta[t])) \tag{1.3.3}$$

$$a_{L/R} = \overline{a}_{CD} \pm \frac{\Delta a_{CD}}{2} \tag{1.3.4}$$

where I_0 is the initial intensity of the light entering the PEM, $\delta(t)$ is the time dependent phase difference of the photoelastic modulator (PEM), $\overline{a}_{CD}$ is the average eulerian absorption (DC voltage on the signal), and Δa_{CD} is the eulerian difference in absorption (AC voltage on the signal). Applying (1.3.3) and (1.3.4) to (1.3.2) and expanding in Bessel functions (see Appendix G), (1.3.2) becomes

$$I[t] = \frac{I_0}{2} e^{-\overline{a}_{CD}}(1 + 2\Delta a_{CD} J_1(\delta_0)\sin(\omega_0 t) + ...) \tag{1.3.5}$$[12].

Likewise in LD spectroscopy the detected signal is,

$$I[t] = I_H e^{-a_H} + I_V e^{-a_V} \tag{1.3.6}$$

where I_H, I_V, a_H, and a_V are the intensities and absorptions for the horizontal and vertical linearly polarized light respectively and are defined as

$$I_{H/V} = \frac{I_0}{2}(1 \pm \cos(\delta[t])) \tag{1.3.7}$$

$$a_{H/V} = \overline{a}_{LD} \pm \frac{\Delta a_{LD}}{2} \tag{1.3.8}$$

applying (1.3.7) and (1.3.8) to (1.3.6), the intensity becomes

$$I[t] = \frac{I_0}{2} e^{-\overline{a}_{LD}} (1 - \Delta a_{LD} J_0(\delta_0) + 2J_2(\delta_0)\cos(2\omega_0 t) + ...) \tag{1.3.9}$$

with the Bessel function expansion (see appendix G for similar derivations) ignoring higher order terms[19]. Both (1.3.5) and (1.3.9) are sums of the DC and AC signal[12]. Therefore, the measure of the ratio of AC to DC (ignoring higher orders) is the CD and LD signal. The CD signal is determined by

$$\frac{\Delta I_{CD}}{\overline{I}} = \frac{-2\Delta a_{CD} J_1(\delta_0)}{1} \tag{1.3.10}$$

and the LD signal is determined by

$$\frac{\Delta I_{LD}}{\overline{I}} = \frac{-\Delta a_{LD} J_2(\delta_0)}{1 - \frac{\Delta a_{LD}}{2} J_0(\delta_0)} \tag{1.3.11}$$

where $\overline{I}$ is the average intensity of the signal, ΔI_i is the difference in intensity of the signal, $\frac{\Delta I_{CD}}{\overline{I}}$ and $\frac{\Delta I_{LD}}{\overline{I}}$ are the detected signal (AC to DC ratio) of CD and LD respectively, δ_0 is the phase-difference amplitude on the PEM, and Δa is the difference in absorption (CD or LD). Equations (1.3.10) and (1.3.11) are the measured CD and LD for the case when the photoelastic modulator does not exhibit static birefringence. Chapter 3 discusses how (1.3.10) and (1.3.11)

changes with the presence of static birefringence in the photoelastic modulator crystal and the effects of the amplitude on the signal.

1.4 PHOTOELASTIC MODULATOR

The photoelastic modulator (PEM) is a device made up of a piezoelectric transducer coupled to a crystal (typically quartz). By coupling the quartz crystal to a piezoelectric transducer, a voltage can be applied to stress the crystal and control the phase difference (δ) of the two linear polarization states, which takes advantage of the quartz birefringence. This is how circular and linear polarized light is created. The crystal has a resonant frequency (about 50 kHz) that is used to oscillate between polarization states. This is done by applying an AC voltage to the piezoelectric transducer, which then applies a stress, "stretching" and "compressing" the crystal. To create circularly polarized light, the phase difference, δ, is a quarter waveplate ($\delta = \pi/2$). To create linearly polarized light, δ is a half waveplate ($\delta = \pi$).

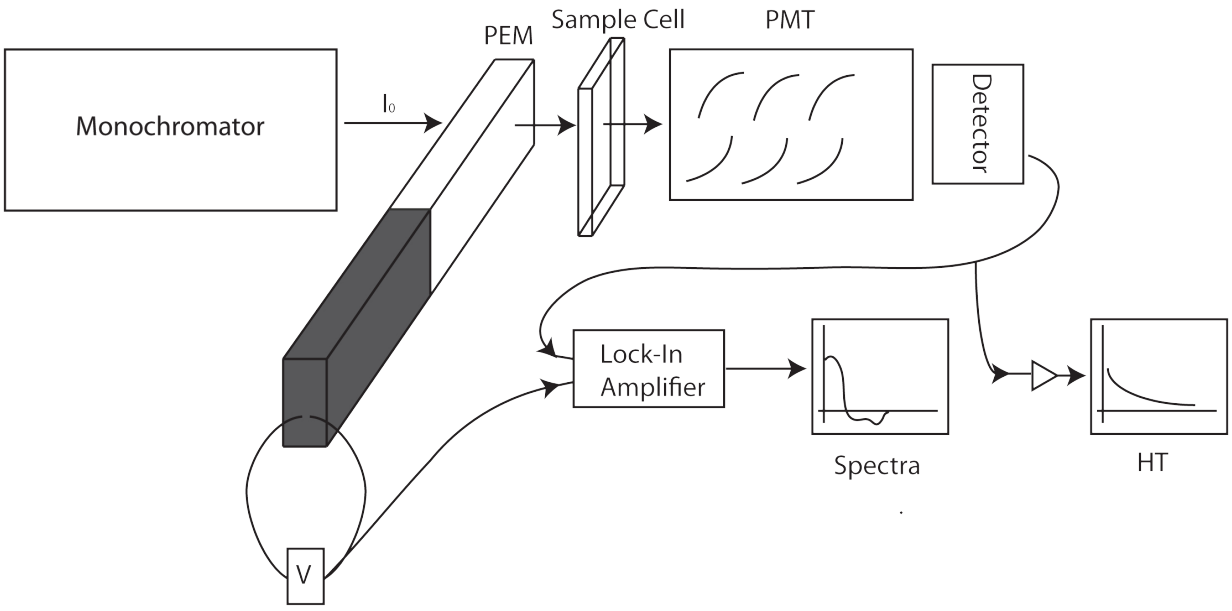

Figure 2: Diagram of the main optical and detecting components in the CD spectrometer used to detect the CD and HT.

The phase difference is measured traditionally by placing linear polarizers of cross linearity on either side of the PEM and the signal from the PMT is observed on an oscilloscope (discussed in Chapter 3). The technique described in Chapter 3 did not produce data of sufficient precision for the sensitive measurements made here due to the noise on the observed signal, therefore a new technique was developed and implemented to determine the phase difference with more accuracy using the same set up with a rotatable polarizer and the voltage-to-gain relationship of the photomultiplier tube determined in Chapter 2.

Quartz may experience a phenomenon where a phase difference in the crystal naturally occurs. This is called static birefringence, δ_s. There have been a few attempts measuring the static birefringence of the quartz crystal[20,21,22], but have an incomplete model or no method to measure the static birefringence. The presence of static birefringence has been observed and will

be discussed with a complete model and method of measuring the static birefringence in Chapter 3.

1.5 SPECIFIC AIMS

This study addresses types and characteristics of noise present in CD and LD spectroscopies. Types of noise include shot noise (Poisson distributed noise), dark current and stray light. Characteristics of and uncertainties in the noise include drift in the signal, mechanical (e.g. slit alignment), instrument settings (e.g. voltage applied to the PEM, choice of phase-difference amplitude, etc.), and fractional change in the signal. Characterizing the noise aids in determining what types and characteristics of noise have the greatest effect on the spectrometer (e.g. light detection, spectral determination, analysis of CD and LD).

Characterizing the noise and gain of the photomultiplier tube will improve the accuracy for determining the phase-difference amplitude (δ_0) and static birefringence (δ_s) in the PEM. A novel approach to determining the phase-difference amplitude and static birefringence is outlined and implemented. Determination of the appropriate phase-difference amplitude and static birefringence allows wavelength-scanable electronics to provide a voltage that more accurately defines the phase-difference amplitude setting for the photoelastic modulator.

This new approach was also used to measure the Stokes parameters (by adding a quarter waveplate to the analyzer) to analyze the light produced by the photoelastic modulator for CD and LD spectroscopy. Phase difference settings were implemented and used for Camphorsulfonic Acid (in CD) and Chrysazin (in LD) to observe the significance of the fractional change in the signal. Each of the methods addressed in this study provided useful information to improve the accuracy and purity (or fidelity) of spectra in CD and LD spectroscopy.

This study addresses the types and characterization of noise in the CD spectrometer. It also addresses the function of the photoelastic modulator. It is hoped that this study will result in suggestions for operating the CD spectrometer with more efficiency and fidelity and improve the data collection of biomolecules exhibiting both CD and LD. In general, this research will open up new opportunities for advances in measuring CD and LD.

CHAPTER 2: CHARACTERIZATION OF THE CD SPECTROMETER

There are some contributions in CD spectroscopy that are not taken into full consideration such as types and characteristics of noise[5,6]. In this chapter, the CD spectrometer will be characterized for contributing sources of noise (signal to noise ratio) and artifacts specific to the photomultiplier tube (PMT); stray light, dark current, and voltage to gain conversion. Data was collected on a Jasco J810 and J815 CD spectrophotometer.

The presence of stray light and dark current can modify the signal in CD spectroscopy. By characterizing the presence of both in the PMT, this will indicate data significance that is collected under certain parameters exhibiting either phenomenon. Stray light and dark current are experimentally determined by observing the DC voltage and high tension (or high voltage, V_0) from the PMT simultaneously.

2.1 SIGNAL TO NOISE RATIO

The signal to noise ratio (SNR) in CD spectroscopy is Poisson distributed and can be defined in terms of the number of photons n entering the detector (current output from the PMT). The SNR can be defined as

$$SNR(\lambda_i) = \frac{n}{\sqrt{n}} = \sqrt{n} \qquad (2.1.1).$$

For CD Spectroscopy, the PMT gain varies to maintain a constant output[23]. This and a high photon flux affects the ability to do single photon counting, so an indirect approach is used to theoretically calculate and experimentally measure the noise. Experimentally the SNR is

$$SNR(\lambda_i) = \frac{\Delta a_{CD}(\lambda_i)}{\sigma(\lambda_i)} \qquad (2.1.2)$$

where $\sigma(\lambda_i)$ is the standard deviation (considered to be a standard measure of noise) of the CD signal (experimentally measured in mdeg) $\Delta a_{CD}(\lambda_i)$ and $\Delta a_{CD}(\lambda_i)$ is the average of the signal at a specific wavelength (in mdeg).

The SNR is determined by taking the ratio of two SNR's, which removes the signal because the signal is identical in both cases and leaves only the ratio of the noise. The theoretical (calculated) RSNR is defined as,

$$RSNR(\lambda_i) = \frac{SNR_1(\lambda_i)}{SNR_2(\lambda_i)} = \frac{\sqrt{n_1}}{\sqrt{n_2}} \tag{2.1.3}$$

where n_1 and n_2 are measures of the number of photons. The experimentally measured RSNR is given by,

$$RSNR(\lambda_i) = \frac{SNR_1(\lambda_i)}{SNR_2(\lambda_i)} = \frac{\sigma_2(\lambda_i)}{\sigma_1(\lambda_i)} \tag{2.1.4}$$

where $\sigma_i(\lambda_i)$ is the corresponding experimental standard deviation of the CD signal $\Delta a_{CD}(\lambda_i)$ (in mdeg). Similar to the theoretical representation of the SNR, the CD signal will be the same for every experiment, but the noise, of which $\sigma(\lambda_i)$ is a measure, varies. Hence the relationship between the experimental and theoretical determination of the photon count and noise is given by,

$$RSNR(\lambda_i) = \frac{\sqrt{n_1}}{\sqrt{n_2}} = \frac{\sigma_2(\lambda_i)}{\sigma_1(\lambda_i)} \tag{2.1.5}$$

where determining RSNR experimentally is a test of the hypothesis that the noise is Poisson-distributed shot noise.

This hypothesis was tested by changing one scanning parameter and holding the others constant. The parameters that were varied are; average number of scans, bandwidth, slit width,

scan speed and response time. A few of the parameters have mechanical functions that can effect how the hypothesis is applied to the data collected and need to be addressed. Bandwidth is a function of slit width. As the wavelength changes through scanning so does the slit width to maintain a constant bandwidth. In addition, this particular CD spectrometer contains a double monochromator with a slit after each prism through which the light passes and therefore the number of photons depends on the square of the bandwidth. The same situation applies for slit width because as wavelength changes, bandwidth varies. According to information provided by Jasco, roughly 1 nm bandwidth corresponds to 10 μm slit width in the visible light region and 1 nm of bandwidth corresponds to 1 mm of slit width in the UV. Finally, it was experimentally shown that scan speed noise was not Poisson distributed (see Figure 3) and therefore was selected in accordance with response time to show Poisson noise contributions when running in maximum allowed combination specifications of scan speed and response time in the program provided by Jasco. Chosen scan speed and response time is shown in Table 1.

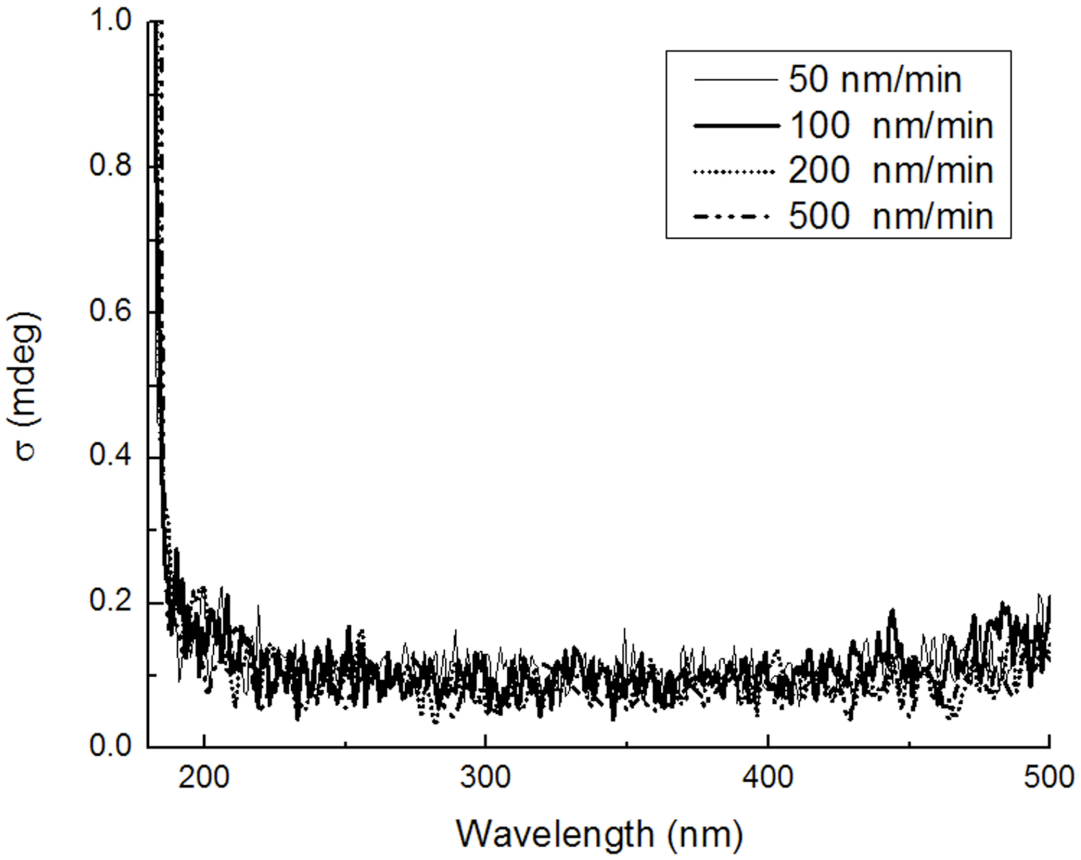

Figure 3: Noise (σ) vs. wavelength for scan speed with response time held at 1 sec.

Indicated in Table 2 are the ranges and tests that exhibit the largest deviation from a Poisson distributed RSNR. The largest deviation came from narrower bandwidths and longer wavelengths. Data collection on the J810 indicated that at higher wavelength ranges (480 -700 nm), the bandwidth-dependent RSNR does not always follow a Poisson distribution with the presence of some deviation from linearity. There was no apparent bandwidth-dependent RSNR nonlinearity on the J815, but it suffered the largest deviation experimentally. Analysis indicates that in these ranges, the noise in the CD signal cannot simply be only Poisson distributed but

may have been complicated by systematic error (slit alignment, etc.). Likewise, Table 3 indicates more ranges and tests that exhibit Poisson distributions, but exhibit some divergence between predicted and experimentally determined RSNRs. All other ranges and tests follow Poisson statistics and coincided with theoretical predictions; particularly response time and averaged number of scans.

Optimal parameters on the J810 and J815 are 1-4 sec response time at a 50-200 nm/min scan speed and a 1-8 nm bandwidth. Note that when using a larger bandwidth, the width and strength of the spectral feature need to be considered. In addition, there is a significant increase in the SNR when HT exceeded 400 volts and weighted data using a quantitative analysis technique that involves the integration of data over a range of HT would be beneficial (Figure 4) and indicate the relationship between SNR and HT.

Response Time (s)	**Scan Speed (nm/min)**	**Scan Speed (Max) (nm/min)**
0.25	1000	-
0.5	500	1000
1	200	500
2	100	200
4	50	100
8	-	50

Table 1: Parameter choices for scan speed and response time experiments

Jasco J810		
Parameter	**Range (nm)**	**Test**
Bandwidth	480-700	1 vs. 2 nm
Bandwidth	480-700	1 vs. 4 nm
Bandwidth	480-700	1 vs. 8 nm
Bandwidth	480-700	2 vs. 4 nm
Bandwidth	480-700	2 vs. 8 nm
Jasco J815		
Parameter	**Range (nm)**	**Test**
Bandwidth	180-480	1 vs. 4 nm
Bandwidth	480-700	1 vs. 4 nm
Bandwidth	480-700	1 vs. 8 nm
Bandwidth	480-700	2 vs. 4 nm
Bandwidth	480-700	2 vs. 8 nm

Table 2: Ranges where RSNR is not normally distributed.

Jasco J810		
Parameter	**Range (nm)**	**Test**
Bandwidth	180-480	1 vs. 4 nm
Bandwidth	480-700	4 vs. 8 nm
Slitwidth	180-500	100 vs. 500 um
Slitwidth	180-500	100 vs. 1000 um
Slitwidth	500-700	100 vs. 500 um
Slitwidth	500-700	100 vs. 1000 um
Slitwidth	500-700	500 vs. 1000 um
Averaged Scans	500-700	1 vs. 4 averaged scans
Jasco J815		
Parameter	**Range (nm)**	**Test**
Bandwidth	480-700	1 vs. 2 nm
Bandwidth	480-700	4 vs. 8 nm
Slitwidth	500-700	500 vs. 1000 um

Table 3: Data collected that has some discrepancies in linearity.

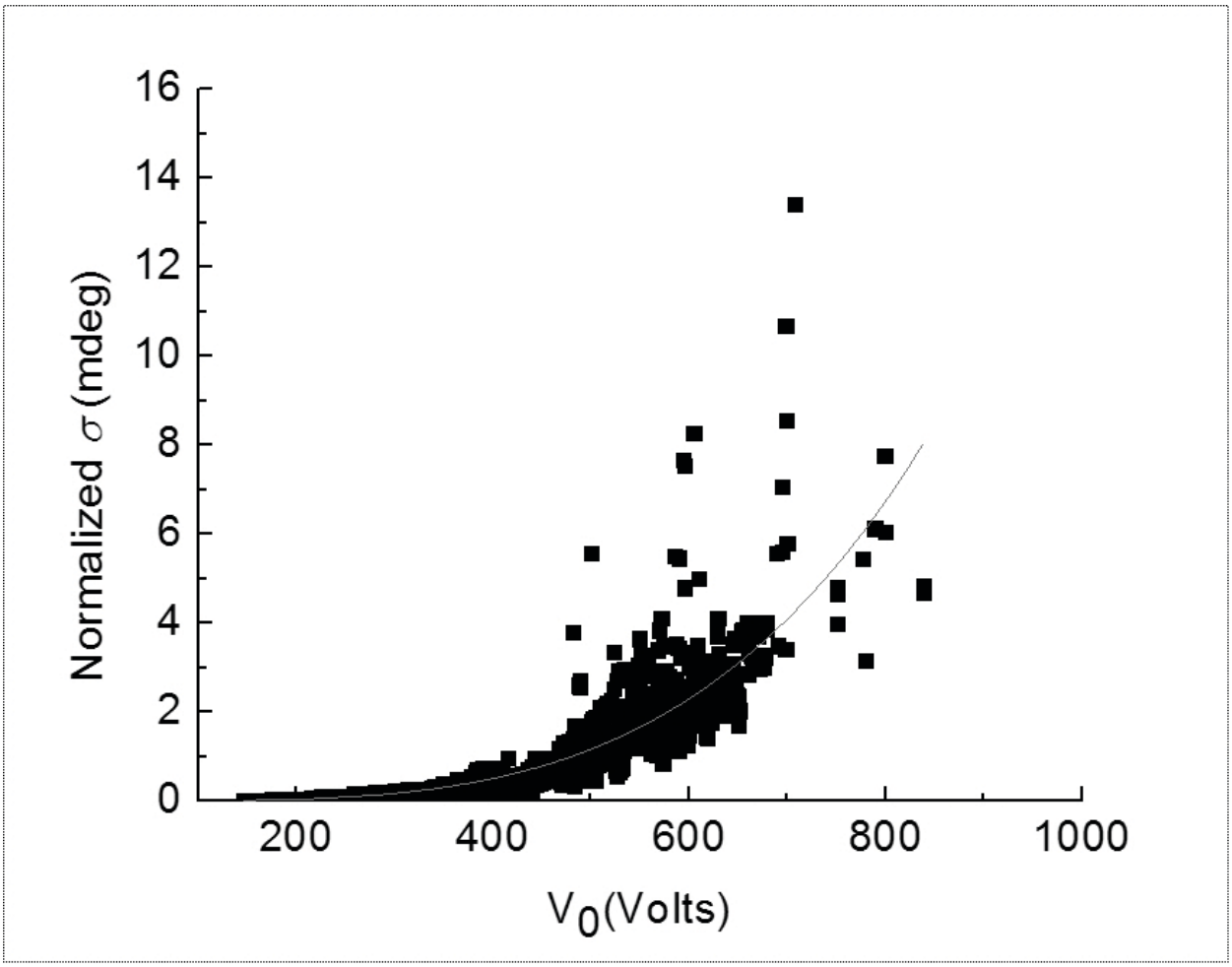

Figure 4: Normalized σ of the CD vs. HT used to weight data that is integrated or combined.

2.2 DARK CURRENT AND STRAY LIGHT

The DC voltage, *v*, (the time average signal from the PMT) is a product of two gains and the sum of three cathode currents,

$$v(\lambda_i) = G_{i/v} G_{PM}[V](j_p + j_s + j_d) \qquad (2.2.1)$$

where $G_{i/v}$ is the gain of the current-to-voltage converter for the PMT, $G_{PM}[V]$ is the gain provided by the Jasco company (relationship between the gain and HT of the PMT), and the three currents that represent the cathode current due to: the primary light beam (j_p), stray light

(j_s), and dark current (j_d)[24]. Normally, the HT on the PMT ($V_{0/f}$) is adjusted to maintain a constant time average DC output ($v_{0/f}$) for the CD spectrophotometer,[25] but when there is too little light, the $V_{0/f}$ limit is met and as a result $v_{0/f}$ is no longer constant and begins to decrease. By measuring the gain on the PMT and the DC output as a function of wavelength simultaneously, the fraction ($v_{fraction}$) of light due to dark current and stray light is,

$$v_{fraction} = \frac{v_f G_{PM}[V_0]}{v_0 G_{PM}[V_f]} \qquad (2.2.2)$$

where V_0 and v_0 are the HT and DC signal under normal operating conditions and V_f and v_f are the HT and DC under exceptional conditions. The subscript *f* indicates the presence of a cutoff filter. Implementing a cutoff filter allows for the stray light and dark current contribution to be separated from the main contribution of the signal. Likewise to separate the stray light from the dark current, the PMT window is blocked (using aluminum foil) and V_f and v_f are replaced by V_{dark} and v_{dark}.

It is observed that when the HT reaches its saturation point the DC voltage decreases (see Figure 6, Figure 7, and Figure 8**)**. In Figure 5, $v_{fraction}$ indicates that the amount of stray light is about 3.0(1)% and dark current is about 0.1(1)% between 290 nm and 184 nm. V_0 reaches its saturation point around 190 nm resulting in the stray light dominating and dark current being a small but measurable contribution (v = 0.32(1)) between 190 nm and 170 nm. Therefore, as V_0 approaches 900 volts, stray light and dark current dominate the signal. On the other hand, stray light and dark current are of little consequence when $V_0 < 600$ volts.

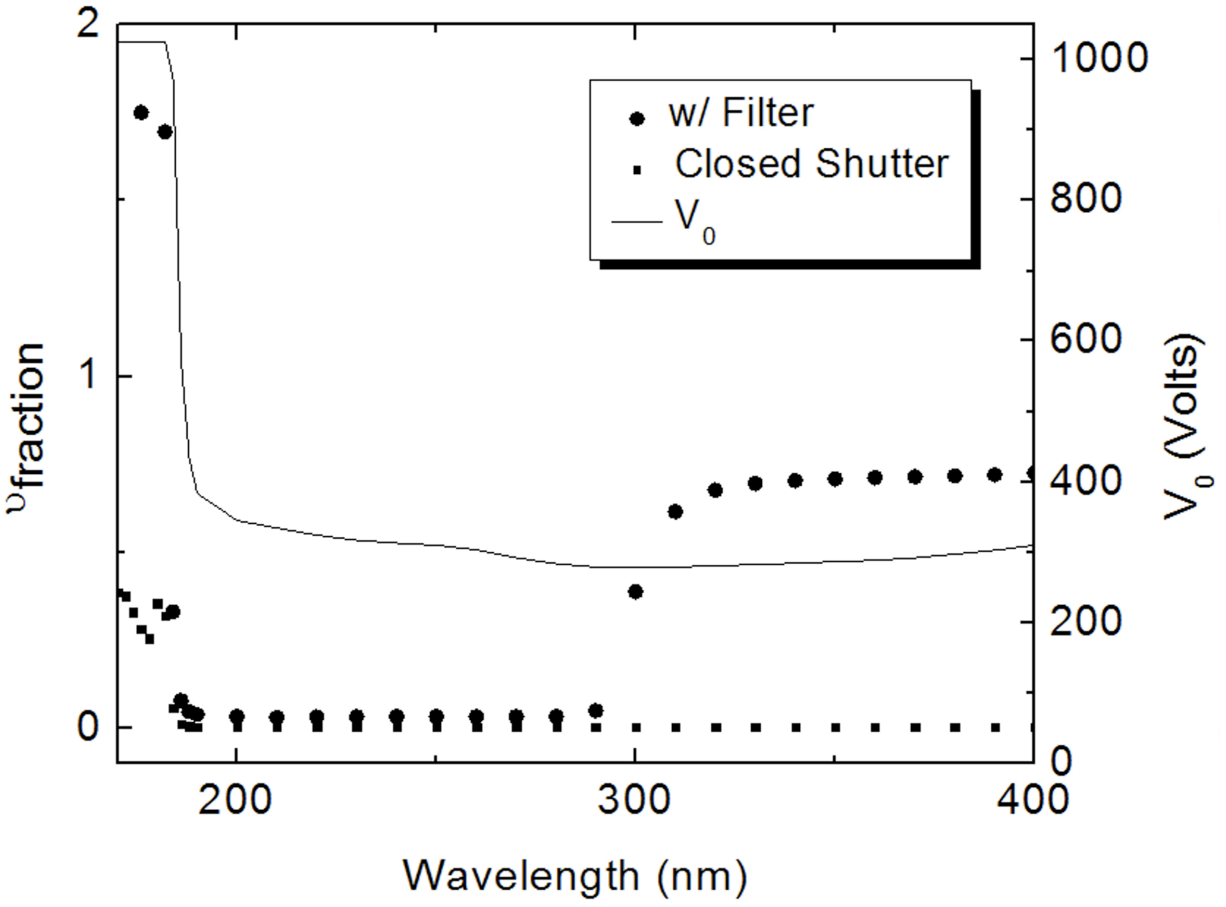

Figure 5: $\upsilon_{fraction}$ and V_0 vs. wavelength determined when a filter is present or the shutter is closed in the Jasco J810 CD spectrometer.

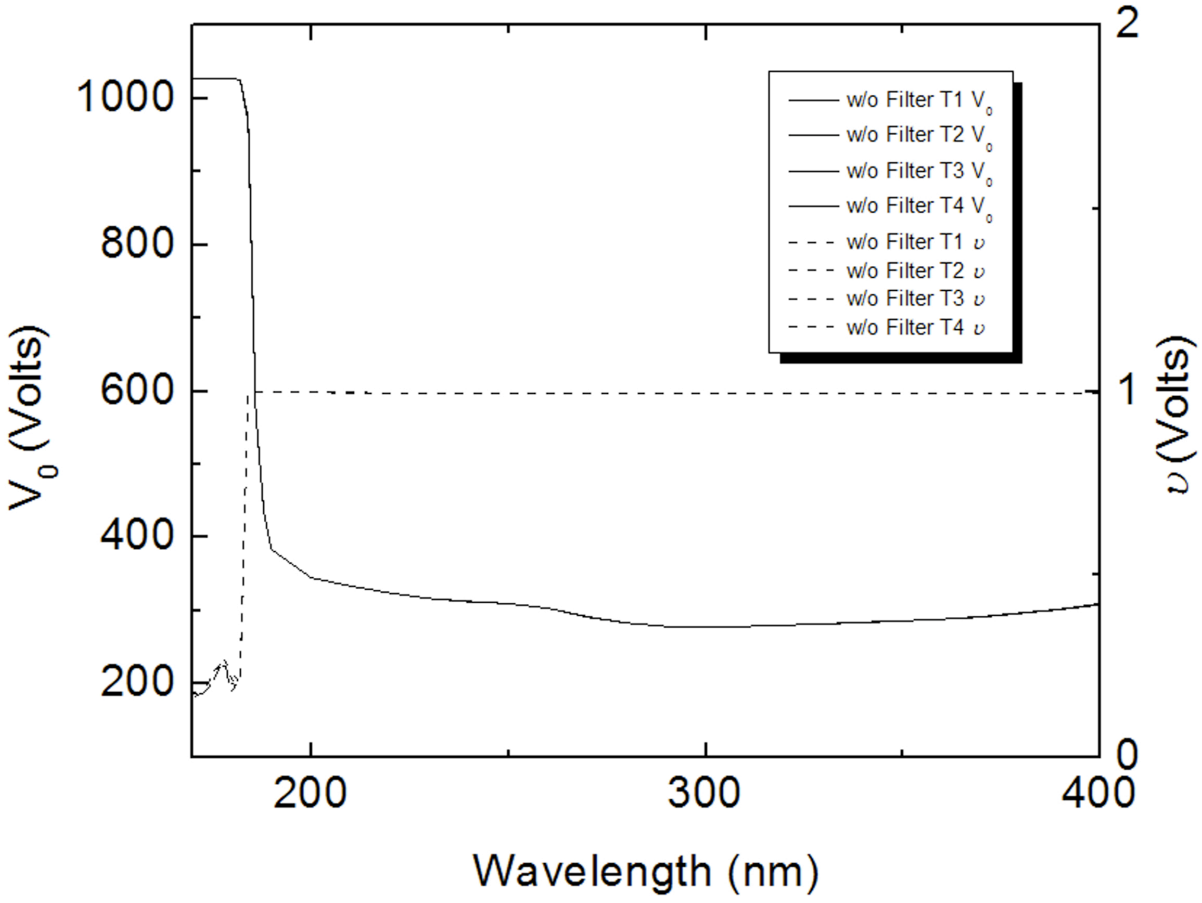

Figure 6: Four trials of V_0 and υ (constant DC output) measured on J810 without a filter.

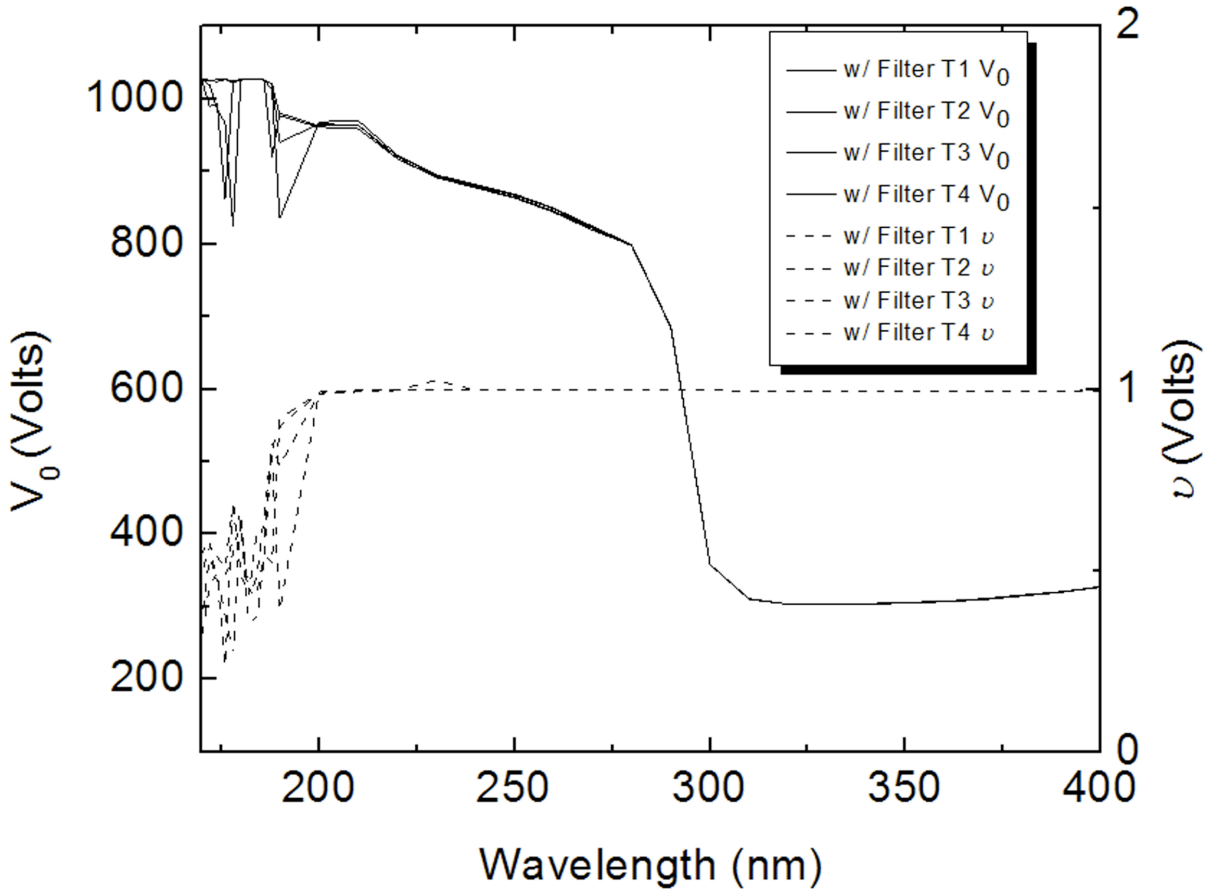

Figure 7: Four trials of V_0 and υ measured on J810 with a 300 nm filter.

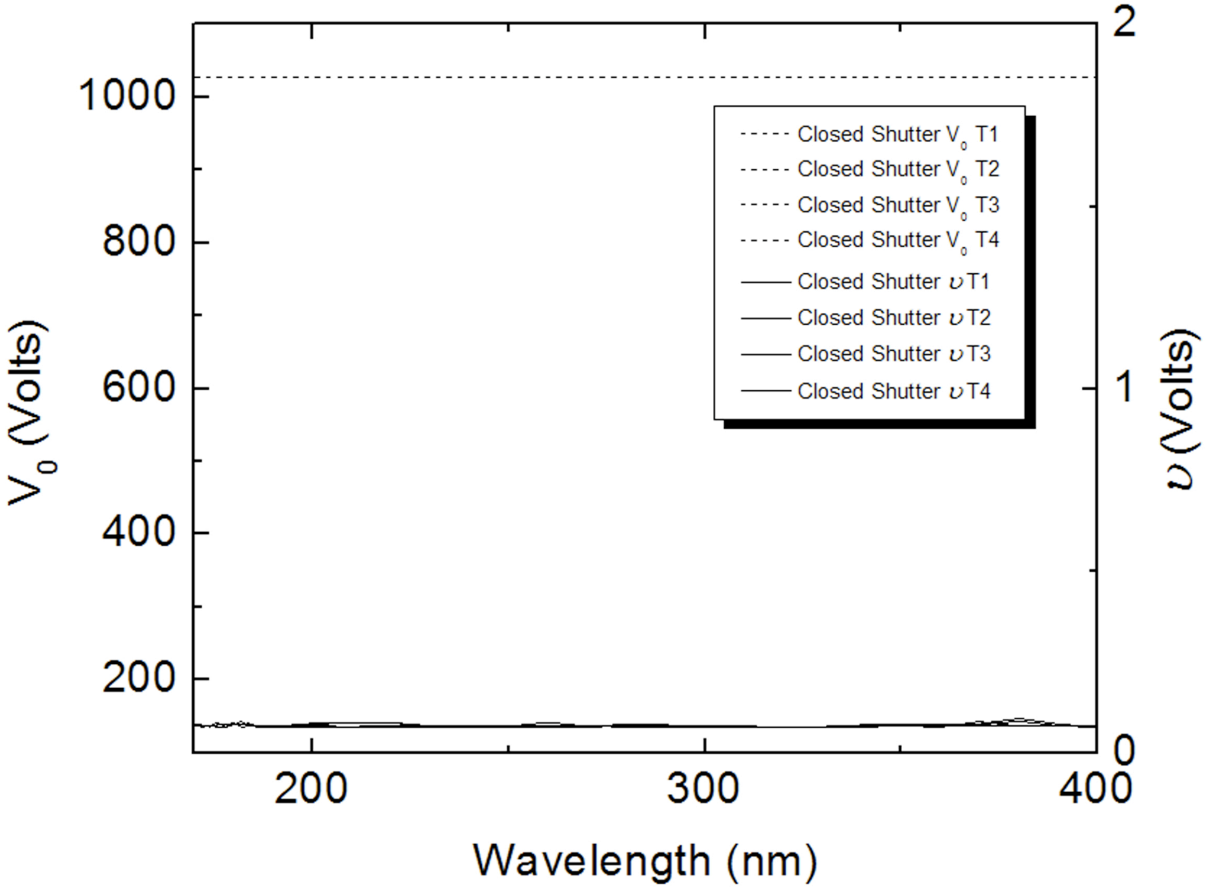

Figure 8: Four trials of V_0 and υ measured on J810 with a closed shutter.

2.3 PHOTOMULTIPLIER TUBE DETECTOR

An ideal PMT (see Figure 9) has a number of dynodes p with a dynode voltage V_d that is equal across every dynode. The HT voltage, V_0, applied to the PMT is equally divided by a voltage divider and the voltage at each dynode is

$$V_d = \frac{V_0}{p+2} \qquad (2.3.1)$$

where V_0 is the total voltage applied to the PMT and p is the number of dynodes in the PMT. The "+ 2" includes the potential drop between the cathode and first dynode and the anode and last dynode assuming voltage drops across each dynode are the same. The gain of each dynode is the number of secondary electrons per primary electron, and can be defined as

$$G_{d_i} = kV_{d_i} \tag{2.3.2}$$

where k is the number of electrons produced per volt of electric potential across a single dynode assuming the material and geometry of the dynodes are identical. For the ideal PMT described, the V_{d_i} are equal and hence the G_{d_i} are equal so that the total gain G_{PM} of the PMT would be

$$G_{PM} = (G_{d_i})^p = (kV_{d_i})^p \tag{2.3.3}.$$

Substituting in (2.3.1),

$$G_{PM} = \frac{k^p}{(p+2)^p}(V_0)^p \tag{2.3.4}$$

and hence,

$$\ln(G_{PM}) = p\ln\left(\frac{k}{p+2}\right) + p\ln(V_0) \tag{2.3.5}$$

which provides a linear relationship between the natural log of the gain and the natural log of the applied voltage, V_0. In practice, however, the photomultiplier tube (Hamamatsu R376 in the Jasco J810 and J815) does not behave perfectly as the ideal case described. It is linear on a log-log scale as described in (2.3.5), but the slope does not equal the integer number of dynodes in the PMT. Results for experimental (2.3.5) are as follows for the two Jasco CD spectrometers being tested as well as data from Hamamatsu,

$$Amplification = 7.44 \times SampleVoltage - 15.7 \qquad \text{R376 Hamamatsu}$$

$$\ln(\sigma^2) = 6.4(3) \times \ln(V_0) - 17.4(7) \qquad \text{Jasco J815}$$

$$\ln(\sigma^2) = 7.5(6) \times \ln(V_0) - 20(1) \qquad \text{Jasco J810.}$$

It is observed that the voltage divider is not functioning as ideally described above, so the theoretical number of dynodes predicted is not the number determined experimentally. Nevertheless, the voltage-gain performance is calibrated and functions as described by the PMT manufacturer.

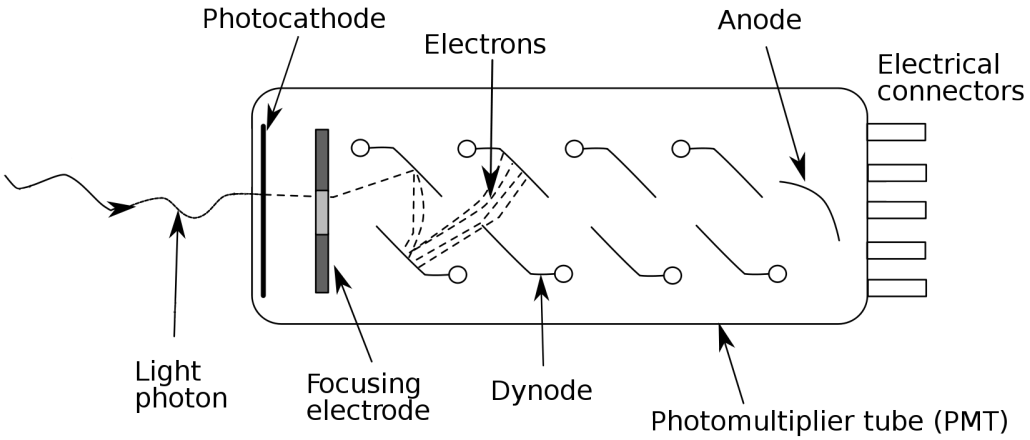

Figure 9: Inside a photomultiplier tube where a photon is incident on the photocathode. The photon is then converted to electrons.

Gain is not a simple function of wavelength, but by combining the above relationship between Gain and HT and information from Section 2.1, describing the relationship between relative SNR and HT, and the initial data collection where HT is recorded with the CD signal, the relative SNR at different wavelengths can be determined (see Figure 4). The HT is therefore useful in determining the significance of the CD data as a function of SNR. For more information see reference 6.

2.4 CONCLUSIONS

Noise in CD spectroscopy was shown to follow Poisson statistics by studying changes in shot noise when varying machine parameters such as number of scans, bandwidth, slit width, and response time on the Jasco J810 and J815 spectrometers. The hypothesis that noise in CD spectroscopy follows Poisson distributed shot noise was verified for all parameters with a few exceptions at longer wavelength ranges. Deviations (systematic error) occur in bandwidth and slit width, as they are both related to each other. Slit width is adjusted in the CD monochromator to allow for a constant bandwidth because the dispersion of the prism in the monochromator is wavelength dependent. Bandwidth deviation increases as bandwidth decreases and also begins to stray from Poisson distribution between 480-700 nm wavelength range. This may be the result of a baseline drift that is more evident in the longer wavelength ranges and may become an issue for CD studies using the longer wavelength ranges. Some slight misalignment in the slits may also be a contributing factor. Similarly, deviations from Poisson distribution in slit width come from a changing bandwidth over wavelength.

It is evident that the SNR, for number of scans and response time parameters, does follow Poisson distribution. Nevertheless, time-dependent systematic errors such as drift are applicable to averaging scans and exhibit the deviations as bandwidth and slit width experiments. It is worth noting that in this regard the J815 performed superior to the J810. It has been demonstrated that the signal is Poisson distributed by quantitatively predicting shot noise.

When implementing the 300 nm filter, dark current and stray light in the PMT where minimal in the higher wavelength range ($\lambda < 300$ nm). Below 300 nm the HT detector voltage, V_0, increases and begins to saturate ($V_0 > 900$ volts) causing the signal to be dominated by stay

light and dark current. For detector voltage below 600 volts, stray light and dark current are negligible and do not produce a false signal.

The final result for this study was the demonstration of the functional dependence of a significant spectral data set. The functional dependence is measured through the relative SNR and V_0, which is a measure of gain, which allows a relationship between gain and wavelength that can be used to weight the significance of data. The results are expected to impact experimental analysis that depends on integrating or combining data, which have a notable variation in V_0 over wavelength.

CHAPTER 3: CHARACTERIZING THE PHOTOELASTIC MODULATOR

A photoelastic modulator (PEM) is an optical device, made of fused silica attached to a piezoelectric transducer that can change the polarization state of the light by varying the applied voltage. The applied voltage changes the delay between the parallel and perpendicular (to the horizontal) electric field inducing a phase change (δ). In CD and LD spectroscopy the PEM is used to oscillate between left and right circularly polarized light or parallel and perpendicular linearly polarized light respectively. In order to oscillate between the two states, an AC voltage is applied to the PEM with a resonant frequency $f \approx 50$ kHz for CD and LD[1]. The light exiting from the oscillating PEM can be described in terms of Stokes parameters as

$$I'(\delta[t]) = \begin{bmatrix} 1 \\ \cos(\delta[t]) \\ 0 \\ -\sin(\delta[t]) \end{bmatrix} \qquad (3.1),$$

where δ is the phase difference between parallel and perpendicular linearly polarized light (see appendix E for derivation) and

$$\delta[t] = \delta_0 \sin(\omega_0 t) \qquad (3.2),$$

where δ_0 is the amplitude and ω_0 ($=2\pi f$) is the angular frequency. It has been observed that a mechanical phase difference (static birefringence) is present in the PEM[8], which (3.2) can be redefined as

---

[1] In LD, PEM oscillates at 50 kHz, but LD measurements are made at $2f$ separately.

$$\delta[t] = \delta_0 \sin(\omega_0 t) + \delta_s \qquad (3.4).$$

where δ_s is phase difference for the static birefringence. The presence of static birefringence changes (1.9) and (1.10) to

$$\frac{\Delta I_{CD}}{\overline{I}} = \frac{-\Delta a_{CD} J_1(\delta_0)\cos(\delta_s)}{1 - \frac{\Delta a_{CD}}{2}\sin(\delta_s) J_0(\delta_0)} \qquad (3.5a)$$

$$\frac{\Delta I_{LD}}{\overline{I}} = \frac{-\Delta a_{LD} J_2(\delta_0)\cos(\delta_s)}{1 - \frac{\Delta a_{LD}}{2}\cos(\delta_s) J_0(\delta_0)} \qquad (3.5b).$$

This chapter describes how the polarization of the light (electric field) is controlled in CD and LD spectroscopy. The light is described by Stokes parameters and the effect of various optical elements (defined in terms of Muller Matrices) on the light. The PEM's time-averaged phase difference is determined theoretically and experimentally and application of phase difference changes on the PEM in the Jasco J810 CD spectrometer. In addition, the application for determining the phase-difference changes will be used to measure the static birefringence of the PEM crystal.

3.1 ELECTRONICS

A wavelength-dependent phase difference is calibrated by Jasco by applying an AC voltage to the J810 PEM. The specific aim of this work is to determine the inherent phase difference of the PEM, and to predict and generate the corresponding phase difference when a specific (external control) voltage is applied. A computer-controlled voltage is externally applied to the PEM circuitry to adjust the PEM-signal amplitude. The computer-controlled electronics (LabVIEW) comprise: an externally controlled wavelength gain change, directly application of a

specific voltage, and the capability to switch between external and internal (standard J810) control.

3.1.1 Understanding the Circuitry of the PEM

The PEM oscillates at a resonant frequency of ≈ 50 kHz driven by an LC-circuit made of Capacitor 7, Capacitor 8, and Inductor 1 (C7, C8, and L1) on the PEM driver board (Jasco schematic PEM Driver 6775-513CA). The driving frequency is fed back through J501 pin 3 to the PEM drive circuit to control the oscillation frequency and eventually through IC3B (difference amplifier) to sum with the DC voltage used to adjust the gain on the AC voltage. There are limitations on the amount of DC voltage that can be mixed with the AC signal. This limit is 2.3 VDC and is controlled by IC3A on the PEM Driver board. The DC voltage can be manually adjusted by actuating SW1 on the PEM Driver board and manually adjusted via potentiometer RV7.

3.1.2 Changes Made on the PEM Driver Board

Switch 1 (SW1) (Jasco schematic PEM Driver 6775-513CA) was replaced with a non-spring loaded switch to allow the external (computer) control voltage to be applied without having to hold the switch back (thus allowing fixed switching between auto and manual mode). The potentiometer RV7 (controls the applied DC voltage on the PEM) was removed and replaced by a 1kΩ resistor so as to not alter the current of the circuitry (limits current). The computer is controlled by placing the computer input through J502 pin 1 and pin 4 and the output through J505 pin 1 and 2 CB-68LP which is connected to the computer. The computer-controlled program (in LabVIEW; see Appendix C) was designed by Chris Bonnerup in the ECU

electronics shop. It allows for a wavelength scanable VDC applied voltage and an automatic set voltage used to set the VDC to 0 volts (an attempt to emulate the PEM being turned off).

The computer program uses the internal VDC to the PEM and converts it to the appropriate external VDC to be applied to the PEM. As the Jasco CD or LD program is running, the internal VDC changes with wavelength and thus the external VDC changes respectively with wavelength.

3.2 DETERMINING THE VOLTAGE APPLIED TO THE PEM

The measured signals for determining CD and LD follow (3.5a) and (3.5b). Using (3.5a) and (3.5b) as a model to allow appropriate choices to maximize the signal and minimize unwanted contributing factors can be done by changing δ_0 (see Figure 10). The appropriate voltage to be applied to the PEM is in conjunction with the phase difference of the PEM. For CD, choosing δ_0 so that $J_1(\delta_0)$ is maximized

$$J_0(0.587\pi) = 0.314 \qquad (3.2.1)$$

will increase the amplitude of the CD signal to its highest point. Likewise, for LD, $J_0(\delta_0)$ is a contributing factor to the DC voltage and should be minimized ($J_0(\delta_0) = 0$),

$$J_0(0.765\pi) = 7.83 \times 10^{-4} \qquad (3.2.2)$$

so that $J_2(\delta_0)$ is the only phase difference contributing factor. Note that in (3.5a), $J_0(\delta_0)$ is a contributing factor. This will be discussed at length in Chapter 4.

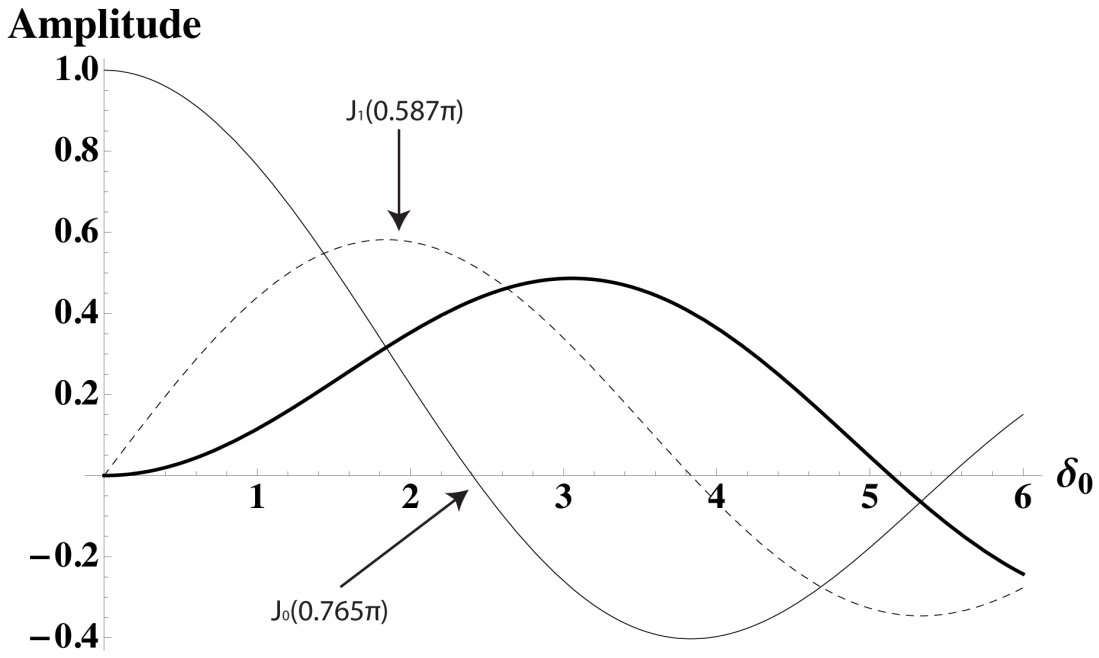

Figure 10: Bessel Functions used in the expansion of the CD and LD signals. Thin black is $J_0(\delta_0)$, dashed is $J_1(\delta_0)$, and thick black is $J_2(\delta_0)$. Traditional settings for the Bessel functions are indicated for CD $J_1(\delta_0) = 1.84$ and LD $J_0(\delta_0) = 2.405$.

Now that δ_0 has been theoretically determined for the PEM, the next step is to determine what voltage needs to be applied for the PEM to produce δ_0. In the past, the determination of the voltage applied to the PEM to produce δ_0 was done by observing the PEM acting as a half-wave plate, where $\delta_0 = \pi$, and then determining the appropriate voltage to be applied to the PEM where, for CD, $\delta_0 = 0.587\pi$ and for LD, $\delta_0 = 0.765\pi$.

3.2.1 Determination of Phase Difference by Traditional Methods

Determination of the phase difference, δ, for the PEM in CD and LD spectroscopy was originally achieved by placing two linear polarizers of cross linearity on either side of the PEM resulting in an AC signal observed on an oscilloscope. This is modeled theoretically by,

$$S_{Analyzer} = M_V M_{PEM}(45^\circ, \delta) M_H S \tag{3.2.3}$$

where M_H is horizontal polarization matrix, M_{PEM} is the matrix for the PEM rotated to 45° with phase difference δ, and M_V is the vertical polarization matrix. Carrying out the calculation, the Stokes parameters become

$$S_{Analyzer} = \frac{1}{2}(1 - \cos(\delta(t)) \begin{bmatrix} 1 \\ -1 \\ 0 \\ 0 \end{bmatrix} \tag{3.2.4}$$

with intensity

$$I_{Analyzer} = \frac{1}{2}(1 - \cos(\delta(t))) = \frac{1}{2}(1 - \cos(\delta_0 \sin(\omega_0 t)) \tag{3.2.5}$$

where δ_0 is the amplitude of the phase difference and is tuned to π by observing a flat top on the trace signal (see Figure 11)[7].

The signal follows $I_{Analyzer}$ (in LD mode) and appears as an oscillating signal with a flat top when δ_0 is equal to π (or a half waveplate). For the bench top machine, noise is a contributing factor and makes it difficult to clearly identify the voltage that must be applied to the PEM (see Figure 15). No difference in signal shape was observed until δ_0 was changed by 6.0(1)% (see Figure 12, which shows a dramatized version of the signal shape change). This makes it difficult to accurately determine δ_0 and the corresponding voltage required to create a half wave retardation. Another technique was developed to accurately calibrate the phase difference of the PEM and is discussed in section 3.2.2.

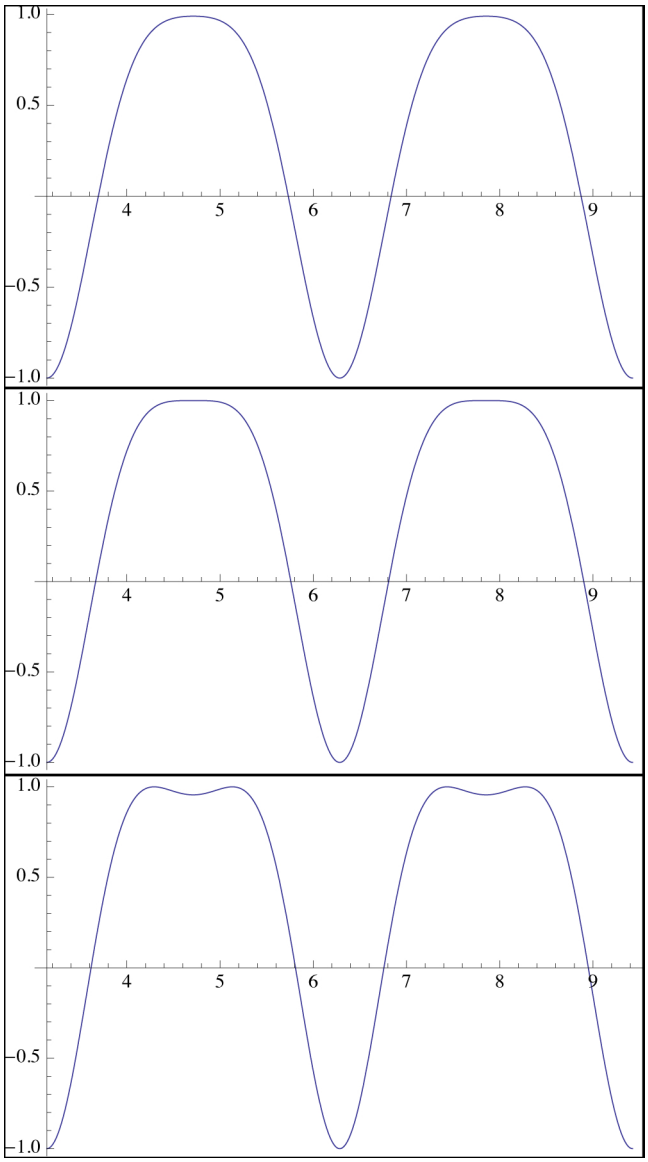

Figure 11: Theoretical representation of LD signal for measuring the phase difference on the PEM (a) 5% below $\delta_0 = \pi$, (b) $\delta_0 = \pi$, and (c) 5% above $\delta_0 = \pi$.

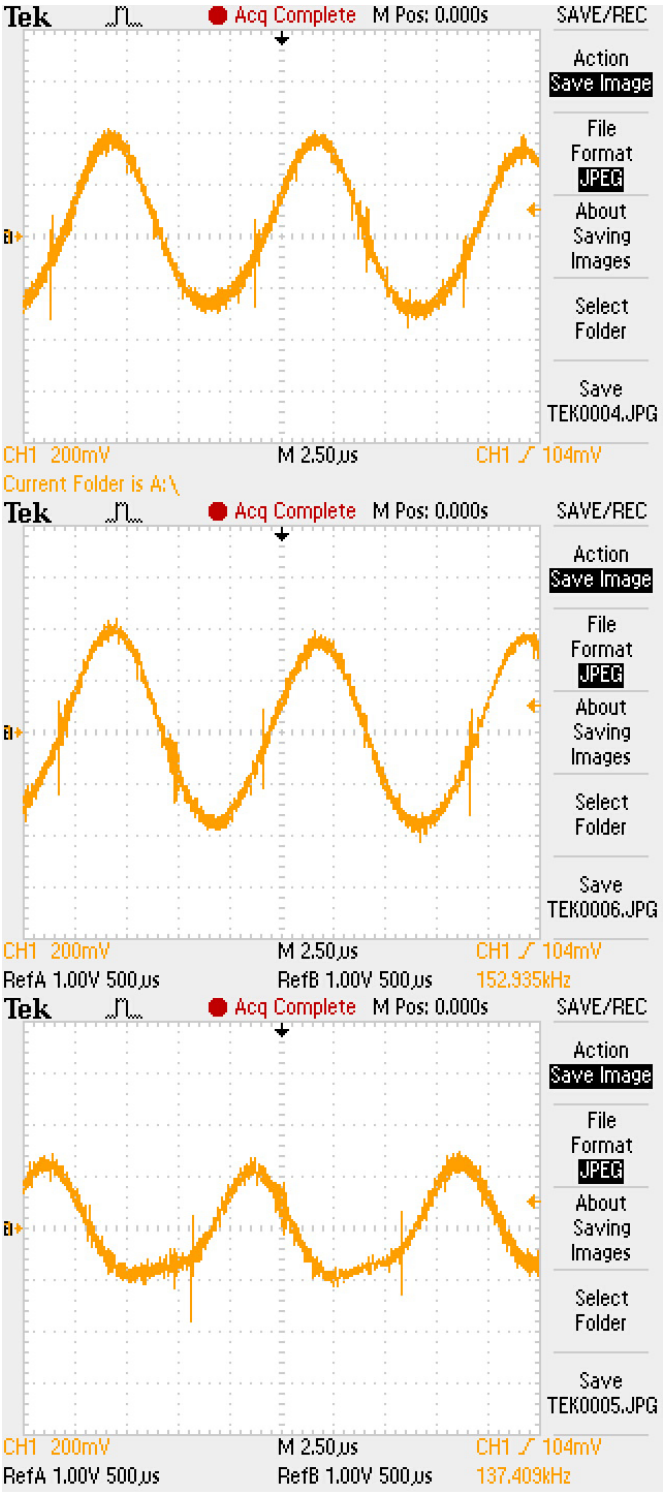

Figure 12: Experimental LD signal for measuring the phase difference on the PEM. (a) ≈ 40% below $\delta_0 = \pi$, (b) $\delta_0 = \pi$, and (c) ≈ 40% above $\delta_0 = \pi$.

3.2.2 Theoretical Setup

Due to the difficultly in determining δ_0, a new approach was taken. This technique uses the same setup only instead of observing the output signal, two intensity measurements are made by changing the angle of the analyzing linear polarizer; one parallel and one perpendicular to the polarizer before the PEM (in our case horizontally and vertically polarized). The Stokes parameters are represented as follows,

$$S_{Analyzer}(\theta_1,\delta) = M_{LP1}(\theta_1)M_{PEM}(\theta_P,\delta)M_H S \tag{3.2.6}$$

where δ is the phase difference of the PEM, θ_1 is the angle of the LP1, θ_p is the angle of rotation of the PEM. It is now possible to determine δ by changing θ_1 to measure the intensities of the Stokes parameters. The resulting Stokes parameters are

$$S_{Analyzer}(0^\circ,\delta) = M_{LP1}(0^\circ)M_{PEM}(45^\circ,\delta)M_H S \tag{3.2.7a}$$

$$S_{Analyzer}(90^\circ,\delta) = M_{LP1}(90^\circ)M_{PEM}(45^\circ,\delta)M_H S \tag{3.2.7b}$$

resulting in

$$S_{Analyzer}(0^\circ,\delta) = \frac{1}{4}(1+\cos(\delta))\begin{bmatrix} 1 \\ 1 \\ 0 \\ 0 \end{bmatrix} \tag{3.2.8a}$$

$$S_{Analyzer}(90^\circ,\delta) = \frac{1}{4}(1-\cos(\delta))\begin{bmatrix} 1 \\ -1 \\ 0 \\ 0 \end{bmatrix} \tag{3.2.8b}$$

with intensities of

$$I_{Analyzer}(0^{\circ},\delta)=\frac{1}{4}(1+\cos(\delta)) \tag{3.2.9a}$$

$$I_{Analyzer}(90^{\circ},\delta)=\frac{1}{4}(1-\cos(\delta)) \tag{3.2.9b}$$

Comparing the two intensities to determine δ gives,

$$\frac{I_{Analyzer}(0^{\circ},\delta)-I_{Analyzer}(90^{\circ},\delta)}{I_{Analyzer}(0^{\circ},\delta)+I_{Analyzer}(90^{\circ},\delta)}=\frac{\frac{1}{4}(1+\cos(\delta))-\frac{1}{4}(1+\cos(\delta))}{\frac{1}{4}(1+\cos(\delta))+\frac{1}{4}(1+\cos(\delta))}=\cos(\delta) \tag{3.2.10}.$$

In the case of CD spectroscopy, the PEM is oscillating, so a time average must be implemented. Assuming no static birefringence,

$$\delta[t]=\delta_0\sin(\omega_0 t) \tag{3.2.11}$$

where δ_0 is the phase difference and ω_0 is the angular frequency of the PEM, the time averaged phase difference for the two intensity measurements becomes,

$$I_{Analyzer}(0^{\circ},\delta_0)=\int_0^{t_0}\frac{1}{4}(1+\cos(\delta_0\sin(\omega_0 t)))dt \tag{3.2.12a}$$

$$I_{Analyzer}(90^{\circ},\delta_0)=\int_0^{t_0}\frac{1}{4}(1-\cos(\delta_0\sin(\omega_0 t)))dt \tag{3.2.12b}$$

results in

$$I_{Analyzer}(0^{\circ},\delta_0)=\frac{1}{4\omega_0}(1+J_0(\delta_0)) \tag{3.2.13a}$$

$$I_{Analyzer}(90^\circ,\delta_0)=\frac{1}{4\omega_0}(1-J_0(\delta_0)) \qquad (3.2.13b)^{26}.$$

Now applying (3.2.12a) and (3.2.12b) to (3.2.10), a time-averaged relationship for the phase-difference amplitude, δ_0, is obtained,

$$\frac{I_{Analyzer}(0^\circ,\delta_0)-I_{Analyzer}(90^\circ,\delta_0)}{I_{Analyzer}(0^\circ,\delta_0)+I_{Analyzer}(90^\circ,\delta_0)}=J_0(\delta_0) \qquad (3.2.14).$$

Now taking into account a static birefringence δ_s,

$$\delta[t]=\delta_0\sin(\omega_0 t)+\delta_s \qquad (3.2.15)$$

so that when reapplying the time average to (2.1.13), the intensity becomes

$$I_{Analyzer}(0^\circ,\delta_0)=\int_0^{t_0}\frac{1}{4}(1+\cos(\delta_0\sin(\omega_0 t)+\delta_s))dt \qquad (3.2.16a)$$

$$I_{Analyzer}(90^\circ,\delta_0)=\int_0^{t_0}\frac{1}{4}(1-\cos(\delta_0\sin(\omega_0 t)+\delta_s))dt \qquad (3.2.16b)$$

and (3.2.14) becomes

$$\frac{I_{Analyzer}(0^\circ,\delta_0,\delta_s)-I_{Analyzer}(90^\circ,\delta_0,\delta_s)}{I_{Analyzer}(0^\circ,\delta_0,\delta_s)+I_{Analyzer}(90^\circ,\delta_0,\delta_s)}=J_0(\delta_0)\cos(\delta_s) \qquad (3.2.17).$$

3.2.3 Experimental Setup

Intensities are measured using the HT of the PMT. The HT is then converted to gain[6]. For CD and LD spectroscopy, as the intensity decreases the gain of the PMT is increased to maintain the constant DC output, therefore,

$$I \propto \frac{1}{G} \tag{3.2.18}$$

and equation (2.2.14) becomes

$$\frac{G(90^{\circ},\delta_0,\delta_s)-G(0^{\circ},\delta_0,\delta_s)}{G(90^{\circ},\delta_0,\delta_s)+G(0^{\circ},\delta_0,\delta_s)} = J_0(\delta_0)\cos(\delta_s) \tag{3.2.19}$$

allowing for the time-averaged δ_0 and δ_s to be measured experimentally.

As observed[8], $\delta_s \neq 0$ for our PEM, therefore boundary conditions must be implemented in order to determine both δ_0 and δ_s. It is expected that when no voltage is applied to the PEM, $\delta_0 = 0$ and δ_s can be determined. This would mean the PEM would be turned off and light would still pass through the PEM to the detector. In our case, the PEM cannot be turned off without major changes to the manufactured instrument; therefore a different approach is used.

3.3 MEASURMENTS AND ANALYSIS OVERVIEW

3.3.1 Measurements for δ_s

In the case of our Jasco J810, the PEM cannot be prevented from oscillating (voltage is always applied to the PEM driver). Therefore δ_s is determined by an iterative approach. δ_s is measured by applying different voltages to the PEM and applying (3.2.19) to the intensity measurements. Using the boundary condition that when no voltage is applied to the PEM, $\delta_0 = 0$, δ_s can be determined by fitting (3.2.19) with a 99% confidence interval,[27] which is done by solving (3.2.19) for $J_0(\delta_0)$ and then changing (guess and check approach) δ_s until the amplitude on the fit is 1.

3.3.2 Analysis of δ_s

It is determined, through experimental measurement, that the static birefringence is neither constant nor linear in wavelength (Figure 14). Different parameters such as wavelength dependence and index of refraction (related to stress induced on the crystal) can complicate how the PEM operates. Index of refraction is related to the stress induced on the crystal used for modulating polarization states. The static birefringence can be defined in terms of the difference in index of refraction, which is related to the stress induced on the crystal,

$$\delta_s = \frac{2\pi d}{\lambda}\Delta n \rightarrow \frac{2\pi d}{\lambda}CS \qquad (3.3.1)^{28}$$

where d is the path length of the PEM, λ is the wavelength, S is the stress applied to the optical element by the piezoelectric transducer, C is the stress optical constant, and Δn is the difference in index of refraction parallel and perpendicular to the optical axis of the PEM[29]. Analysis of Δn is done because the function of Δn with respect to λ (see Figure 13) is not well understood. The process is described in (3.3.1) and is used to determine Δn, which is done by applying a stress to the crystal through the piezoelectric transducer, which changes Δn to create a phase difference. In the case for no stress (determining δ_s) zero volts are applied to the PEM and Δn is the static difference in index of refraction. It is observed that Δn (and stress applied to the crystal) has a linear-like relationship with wavelength (see Figure 13) implying that the coupling of the piezoelectric transducer and the crystal introduce a stress that is linear with respect to wavelength.

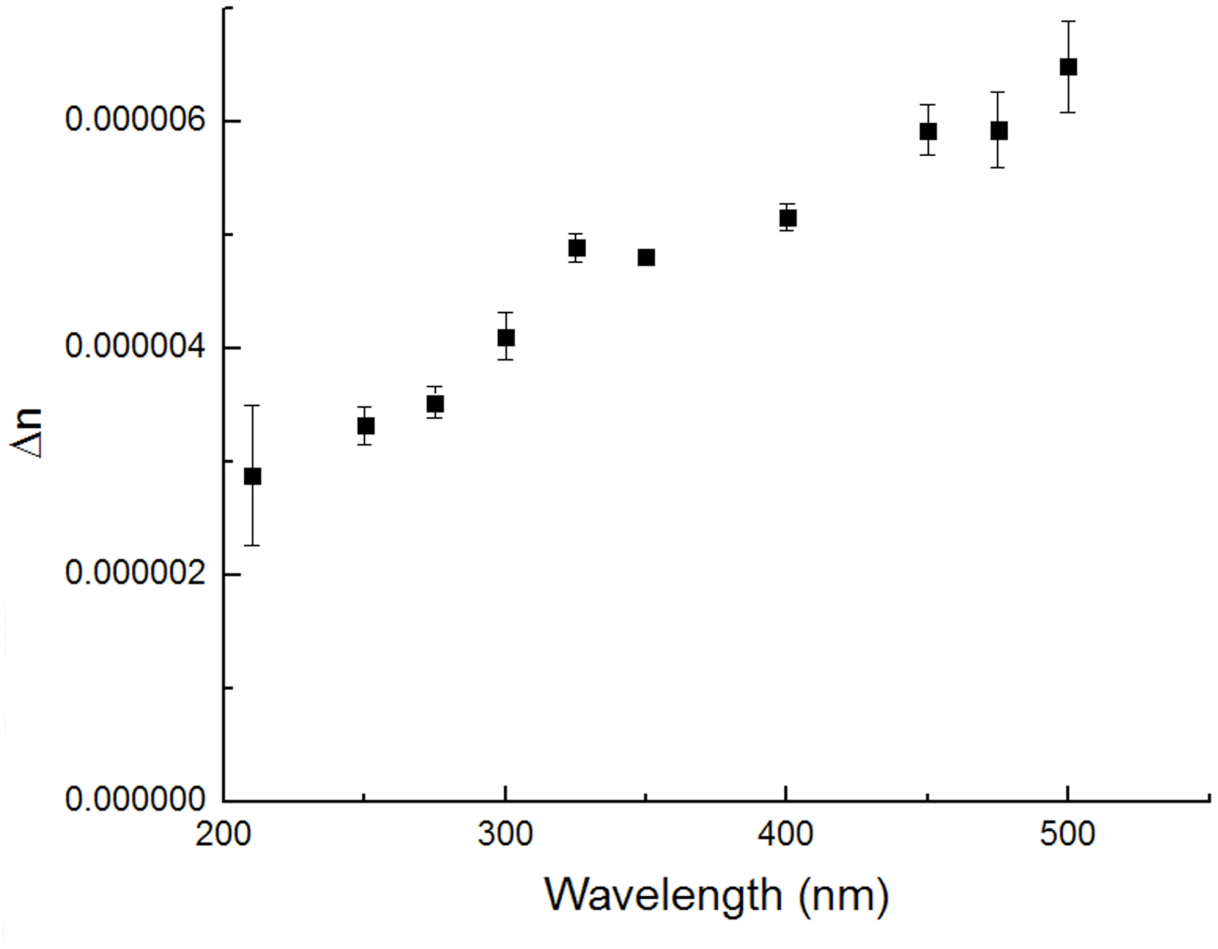

Figure 13: Difference in index of refraction vs. wavelength of the photoelastic modulator in the Jasco J810.

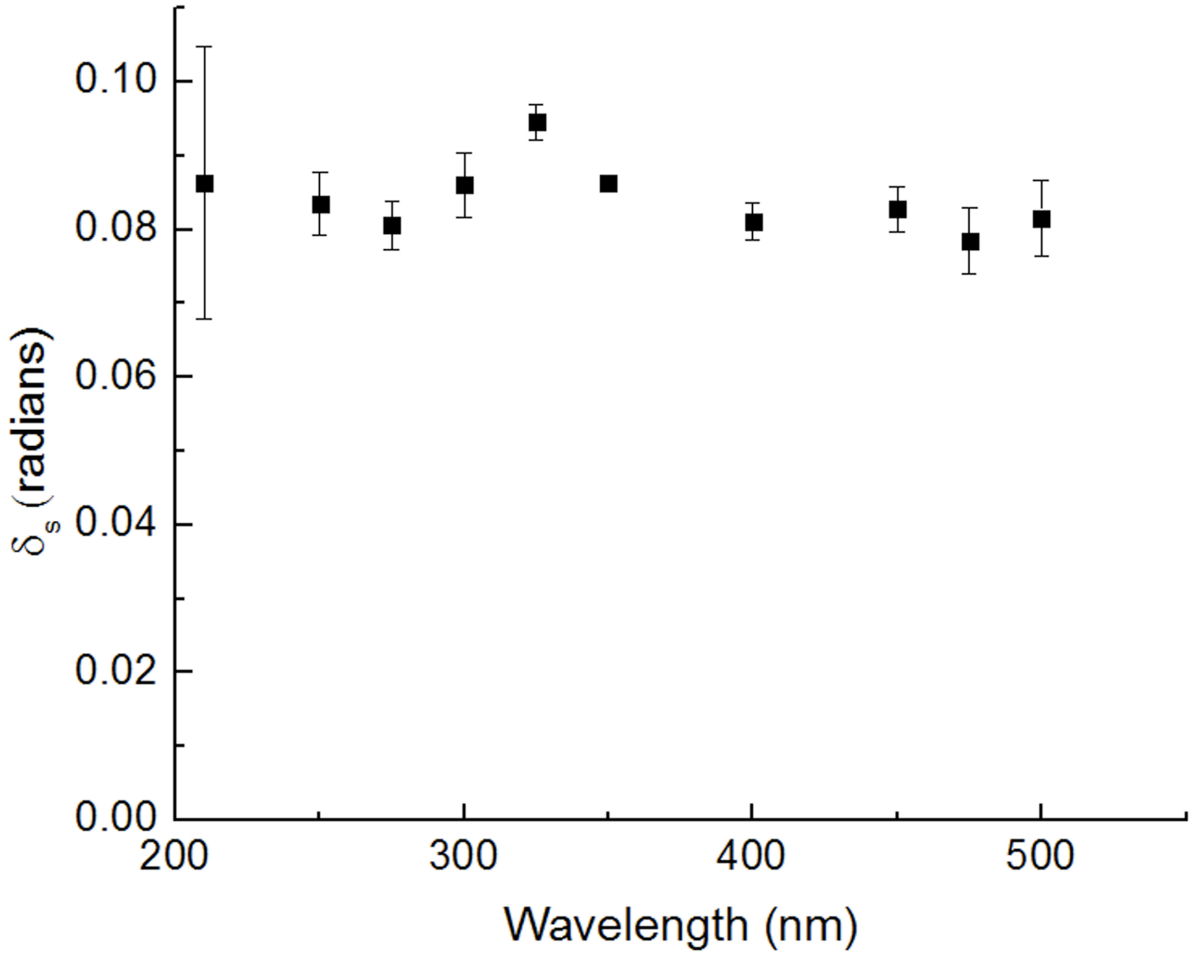

Figure 14: Measure of the static birefringence of the photoelastic modulator vs. wavelegnt in the Jasco J810 spectrometer.

Now that δ_s is determined, the voltages applied to the PEM to create a specific δ_0 are measured. The voltages are determined by implementing (3.2.19) and the measured δ_s. Figure 15 is the voltages for CD and LD measurements. For CD, the voltages matched between 350-400 nm and deviate from each other above and below these wavelengths. For LD, the voltages matched at around 500 nm but deviate as the wavelengths get shorter.

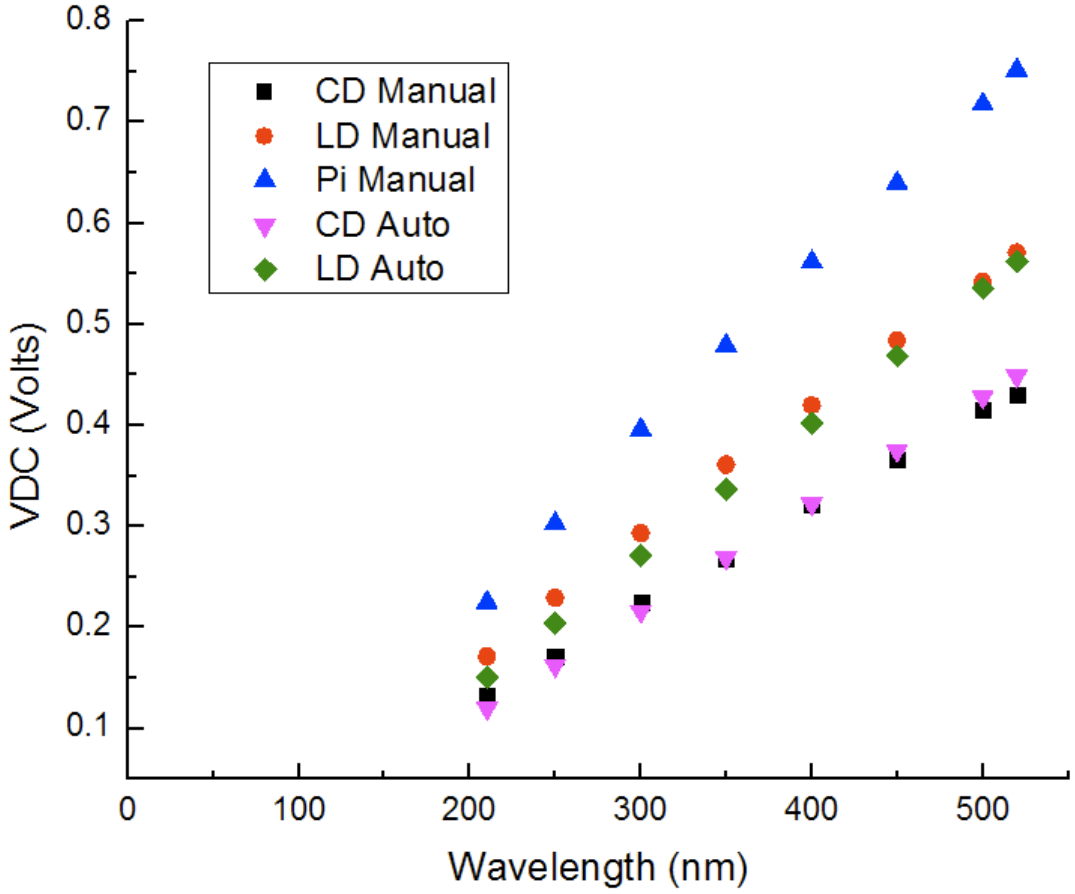

Figure 15: Voltages applied to the PEM for CD and LD auto (Jasco calibration) and CD and LD manual (lab determined) calibration.

3.4 CONCLUSIONS

Described in this chapter is a theoretical model and experimental technique used to measure the time-averaged static birefringence δ_s and the amplitude of the induced phase difference δ_0 for the PEM. Placing an analyzer down stream from the PEM, the model predicts the appropriate phase difference required to detect CD and LD signals. By rotating the analyzer, intensity measurements are made and then used to determine δ_0. The model is then implemented

to determine the corresponding voltage that must be applied to the wavelength-dependent PEM. This experimental technique is a more accurate way of determining δ_0 than traditional methods.

The same technique was used to measure δ_s by fitting collected data on δ_0 to (3.2.19). This was done for a broad wavelength spectrum (210-550 nm). A non-linear relationship between δ_s and wavelength was observed. It is possible that the non-linearity arises due to the non-linear index of refraction over wavelength[30].

A static birefringence presence was observed and will affect the definition of the measurement of CD and LD. Equations (3.5a) and (3.5b) will be used as the new model for measurements of CD and LD in the rest of this study. The choice of an appropriate δ_0 for CD and LD will be discussed in Chapter 4 by determining the Stokes parameters of the PEM.

CHAPTER 4: STOKES PARAMETERS OF THE PHOTOELASTIC MODULATOR

4.1 MEASURING STOKES PARAMETERS

Measuring the Stokes parameters, for the Jasco J810, is done by introducing an analyzer that contains a linear polarizer (LP) and an adjustable waveplate (WP) into the light path after the PEM (see Figure 16). The Stokes parameters will give information about the time averaged mixing of polarization states for CD and LD. By making Stokes parameter measurements, the voltage applied to the PEM can be adjusted to compensate for non-uniform mixing of polarization states.

4.1.1 Method for Measuring Stokes Parameters

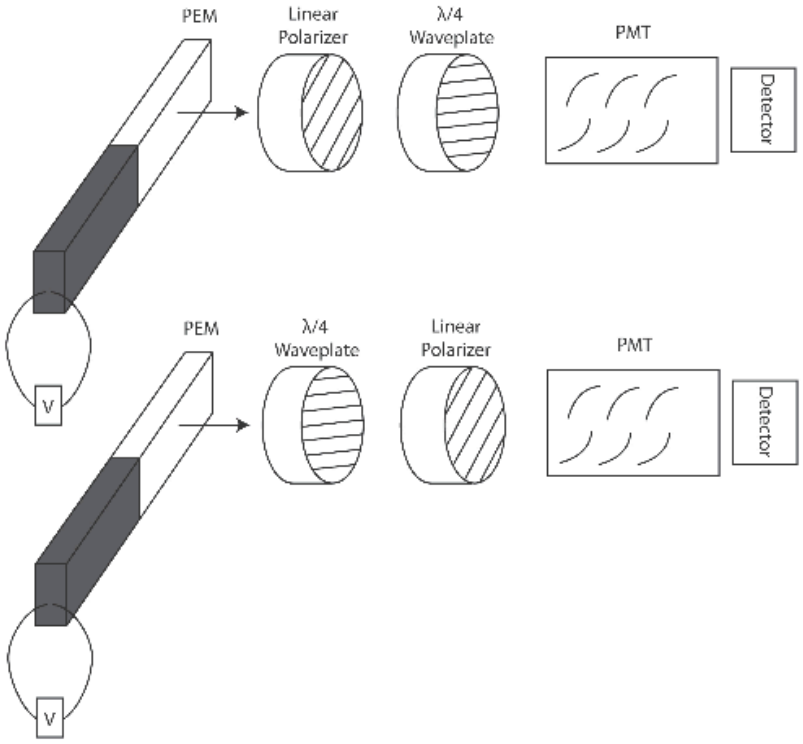

Figure 16: The experimental setup to measure the Stokes parameters of the PEM. The lines through the waveplate and linear polarizer indicate the transmission optical axes.

Beginning with the general case of a Stokes vector

$$S = \begin{bmatrix} S_0 \\ S_1 \\ S_2 \\ S_3 \end{bmatrix} \tag{4.1.1}$$

where S_0 corresponds to total intensity of the system, S_1 is the linear polarized component, S_2 is the $\pm\pi/4$ component, and S_3 is the circular polarized component of the total intensity. These parameters indicate what type of light is present. In order to create circular light from an incident source, first add a linear polarizer then a wave-plate downstream from the light source. The Muller matrices of the analyzer are as follows

$$M_{WP} = \begin{bmatrix} 1 & 0 & 0 & 0 \\ 0 & 1 & 0 & 0 \\ 0 & 0 & \cos(\psi) & \sin(\psi) \\ 0 & 0 & -\sin(\psi) & \cos(\psi) \end{bmatrix} \tag{4.1.2}$$

where ψ is the angle of retardation in the wave-plate and

$$M_{LP} = \frac{1}{2}\begin{bmatrix} 1 & \cos(2\varphi) & \sin(2\varphi) & 0 \\ \cos(2\varphi) & \cos^2(2\varphi) & \sin(2\varphi)\cos(2\varphi) & 0 \\ \sin(2\varphi) & \sin(2\varphi)\cos(2\varphi) & \sin^2(2\varphi) & 0 \\ 0 & 0 & 0 & 0 \end{bmatrix} \tag{4.1.3}$$

where φ is the angle of the polarizer's transmission axis with respect to the horizontal. Therefore the equation for the Stokes parameters becomes[31],

$$S_L(\varphi, \theta_{WP}, \psi) = M_{LP}(\varphi) M_{WP}(\theta_{WP}, \psi) S \tag{4.1.4}$$

and carrying out the matrix multiplication where, $\varphi = 0$, $\theta_{WP} = \pi/4$, and $\psi = \pi/2$ to give a quarter wave retardation, S_L reduces to

$$S_L = \frac{1}{2}(S_0 + S_3)\begin{bmatrix} 1 \\ 0 \\ 1 \\ 0 \end{bmatrix} \tag{4.1.5}$$

where S_L is the Stokes parameters of the output light that is linearly polarized at 45°. To produce horizontally or vertically polarized light, a simultaneous rotation of the linear polarizer and quarter waveplate combination by angle ϕ is done

$$S_L(\varphi,\phi,\psi) = M_{LP}(\varphi,\phi+45^\circ)M_{WP}(\phi,\psi)S \tag{4.1.6}$$

and becomes the output light produced by the rotated circular polarizer.

$$S_L(\phi) = \frac{1}{2}(S_0 + S_3)\begin{bmatrix} 1 \\ -\sin(2\phi) \\ \cos(2\phi) \\ 0 \end{bmatrix} \tag{4.1.7}$$

where ϕ is the angle of rotation of the analyzer. By setting $\phi = \pi/4$, (4.1.7) reduces to

$$S_L(\frac{\pi}{4}) = \frac{1}{2}(S_0 + S_3)\begin{bmatrix} 1 \\ -1 \\ 0 \\ 0 \end{bmatrix} \tag{4.1.8}$$

where the only contributing component is horizontal linearly-polarized light and the intensity is

$$I_L(\frac{\pi}{4}) = \frac{1}{2}(S_0 + S_3) \tag{4.1.9}$$

which is dependent on the circularly polarized component, S_3.

The next step is to create circularly polarized light. This is done by changing the order of the polarizer wave-plate combination.

$$S_C(\varphi,\phi,\psi) = M_{WP}(\phi,\psi)M_{LP}(\varphi,\phi+45^\circ)S \tag{4.1.10}$$

Now applying the same rotation as (4.1.7) to (4.1.10), the Stokes parameters become

$$S_C(\phi) = \frac{1}{2}(\sin(2\phi)S_1 + \cos(2\phi)S_2)\begin{bmatrix} 1 \\ 0 \\ 0 \\ 1 \end{bmatrix} \tag{4.1.11}$$

with intensity of

$$I_C(\phi) = \frac{1}{2}(\sin(2\phi)S_1 + \cos(2\phi)S_2) \tag{4.1.12}$$

Note that no matter how the circular polarizer in this configuration is rotated it will never change its polarization state (i.e. circular polarization), thus ϕ can be rotated to $\pi/4$ to accommodate for measuring the linear portion of the light.

Determination of the Stokes parameters individually is done by comparing the intensities for different rotations of the analyzer. Those include

$$S_C(0^\circ) = M_{WP}(0^\circ,90^\circ)M_{LP}(0^\circ,45^\circ)S \tag{4.1.13a}$$

$$S_C(45^\circ) = M_{WP}(45^\circ,90^\circ)M_{LP}(0^\circ,90^\circ)S \quad (4.1.13b)$$

$$S_C(90^\circ) = M_{WP}(90^\circ,90^\circ)M_{LP}(0^\circ,135^\circ)S \quad (4.1.13c)$$

$$S_L(0^\circ) = M_{LP}(0^\circ,45^\circ)M_{WP}(0^\circ,90^\circ)S \quad (4.1.13d)$$

with intensities,

$$I_C(0^\circ) = \frac{1}{2}(S_0 + S_2) \quad (4.1.14a)$$

$$I_C(45^\circ) = \frac{1}{2}(S_0 - S_1) \quad (4.1.14b)$$

$$I_C(90^\circ) = \frac{1}{2}(S_0 - S_2) \quad (4.1.14c)$$

$$I_L(0^\circ) = \frac{1}{2}(S_0 + S_3) \quad (4.1.14d)$$

solving for S_i,

$$S_0 = I_C(0^\circ) + I_C(90^\circ) \quad (4.1.15a)$$

$$S_1 = S_0 - 2I_C(45^\circ) \quad (4.1.15b)$$

$$S_2 = I_C(0^\circ) - I_C(90^\circ) \quad (4.1.15c)$$

$$S_3 = 2I_C(0^\circ) - S_0 \quad (4.1.15d).$$

Now applying the PEM to the situation, where

$$S = M_{PEM}(\theta_{PEM},\delta)S_H \quad (4.1.16)$$

where S_H is the Stokes parameters for horizontally polarized light. S now becomes

$$S = \begin{bmatrix} 1 \\ \cos(\delta[t]) \\ 0 \\ -\sin(\delta[t]) \end{bmatrix} \tag{4.1.17}$$

and applying it to (4.1.13a,b,c,d), the Stokes parameters become

$$S_0 = 1 \tag{4.1.18a}$$

$$S_1 = \cos(\delta[t]) \tag{4.1.18b}$$

$$S_2 = 0 \tag{4.1.18c}$$

$$S_3 = -\sin(\delta[t]) \tag{4.1.18d}$$

and the time averaged Stokes parameters are,

$$S_0 = 1 \tag{4.1.19a}$$

$$S_1 = J_0(\delta_0)\cos(\delta_s) \tag{4.1.19b}$$

$$S_2 = 0 \tag{4.1.19c}$$

$$S_3 = J_0(\delta_0)\sin(\delta_s) \tag{4.1.19d}.$$

4.1.2 Calibrating the Adjustable Waveplate

The waveplate is calibrated by placing two linear polarizers of cross linearity on either side of the waveplate. The incoming light is horizontally polarized and the linear polarizer is

placed after the WP, the phase of the WP can be determined for angles of 45°, -45°. The Muller matrix formula is as follows.

$$S_{WP}(\theta_1,\psi) = M_{LP}(\theta_1)M_{WP}(\theta_{WP},\psi)M_{PEM}(\theta_P,\delta)M_H S \tag{4.1.20}$$

with settings of

$$S_{WP}(0^\circ,\psi) = M_{LP}(0^\circ)M_{WP}(0^\circ,\psi)M_{PEM}(45^\circ,0^\circ)M_H S \tag{4.1.21a}$$

$$S_{WP}(90^\circ,\psi) = M_{LP}(90^\circ)M_{WP}(0^\circ,\psi)M_{PEM}(45^\circ,0^\circ)M_H S \tag{4.1.21b}$$

resulting in,

$$S_{WP}(0^\circ,\psi) = \frac{1}{2}(1+\cos(\psi))\begin{bmatrix} 1 \\ -1 \\ 0 \\ 0 \end{bmatrix} \tag{4.1.22a}$$

$$S_{WP}(90^\circ,\psi) = \frac{1}{2}(1-\cos(\psi))\begin{bmatrix} 1 \\ 1 \\ 0 \\ 0 \end{bmatrix} \tag{4.1.22b}$$

with intensities

$$I_{WP}(0^\circ,\psi) = \frac{1}{2}(1+\cos(\psi)) \tag{4.1.23a}$$

$$I_{WP}(90^\circ,\psi) = \frac{1}{2}(1-\cos(\psi)) \tag{4.1.23b}.$$

Note that this configuration is not dependent on the phase difference, δ, of the PEM. Thus, the phase difference ψ of the WP can be determined by comparing the two intensities.

$$\frac{I_{WP}(0^\circ,\psi)-I_{WP}(90^\circ,\psi)}{I_{WP}(0^\circ,\psi)+I_{WP}(90^\circ,\psi)}=\frac{\frac{1}{2}(1+\cos(\psi))-\frac{1}{2}(1-\cos(\psi))}{\frac{1}{2}(1+\cos(\psi))+\frac{1}{2}(1-\cos(\psi))}=\cos(\psi) \quad (4.1.24)$$

4.1.3 Calibrating the Adjustable Waveplate at Other Waveplate Angles

In order to calibrate the adjustable waveplate, an additional linear polarizer (LP) is needed. Below is the set up including this additional linear polarizer to make the above measurements at 0° and 90°. Note that it will also be used to determine Stokes parameters. A second linear polarizer is place in between the waveplate and PEM.

$$S_{WP}(\theta_2,\psi)=M_{LP2}(\theta_2)M_{WP}(\theta_{WP},\psi)M_{LP1}(\theta_1)M_{PEM}(\theta_P,\delta)M_H S \quad (4.1.25)$$

where θ_2 is the rotation able of the LP2, θ_{WP} is the rotation of the WP, ψ is the phase difference of the WP, θ_1 is the angle of the LP1, θ_p is the angle of rotation of the PEM and δ is the phase delay for the PEM. Looking at the case where the WP is set at 0°, calibration is done by setting the second LP at 45° and -45°.

$$S_{WP}(45^\circ,\psi)=M_{LP2}(45^\circ)M_{WP}(\theta_{WP},\psi)M_{LP1}(45^\circ)M_{PEM}(45^\circ,0)M_H S \quad (4.1.26a)$$

$$S_{WP}(-45^\circ,\psi)=M_{LP2}(-45^\circ)M_{WP}(\theta_{WP},\psi)M_{LP1}(45^\circ)M_{PEM}(45^\circ,0)M_H S \quad (4.1.26b)$$

resulting in

$$S_{WP}(45^\circ,\psi)=\frac{1}{4}(1+\cos(\psi)\begin{bmatrix}1\\0\\-1\\0\end{bmatrix} \quad (4.1.27a)$$

$$S_{WP}(-45^{\circ},\psi)=\frac{1}{4}(1-\cos(\psi)\begin{bmatrix}1\\0\\1\\0\end{bmatrix} \tag{4.1.27b}$$

with intensities of

$$I_{WP}(45^{\circ},\psi)=\frac{1}{4}(1+\cos(\psi)) \tag{4.1.28a}$$

$$I_{WP}(-45^{\circ},\psi)=\frac{1}{4}(1-\cos(\psi)) \tag{4.1.28b}$$

comparing the two intensities to determine ψ

$$\frac{I_{WP}(45^{\circ},\psi)-I_{WP}(-45^{\circ},\psi)}{I_{WP}(45^{\circ},\psi)+I_{WP}(-45^{\circ},\psi)}=\frac{\frac{1}{2}(1+\cos(\psi))-\frac{1}{2}(1-\cos(\psi))}{\frac{1}{2}(1+\cos(\psi))+\frac{1}{2}(1-\cos(\psi))}=\cos(\psi) \tag{4.1.29}.$$

Once calibrated, the second polarizer is removed and the Stokes parameters are measured at that WP setting.

$$S_C(\theta_1,\theta_2)=M_{WP}(\theta_{WP},\psi)M_{LP2}(\theta_2)M_{PEM}(\theta_P,\delta)M_H S \tag{4.1.30a}$$

$$S_L(\theta_1,\theta_2)=M_{LP1}(\theta_2)M_{WP}(\theta_{WP},\psi)M_{PEM}(\theta_P,\delta)M_H S \tag{4.1.30b}$$

The only difficulty that may arise is switching to measure $I_C(0°)$ where the other LP will be removed instead. Note that the LPs chosen for this experiment have been tested to have the same absorption in the CD machine. The measurements for intensities are as follows

$$I_C(0^{\circ})=\frac{1}{2}(S_0+S_2) \tag{4.1.31a}$$

$$I_C(90^\circ) = \frac{1}{2}(S_0 - S_2) \tag{4.1.31b}$$

$$I_C(45^\circ) = \frac{1}{2}(S_0 - S_1) \tag{4.1.31c}$$

$$I_L(0^\circ) = \frac{1}{2}(S_0 + S_3) \tag{4.1.31d}$$

and solved for the stokes parameters in terms of intensities

$$S_0 = I_C(0^\circ) + I_C(90^\circ) \tag{4.1.32a}$$

$$S_1 = S_0 - 2I_C(45^\circ) \tag{4.1.32b}$$

$$S_2 = I_C(0^\circ) - I_C(90^\circ) \tag{4.1.32c}$$

$$S_3 = 2I_L(90^\circ) - S_0 \tag{4.1.32d}.$$

4.2 ANALYSIS

The theoretical model to determine the Stokes parameters is applied to the spectrometer for CD and LD. The measurements of (4.1.31a,b,c,d) for wavelengths 520, 350, 300, 210 nm as shown in Figure 17 for CD and Figure 18 for LD. For both Figure 17 and Figure 18, S_1 is not constant over wavelength, but rather increases with decreasing wavelength. This may be due to factory calibration methods of the Jasco J810 where it is only calibrated at a two wavelengths.

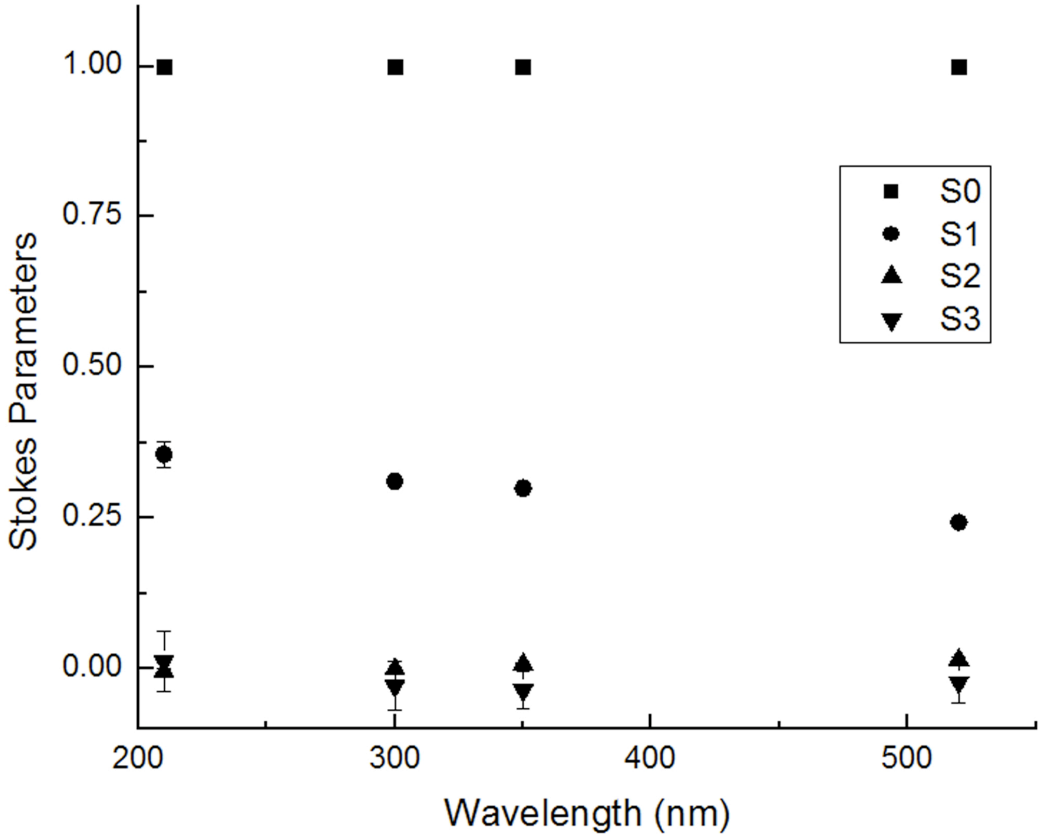

Figure 17: Stokes parameters measured on the Jasco J810 in auto (Jasco Calibration of the PEM) CD mode.

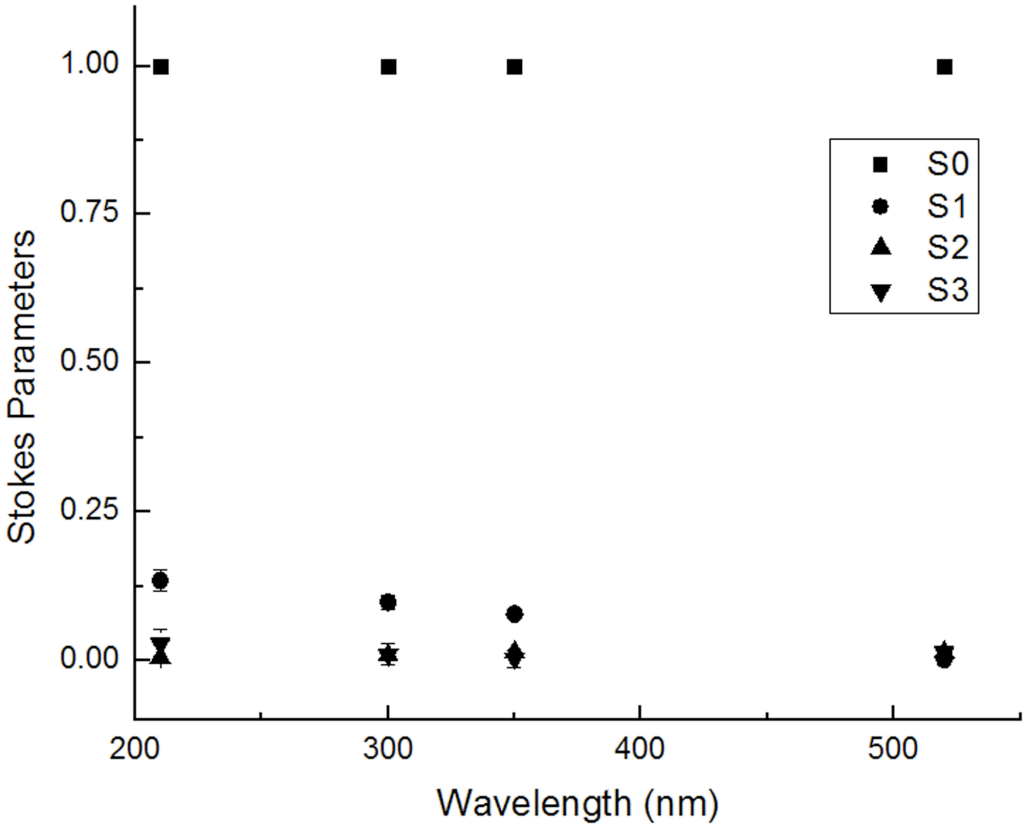

Figure 18: Stokes parameters measured on the Jasco J810 in auto (Jasco Calibration of the PEM) LD mode.

Using the method discussed in chapter 3, new settings for the PEM result in Figure 19 for CD and Figure 20 for LD. Observations in both CD and LD indicate a removal of the S_1 wavelength dependence.

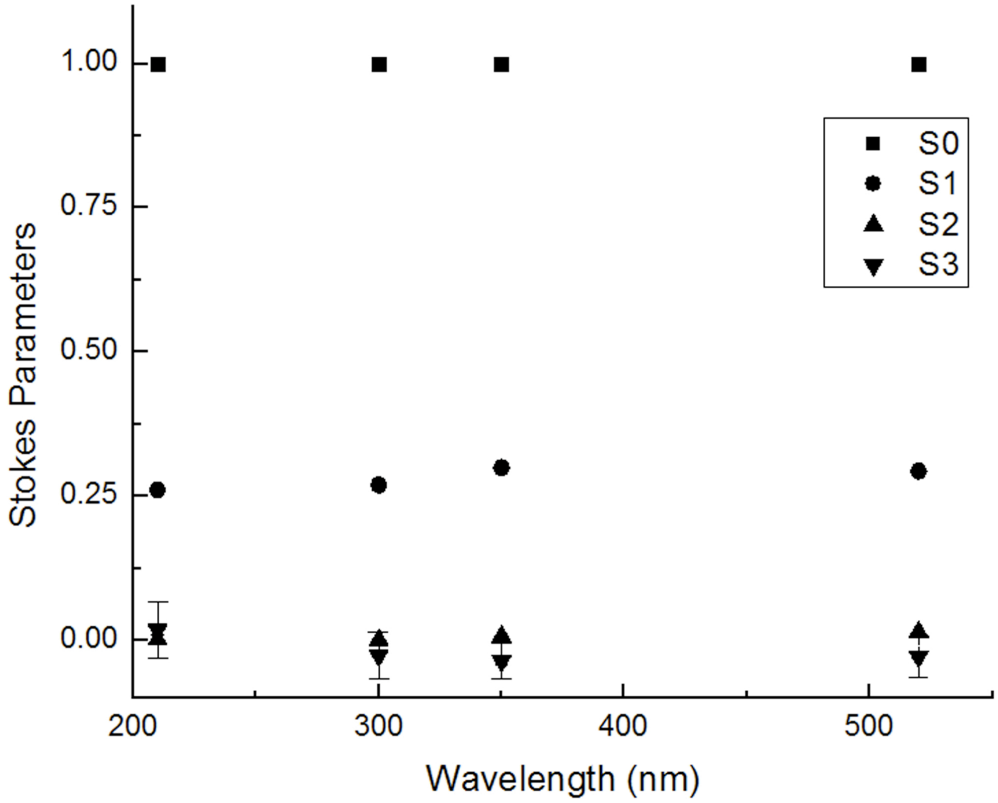

Figure 19: Stokes parameters measured on the Jasco J810 in manual (experimentally determined calibration of the PEM) CD mode.

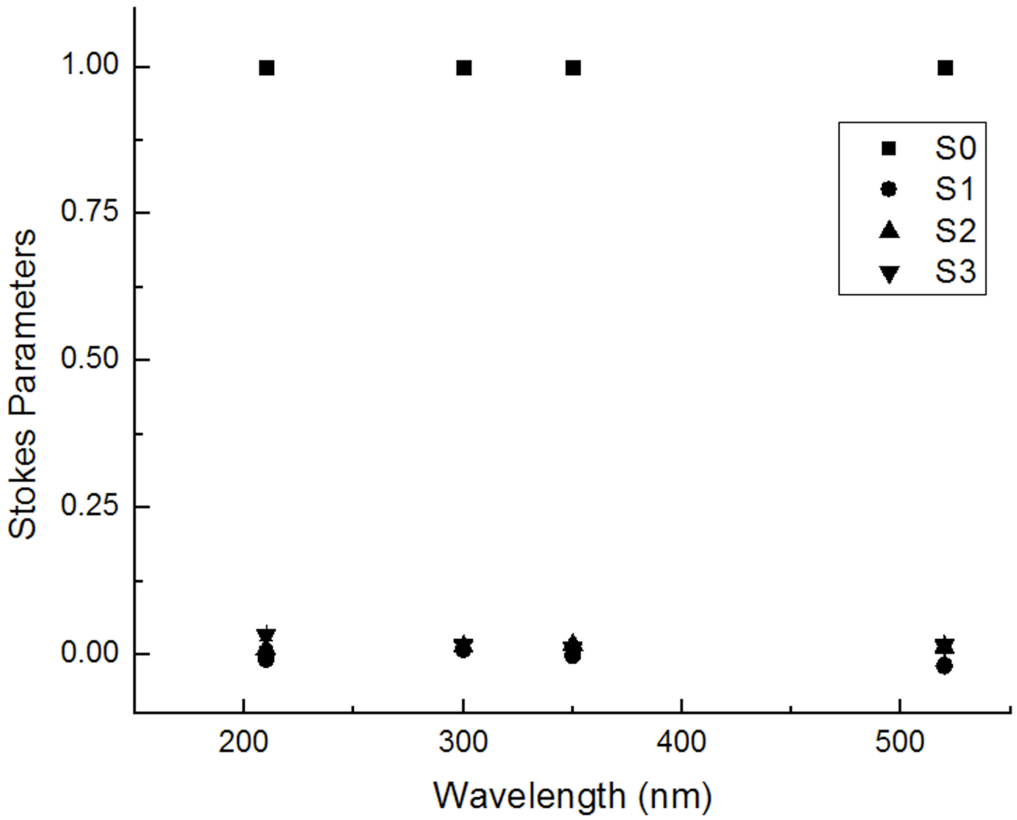

Figure 20: Stokes parameters measured on the Jasco J810 in manual (experimentally determined calibration of the PEM) LD mode.

In CD spectroscopy, S_1 is non-zero. This is due to the choice of δ_0, which follows (4.1.19b). The non-zero S_1 arises from the polarization states that are formed between the left and right circularly polarized states. In this case only horizontal linearly polarized light is formed with no vertical linearly polarized light to compensate for this effect. This is corrected for by applying $\delta_0 = 0.765\ \pi$ and shown in Figure 21 at 350 nm.

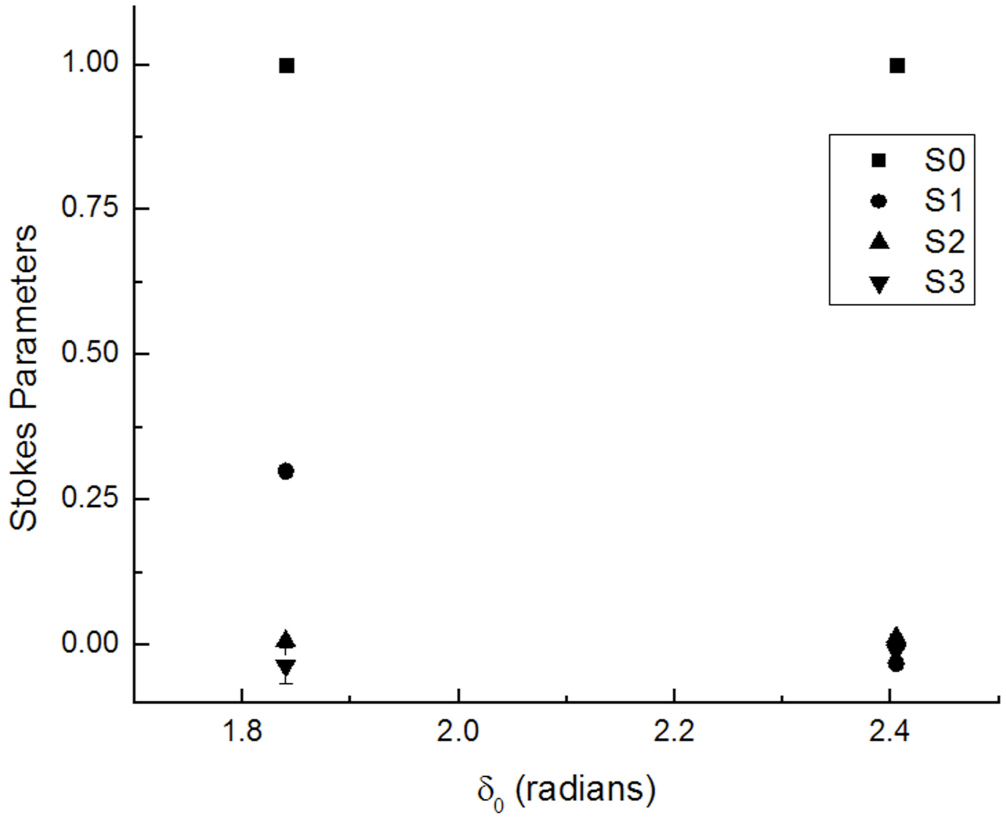

Figure 21: Measurement of Stokes parameters varying δ_0 from 1.84 to 2.405 in CD at 350 nm.

4.3 CONCLUSIONS

Discussed in this chapter is a technique to determine the Stokes parameters for a CD and LD spectrometer. The technique was modeled theoretically by implementing a rotatable circular polarizer containing a quarter waveplate and a linear polarizer then measured using the intensities via HT of the PMT. It was observed that by implementing this new technique to determine the phase difference resulted in constant Stokes parameters over wavelength.

In CD, S_1 was observed to be nonzero. The S_1 contribution can be removed by changing δ_0 to oscillate where $J_0(\delta_0) = 0$ (LD phase setting) with traditional tuning on the lock-in amplifier. Chapter 5 will discuss the fractional change in the intensity of the signals between traditional methods and methods discussed in this chapter.

CHAPTER 5: APPLICATION OF CAMPHORSULFONIC ACID AND CHRYSAZIN

The model for CD and LD was derived with the presence of δ_s in the PEM crystal (equations (3.5a) and (3.5b)). Camphorsulfonic Acid (CSA) and Chrysazin (in low density poly-ethylene (LDPE)) will be used to test this new model. In addition, the effects of the presence of static birefringence (δ_s) causing "cross-talking" or "leaking" into the signal will be tested. The effect of δ_s, in the model, was tested by adjusting δ_0 so that the detected CD and LD were observed to change by a theoretically predetermined fractional change.

5.1 THEORY

The CD and LD signal models associated with the measurements to be made are defined as,

$$\frac{\Delta I_{CD\omega_1}}{\bar{I}} = \frac{-\Delta a_{CD} J_1(\delta_0)\cos(\delta_s)}{1-\frac{\Delta a_{CD}}{2}\sin(\delta_s)J_0(\delta_0)} \tag{5.1a}$$

$$\frac{\Delta I_{CD\omega_2}}{\bar{I}} = \frac{-\Delta a_{CD} J_2(\delta_0)\sin(\delta_s)}{1-\frac{\Delta a_{CD}}{2}\sin(\delta_s)J_0(\delta_0)} \tag{5.1b}$$

where $\frac{\Delta I_{CD\omega_1}}{\bar{I}}$ is the CD signal and $\frac{\Delta I_{CD\omega_2}}{\bar{I}}$ is the LD signal when collecting data on a sample that only exhibits CD and

$$\frac{\Delta I_{LD\omega_1}}{\bar{I}} = \frac{\Delta a_{LD} J_1(\delta_0)\sin(\delta_s)}{1-\frac{\Delta a_{LD}}{2}\cos(\delta_s)J_0(\delta_0)} \tag{5.2a}$$

$$\frac{\Delta I_{LD\omega_2}}{\bar{I}} = \frac{-\Delta a_{LD} J_2(\delta_0)\cos(\delta_s)}{1-\frac{\Delta a_{LD}}{2}\cos(\delta_s)J_0(\delta_0)} \tag{5.2b}$$

where $\frac{\Delta I_{LD\omega_1}}{\bar{I}}$ is the CD signal and $\frac{\Delta I_{LD\omega_2}}{\bar{I}}$ is the LD signal when collecting data on a sample that only exhibits LD (see Appendix G for derivation of 5.1 and 5.2).

In this experiment, the phase difference δ_0 was changed. The appropriate phase difference is determined by a desired fractional change in the LD (or CD) intensity signal,

$$\left(\frac{\Delta I_{LD}}{\bar{I}}\right)_{new} = \left(\frac{\Delta I_{LD}}{\bar{I}}\right)_{old} - \mu\left(\frac{\Delta I_{LD}}{\bar{I}}\right)_{old} \tag{5.3}$$

where μ is fractional change of the signal and μ becomes,

$$\mu = 1 - \frac{\left(\frac{\Delta I_{LD}}{\bar{I}}\right)_{new}}{\left(\frac{\Delta I_{LD}}{\bar{I}}\right)_{old}} \tag{5.4}.$$

Substituting in (5.1b) and varying δ_0 for the new intensity signal holding the old intensity signal at and $\delta_0 = 2.405$, a fractional change is predicted by the model. It was found that for $\frac{\Delta I_{CD_{\omega_1}}}{\bar{I}}$, a 0.36 fractional change will occur when δ_0 is changed from 2.405 to 1.84. Likewise, $\frac{\Delta I_{CD_{\omega_2}}}{\bar{I}}$ will have a 0.1 fractional change when δ_0 is changed from 2.405 to 1.84. It is worth noting again that traditionally CD is run at $\delta_0 = 1.84$, but exhibits a horizontal contribution in the signal via Stokes parameter S_1. Changing the phase-difference amplitude between 1.84 and 2.405 will allow a measurement of the sensitivity effects between $\delta_0 = 1.84$ and $\delta_0 = 2.405$ for CD as previously

theorized[32]. Applying the same model to $\frac{\Delta I_{LD_{\omega_1}}}{\bar{I}}$, will have a 0.1 fractional change and $\frac{\Delta I_{LD_{\omega_2}}}{\bar{I}}$ will have a 0.3 fractional change. To test the model for CD and LD with δ_s present in the crystal, these fractional changes will be determined experimentally in this chapter.

5.2 CAMPHORSULFONIC ACID

Camphorsulfonic Acid (CSA) is a well characterized chiral molecule used as a standard in Circular Dichroism (CD)[33] (Figure 22). The CD spectrum of CSA has two peaks one around 290 nm and the other around 190 nm. CSA has been used to calibrate CD machines for years using these two peaks, because of its well-known secondary structure[34,35,36]. Therefore, it will be used as a standard to observe effects of phase difference δ_0 changes on the CD and LD spectrum.

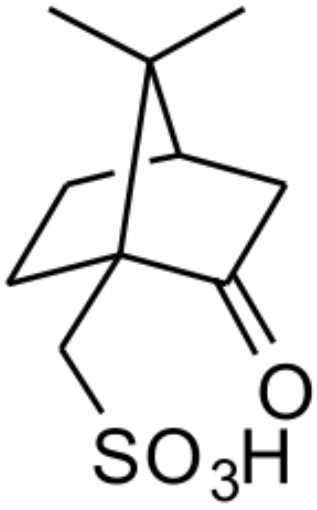

Figure 22: Molecular structure of Camphorsulfonic Acid.

5.2.1 Materials and Methods

A solution of 0.06% (weight per volume) of CSA (Camphorsulfonic Acid, Sigma-Aldrich 99%) was prepared in water and is placed in a 1 mm path length quartz cell. Its CD and LD were

recorded using a Jasco J810 CD spectrometer, which contains an external voltage application to the PEM (section 3.1). The external voltage application will allow the control of δ_0 to be set at δ_0 = 1.84 and δ_0 = 2.405 for CD and δ_0 = 1.9 and δ_0 = 2.405 for LD.

5.2.2 Analysis

Averaging 4 sets of data collected over 4 days, CD of CSA, at 290 nm peak (300-280 nm), has a 0.09(3) fractional change and LD of CSA, at 290 nm peak (300-280 nm), has a 0.22(14) fractional change. The fractional change for both CD and LD fall within one standard deviation of the predicted fractional change. In addition, observed in Figure 25 and Figure 26, is the presence of the CD leaking over into the LD (most apparent at 290 nm). It should be noted that the "leaking" of the LD signal is a small signal and has a lot of noise causing the experimental uncertainties to be quite large though still qualitative and quantitative. In CD, the small fractional change implies that changing the phase-difference amplitude on CD from its traditional setting of 1.84 to 2.405 confirms that it has little effect on the CD amplitude with the added benefit of removing the horizontal (non-CD) component in S_1.

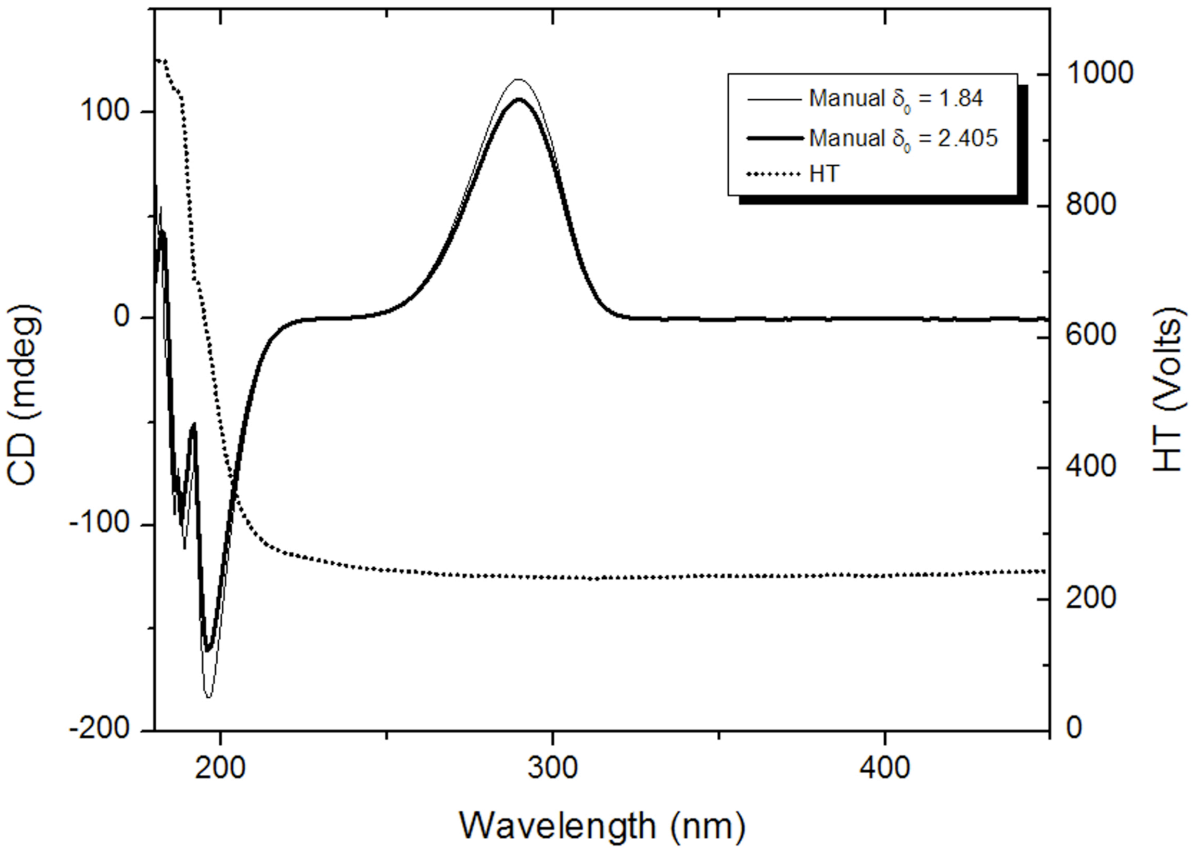

Figure 23: CD spectrum of Camphorsulfonic Acid changing the phase difference from $\delta_0 = 1.84$ to $\delta_0 = 2.405$.

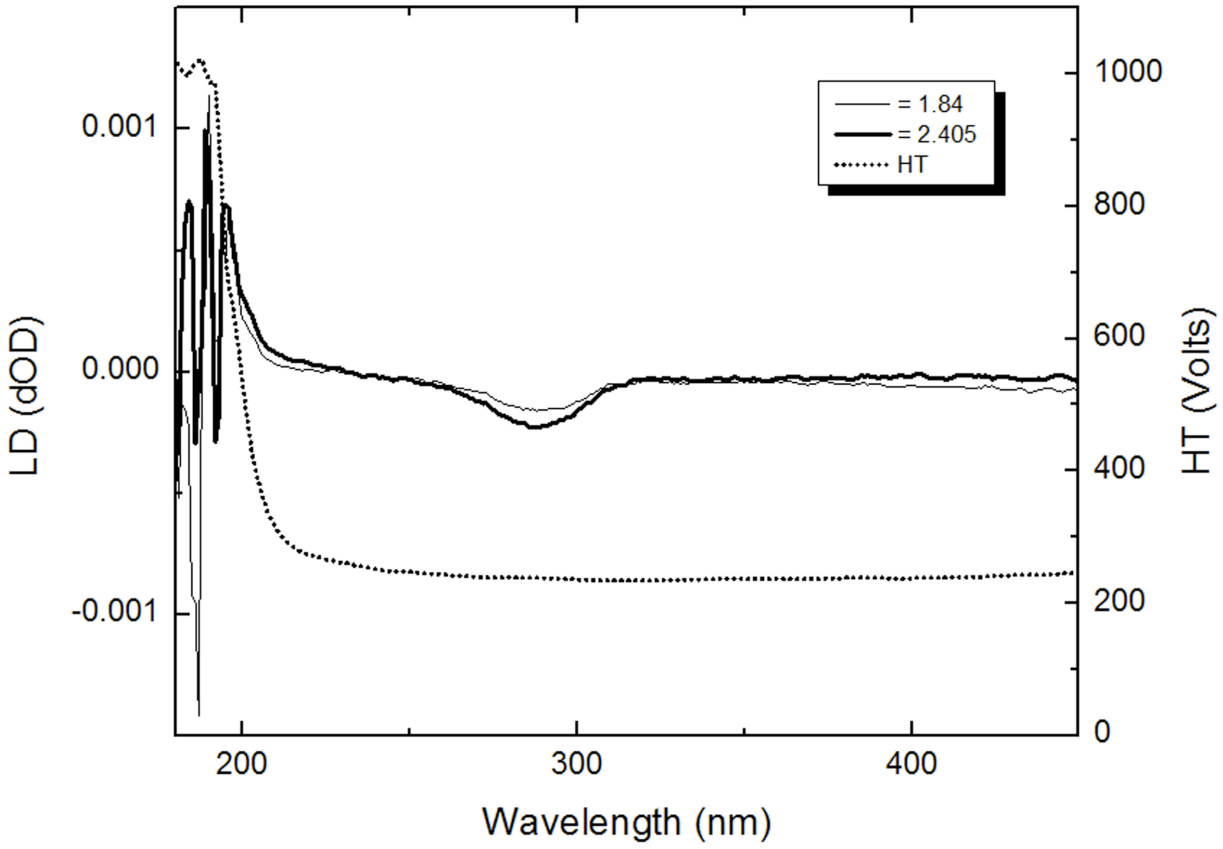

Figure 24: LD spectrum of Camphorsulfonic Acid changing the phase difference from $\delta_0 = 1.84$ to $\delta_0 = 2.405$.

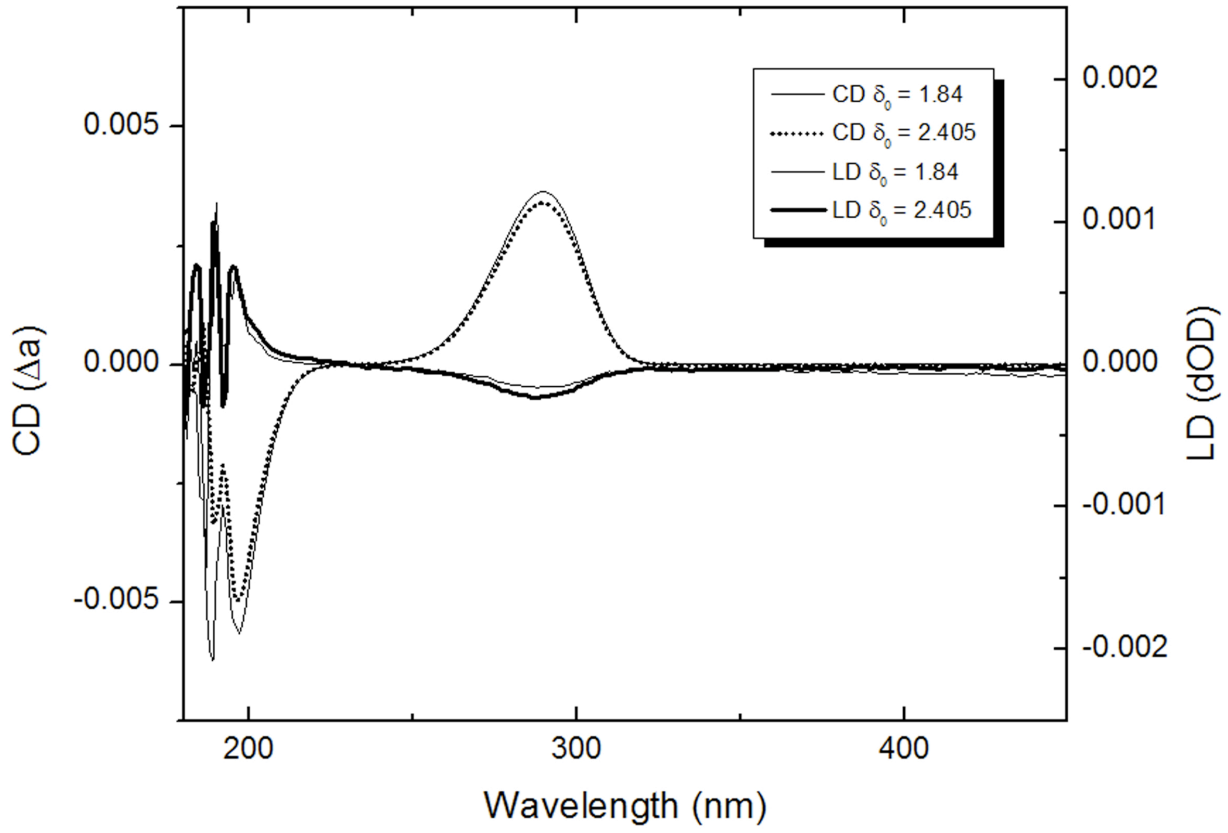

Figure 25: CD and LD of Camphorsulfonic Acid changing the phase difference from $\delta_0 = 1.84$ to $\delta_0 = 2.405$.

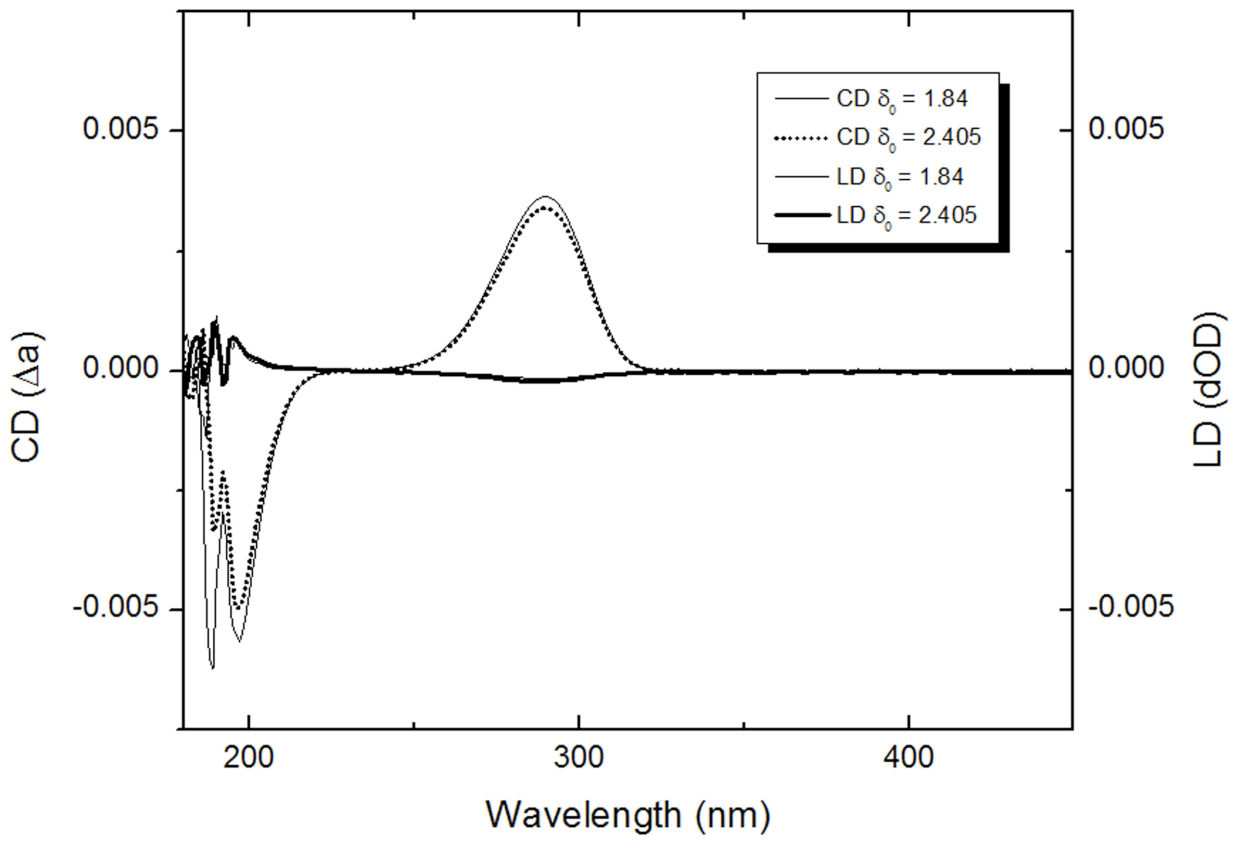

Figure 26: CD and LD of Camphorsulfonic Acid changing the phase difference from $\delta_0 = 1.84$ to $\delta_0 = 2.405$ with comparable units.

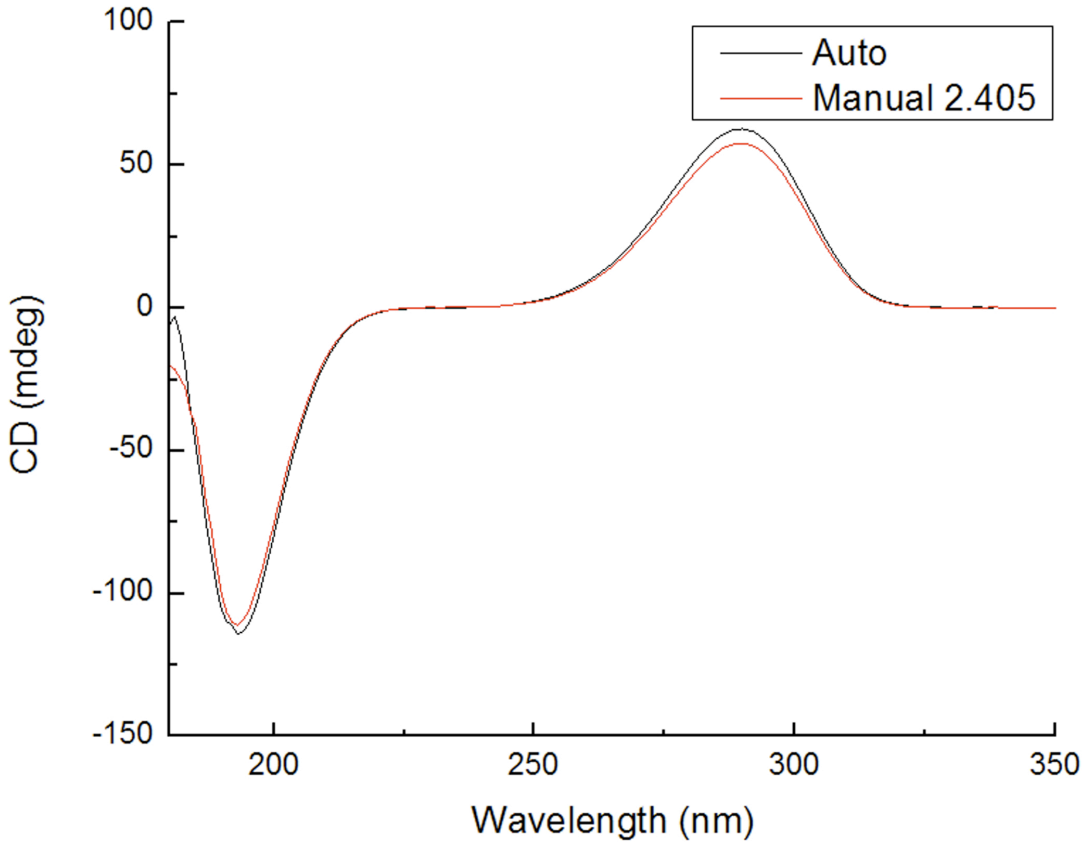

Figure 27: CD of Camphorsulfonic Acid changing the phase difference from Auto to Manual δ_0 = 2.405.

5.3 CHRYSAZIN

Chrysazin is an organic biomolecule that was chosen to analyze the detection of LD because it has no chirality (see Figure 28) and thus is not expected to exhibit CD. Chrysazin was recently analyzed and exhibited LD peaks at 444 nm, 250 nm, and 222 nm when imbedded in low-density polyethylene[37]. This section will repeat methods and experiments described in

reference 49 and analyze the fractional changes (observed when changing δ_0) in the signal at these peaks.

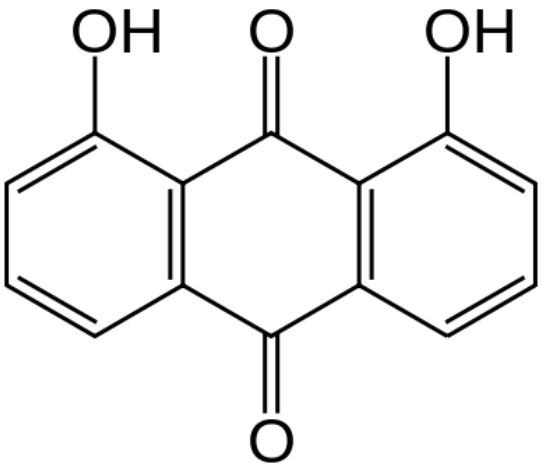

Figure 28: Chrysazin molecular structure.

5.3.1 Materials and Methods

Chrysazin (MP Biomedicals, Inc) was impregnated into low-density polyethylene (pure LDPE 100 μm thick sheet (Hinnum Plast, Vordingborg)) that was obtained from Spanget-Larsen lab in Denmark. This process was done by submerging strips of the LDPE in Chloroform (Acro Organics 99.8% for spectroscopy; stabilized with ethanol) at 50° C for 1 day to remove short residual LDPE that can induce false signals. The strips are then transferred to a Chrysazin saturated Chloroform solution at 50° C for 5 days. Once a day for 30 minutes the solution is sonicated to accelerate the process of impregnation in the LDPE[9,37].

The LDPE strips are then removed from the chloroform solution to allow the chloroform to evaporate and then cleaned with ethanol to remove residual crystallization on the surface of the LDPE. The LDPE is then placed in an in-house built stretcher that stretches the LDPE by

500% in the vertical direction[38,16]. The stretcher (containing the LDPE saturated with Chrysazin) is then placed in the Jasco J810 CD spectrometer and tested in for LD and CD.

5.3.2 Analysis

Chrysazin in LDPE spectra yield peaks at 441 nm, 249 nm, and 227 nm (see Figure 29). These peaks are similar to the work that was previously done and verify the spectrum of Chrysazin as reproducible. The fractional changes for LD in Chrysazin were 0.29(1) (at 441 nm peak (431 nm > λ > 451 nm)), 0.28(1) (at 249 nm peak (239 nm > λ > 259 nm)), and .29(2) (at 227 nm peak (217 nm > λ > 237 nm)). The fractional changes at each peak lie within the theoretical determined 0.3 fractional change. This indicates that the model for LD is correct.

The fractional changes for CD in Chrysazin (see Figure 30) were, 0.02(1) (at 441 nm peak (431 nm > λ > 451 nm)), 0.04(2) (at 249 nm peak (239 nm > λ > 259 nm)), and 0.04(3) (at 227 nm peak, (217 nm > λ > 237 nm)). All three peaks do not fall within one standard deviation of the predicted 0.1 fractional change. This may be due to the size of the signal (See Figure 31 and Figure 32) in comparison to the LD signal.

It was also observed that when comparing the Jasco calibrated PEM to the manual calibration, the spectra were similar in the longer wavelengths, but began to deviate as the wavelength changes. This is due to the difference between Jasco calibration and the manual calibration (See Figure 15 and Figure 33).

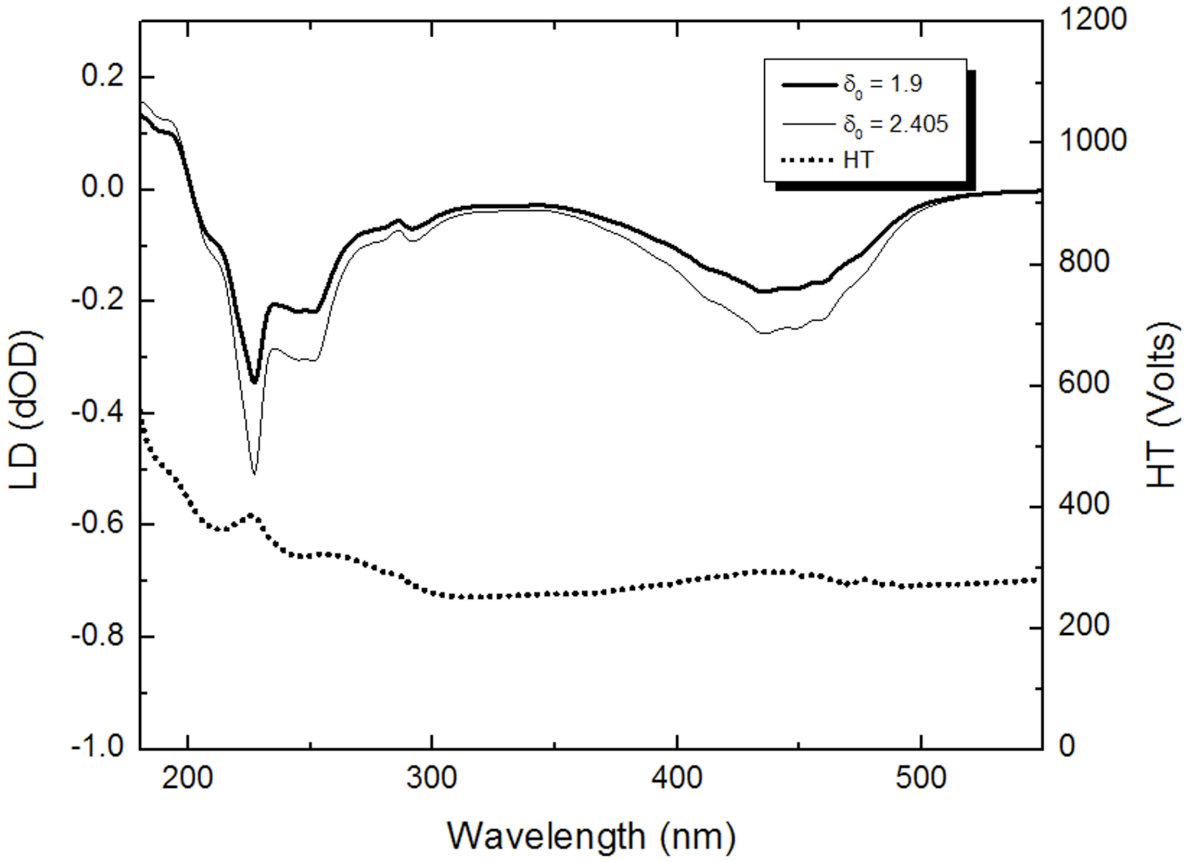

Figure 29: LD spectrum of Chrysazin changing the phase difference from $\delta_0 = 2.405$ to $\delta_0 = 1.9$.

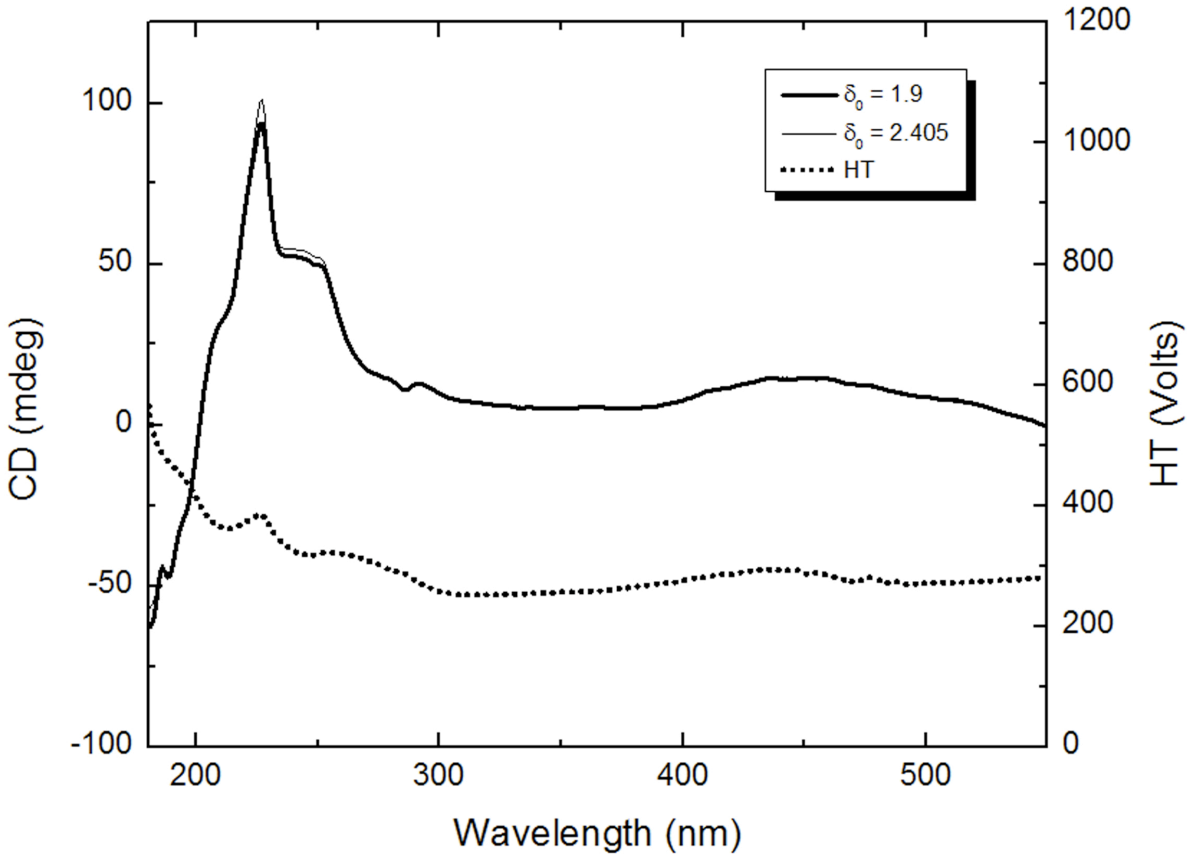

Figure 30: CD spectrum of Chrysazin changing the phase difference from $\delta_0 = 2.405$ to $\delta_0 = 1.9$.

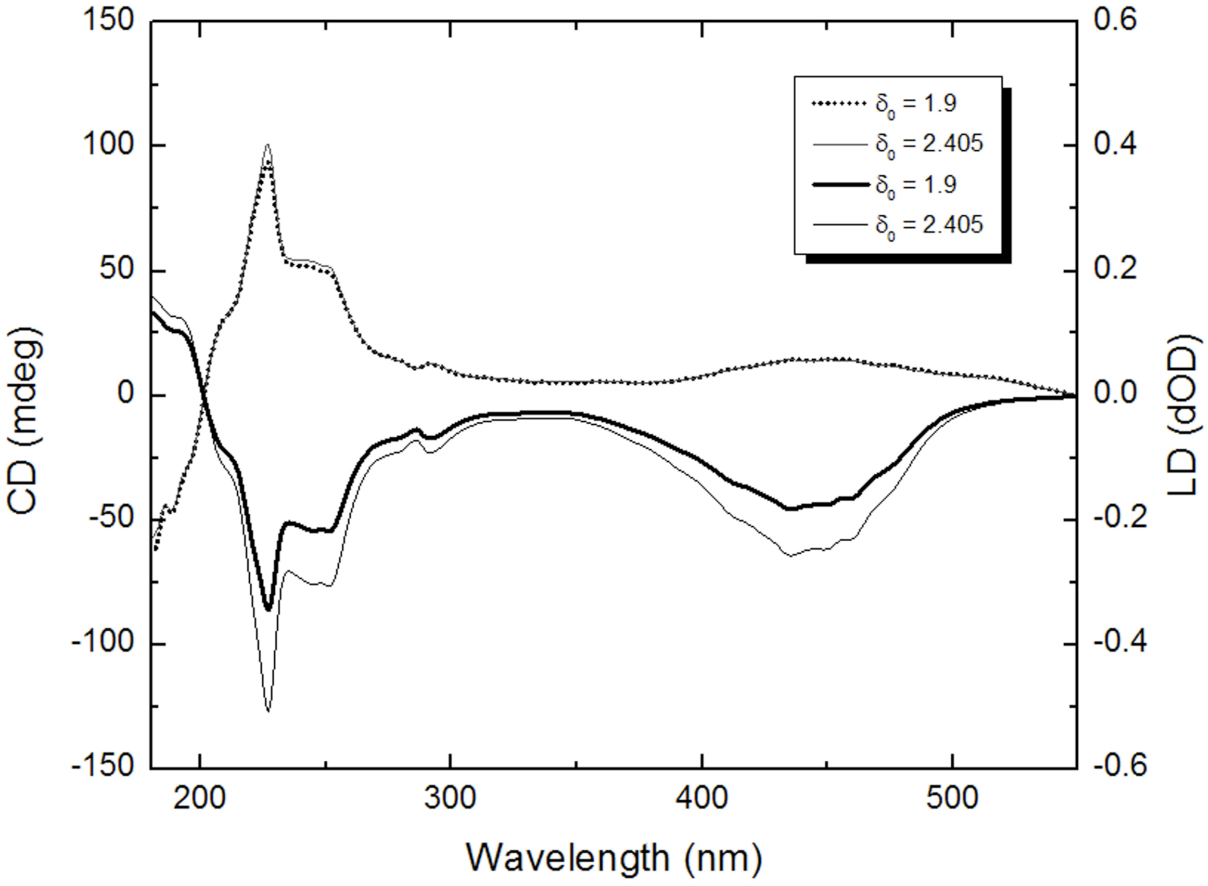

Figure 31: CD (in mdeg) and LD (in dOD) of Chrysazin changing the phase difference from δ_0 = 2.405 to δ_0 = 1.9.

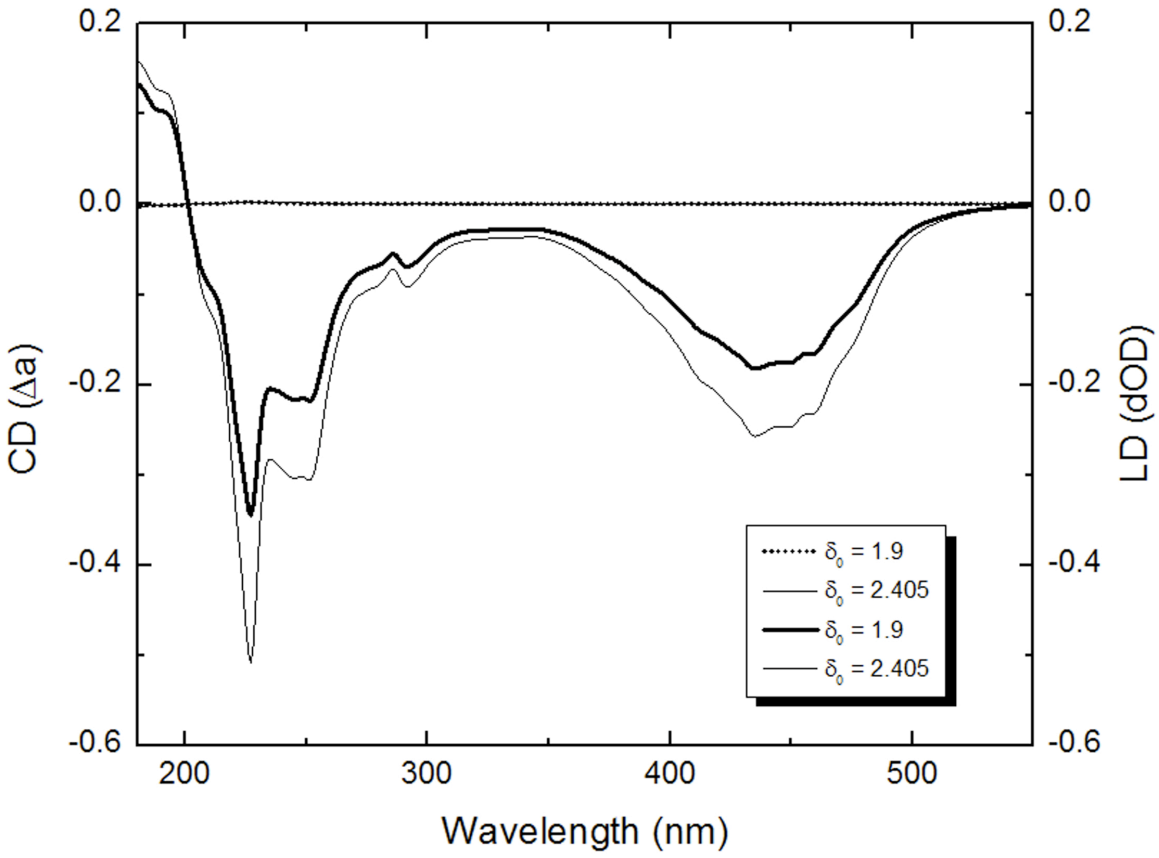

Figure 32: CD and LD of Chrysazin with, comparative units, changing the phase difference from $\delta_0 = 2.405$ to $\delta_0 = 1.9$.

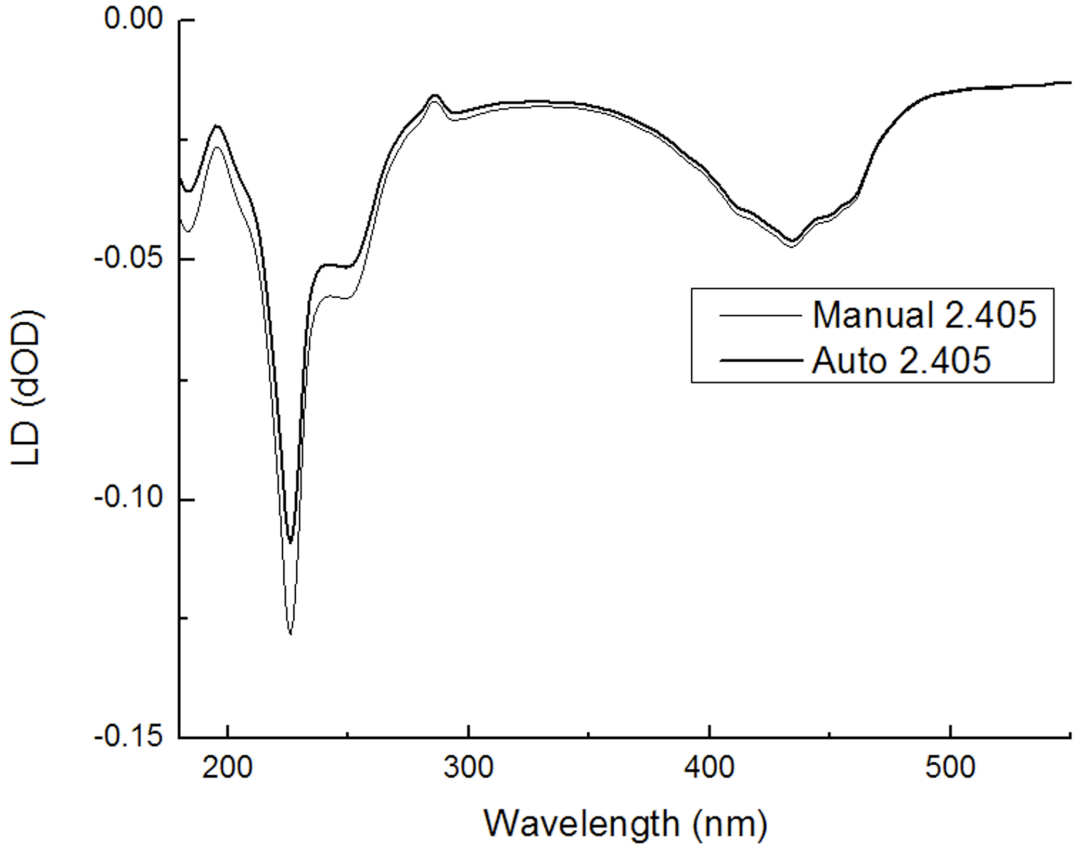

Figure 33: LD of Chrysazin for Auto and Manual where $\delta_0 = 2.405$.

5.3.3 Conclusion

This chapter discussed the measurements of CD and LD of CSA and chrysazin to test the new model of CD and LD signals in the presence of δ_s in the PEM crystal. CSA's well characterized structure and non-chiral structure of Chrysazin in LDPE made these two chemicals ideal to be used as standards for testing the model of the signal and presence of "leaking" of the signal from CD into LD and LD into CD. Applying a phase difference, δ_0, change to CD from

1.84 to 2.405, experimentally showed a .09(2) fractional change, at 290 nm, in the signal intensity of the CD signal of CSA. It is recommended for CD detection that the phase difference on the PEM be set to 2.405 rather than the traditional 1.84 because of the presence of static birefringence. The non-zero S_1 Stokes parameter can be removed to improve the fidelity of the CD signal without major effects to the spectrum, because the fractional change (sensitivity) is small. Changing the phase-difference amplitude may also have an effect on the ratio between the peaks and potentially improve the CSA ratio calibration.

Chrysazin in LDPE was verified to have the same three peaks (441, 249, and 229 nm) in LD[5] and the experimental fractional changes at each peak fell within one standard deviation of the predicted fractional change. The CD of Chrysazin indicated a leakage from the LD signal over into the CD signal. The fractional change at the same peaks was much less that the predicted fractional change of 0.1. This may be due to the size (and thus noise) of the signal leaking over, as CD signals are much weaker than LD signals.

CHAPTER 6: EPILOGUE

This dissertation addressed techniques and methods for characterizing the CD spectrometer. New hardware and software was developed and theoretical models were derived to determine and implement new measurement techniques. Discussed was the methodology for measuring shot noise, the phase-difference amplitude, δ_0, of the PEM and static birefringence, δ_s, of the PEM crystal. New hardware and software control for the voltage applied to the PEM was developed and the theory describing the CD and LD signal dependence on the phase-difference amplitude, δ_0, and static birefringence, δ_s, of the PEM crystal was extended. Lastly camphorsulfonic acid and chrysazin were used to verify the theoretical model developed for this research to describe the CD and LD signal. This work suggests how to improve the fidelity of CD and LD signals by applying a more accurate δ_0 calibration and a novel choice of δ_0 for CD.

The hypothesis that shot noise in CD spectroscopy is Poisson distributed was tested. Characterization of the PMT included measuring the signal to noise ratio, stray light and dark current, and data significance. Deviations from shot noise in the signal were apparently due to systematic error such as drift and mechanical issues with the slit alignment mainly observed when investigating the bandwidth and slit width. These deviations mainly appeared in the longer wavelength ranges (480-700 nm). Systematic errors may be cause for concern when determining the significance of the data in the longer wavelength ranges of CD studies and should be taken into consideration when collecting data above 480 nm. Even though response time and average number of scans SNR's follow Poisson distributions, it is important to remember time-dependent systematic errors still exist and time should be considered when choosing the number of scans to average over or how long a single data collection run takes so as to not have drift occur.

Noise in the photomultiplier tube caused by dark current or stray light was observed to be minimal above 300 nm (detector voltage below 600 volts). As the detector voltage (V_0) increases above 600 volts, stray light and dark current are no longer negligible and need to be considered. This is because as V_0 increases to saturation (V_0 > 900 volts) the output DC voltage on the detector can no longer maintain a constant voltage causing stray light and dark current to dominate. It is recommended that data collected with an associated V_0 above 600 volts be considered to be dominated by noise and should be weighted differently with respect to the rest of the spectrum because of the sensitivity to stray light and dark current above 600 volts.

A functional dependence for the significance of spectral data was determined by the relative SNR and V_0 (measure of gain). The measure of the gain on the photomultiplier tube allows for an experimentally determined relationship between gain and wavelength used to weight the significance of collected data (see Figure 4). These results should impact data analyses that involve integrating or combining data that have a variation in V_0.

The photoelastic modulator was characterized for phase-difference amplitude and static birefringence. The light intensity was modeled by placing a rotatable linear polarizer downstream from the photoelastic modulator using Stokes parameters and then implemented experimentally by measuring a time-averaged V_0. The phase-difference amplitude was used to determine the appropriate phase difference required to detect CD and LD signals (i.e. the appropriate voltage to be applied to the photoelastic modulator at a specific wavelength). This method was observed to be a more accurate and effective way to determine the phase difference than traditional methods and can be implemented for other CD spectrometers.

The static birefringence was determined to be nonlinear (presumably due to nonlinearity of index of refraction) with wavelength. This affected the measurements of the CD and LD by

causing “leaking” of one signal into the other and this was verified (chapter 5). The size of the “leaking” signal was very small in comparison to the proper signal (ratio of 1:100), but nonetheless observed. The “leaking” should not be ignored and its presence, as a spectral feature, should not be mistaken for a real signal when measuring a biomolecule that exhibits both CD and LD.

The measurement of Stokes parameters for the photoelastic modulator were developed by implementing a rotatable circular polarizer that contained a quarter waveplate and a linear polarizer and implemented into CD and LD spectroscopy for a precise calibration. Similar to how the phase-difference amplitude was determined, the time-averaged V_0 was measured for CD and LD. It was observed that for CD, S_1 was nonzero, but all other Stokes parameters for CD and LD were zero. It was also observed that when the PEM oscillated at the manufactured voltage settings, an increase in Stokes parameter S_1 (the linear horizontal component) occurred with a decreasing wavelength. By implementing this new technique, to determine the phase-difference amplitude, appropriate voltages to apply to the photoelastic modulator were determined and removed the effect.

The presence of the S_1 parameter in CD spectroscopy comes from the oscillation between the left and right circularly polarized light where there is a net horizontally polarized component. This can be removed by changing the phase difference from $\delta_0 = 1.84$ to $\delta_0 = 2.405$ (were the J_0 contribution is zero). This change was observed to have minimal effect with respect to the peak amplitude (a 0.09(3) fractional change on the peak signal intensity overall) of the CD signal itself (Chapter 5). It is recommended to set both CD and LD at $\delta_0 = 2.405$ using traditional methods on the lock-in amplifier; i.e. CD collected at resonant frequency f and LD collected at $2f$. This is a significant new development in CD and is verified in chapter 5 using CSA and Chrysazin.

A CD and LD standard were used to determine the new correction (verify the presence of static birefringence in the crystal) to the model of the signal. Camphorsulfonic Acid and Chrysazin were used to test changes made to the spectrometer. Camphorsulfonic Acid was used to test the model on the CD signal as it has a well-known structure and has been used to calibrate CD spectrometers in the past by observing the ratio between two peaks. It was observed to have a 0.09(3) fractional change for the CD signal and a 0.22(14) fractional change for the LD signal. This indicates that there is minimal sensitivity to the CD signal when changing the phase-difference amplitude from 1.84 to 2.405 and will remove the horizontal effects of the S_1 Stokes parameter on the CD signal. Leakage of the CD signal into the LD signal is also observed at the 290 nm peak.

Chrysazin in LDPE was used to test the LD signal fractional change effects. It was chosen because the structure is not chiral and thus should not exhibit CD. The fractional change of the LD fell within one standard deviation of the predicted fractional change, but the CD had fractional changes that fell within three to four standard deviations. This may be due to the size of the CD signal.

The research presented here provides useful information in determining the significance of spectral data collected for CD and LD spectroscopy. From observation and analysis of shot noise, it is recommended to set CD data collection with no more than 4 average number of scans, 50-200 nm/min scan speed, 1-4 sec response time, because of drift. One should take into consideration, that when choosing a bandwidth, what wavelength range data is being collected and the width of the expected peaks, because choosing a bandwidth too large will cause a peak to broaden and too small of a bandwidth can introduce systematic errors (bandwidth between 1-8 nm). When analyzing data collected with a HT above 600 V, noise becomes significant and data

should be weighted as a function of HT. For the photoelastic modulator, a new phase-difference amplitude ($\delta_0 = 2.405$) should be used for CD (same as what LD is run in). This will remove the horizontal component (in S_1) in the signal in CD with minimal change in sensitivity to the signal. It is also important to note that when determining the phase-difference amplitude of the PEM, that more than two points should be measured so as to increase the functional accuracy of the photoelastic modulator.

It has been experimentally determined that in the presence of static birefringence that cross contamination (between CD and LD) can occur. These results may eventually lead to a mitigation strategy which should improve the calibration of the instrument and the fidelity of the signal. Also, the methodology developed here, (to model the function of the detection of CD and LD spectroscopy) particularly and uniquely including the effect of static birefringence, will open up new methods and options in the determination of CD and LD spectra. This work is expected to have an impact on the data collection in the biomedical field for CD and LD spectroscopy.

REFERENCES

1. Pauling L, Corey RB, Branson HR. The Structure of proteins: Two Hydrogen Bonded Helical Conformations of the Polypeptide chain. Proc. National Academy of Science USA 1951;37: 205-211.
2. Yang JT. Remembrance of Things Past: A Career in Chiroptical Research. Fasman GD. Circular Dichroism and the Conformational Analysis of Biomolecules, 1st edition. New York: Plenum Press; 1996.
3. Selkoe DJ. Folding proteins in fatal ways. Nature 2003; 426: 900-904.
4. Greenfield NJ. Applications of circular dichroism in protein and peptide analysis. TrAC Trends in Analytical Chemistry 1999; 18: 236-244.
5. Castiglioni E, Albertini P, Abbate S. Evaluation of Instrumental Errors Built in Circular Dichroism Spectrometers. Chirality 2010; 22: E142-E148.
6. DiNitto JM, Kenney JM. Noise Characterization in Circular Dichroism Spectroscopy. Applied Spectroscopy 2012; 66: 180-187.
7. Oakberg TC, Trunk J, Sutherland JC. Calibration of Photoelastic Modulators in the Vacuum UV. Proc SPIE 2000; 4133: p. 258-262.
8. DiNitto JM, Kenney JM. Novel Technique for Improvement in Calibration of the Photoelastic Modulator in Circular and Linear Dichroism. Applied Spectroscopy; submitted March 2012.
9. DiNitto JM, Kenney JM. New model of CD and LD spectroscopy containing static birefringence applied to Camphorsulfonic Acid and Chrysazin. Applied Spectroscopy; In preparation.

10. Berg JM, Tymoczko JL, Stryer L. Biochemistry, 6th edition. New York: W.H. Freeman and Company; 2007.
11. Rodgers A, Norden B. Circular Dichroism and Linear Dichroism, 1st edition. New York: Oxford University Press; 1997.
12. Sutherland JC. Measurement of Circular Dichroism and Related Spectroscopes with Conventional and Synchrotron light Sources: Theory and Instrumentation. Wallace BA, Janes RW. Modern Techniques for Circular Dichroism and Synchrotron Radiation Circular Dichroism. Netherlands: IOS Press 2009.
13. Crabbe' P. ORD and CD in Chemistry and Biochemistry: An Introduction : Academic Press; 1972. p. 8.
14. Djerassi C. Optical Rotatory Dispersion. Ann Arbor, Michigan: A Xerox Company; 1960. p. 31-32.
15. Pollock JB, Cutler PJ, Kenney JM, Gemperline PJ, Burns CS. Characterization of Cu^{2+}-binding modes in the prion protein by visible circular dichroism and multivariate curve resolution. Analytical Biochemistry 2008; 377: 223-233.
16. Norden B, Rodger A, Dafforn T. Linear Dichroism and Circular Dichroism: A Textbook on Polarized-Light Spectroscopy, 1st edition. Cambridge, UK: The Royal Society of Chemistry; 2010.
17. Model J-810 Spectropolarimeter Hardware/Function Manual. Jasco Corporation 1999.
18. Cheng JC, Nafie LA, Allen SD, Braunstein AI. Photoelastic modulator for the 0.55-13 um range. Applied Optics 1976; 15: 1960-1965.
19. Watson GN. A Treatise on the Theory of Bessel Functions, 2nd edition. New York: Cambridge University Press; 1966.

20. Shindo Y, Ohmi Y. 3. Critical Comments on Liquid Crystal Induced Circular Dichroism. American Chemical Society 1985; 107: 91-97.
21. Davidsson A, Norden B. On the problem of obtaining accurate circular dichroism. Calibration of circular dichroism spectrometers. Spectrochimica Acta 1976; 32A: 717-722.
22. Chao YF, Lin PL. Artifactual Circular Dichroism Effect in a Photoelastic Modulator. Optical Com. 2010; 283: 4582-4585.
23. Becker W. Advanced time-correlated single photon counting techniques, 1st edition. New York: Springer; 2005.
24. Sutherland JC. Measurement of the Circular Dichroism of Electronic Transitions, 1st edition. In Press.
25. Wallace BA, Janes RW. Modern Techniques for Circular Dichroism and Synchrotron Radiation Circular Dichroism Spectroscopy: Volume 1 Advances in Biomedical Spectroscopy, 1st edition. Amsterdam: IOS Press; 2009.
26. Dunlap D, Samori B, Bustamante C. Why Does Sinusoidally Modulated Polarization Introduce a Systematic Error in Linear Dichroism Measurements? Analytical and Instrumental Solutions, Samori B, Thulstrup EW. Polarized Spectroscopy of Ordered Systems. Massachusetts: Kluwer Academic Publishers. 1988.
27. Lefebvre M. Applied Probability and Statistics, 1st edition. New York: Springer; 2006.
28. Kemp JC. Piezo-Optical Birefringence Modulators: New Use for a Long-Known Effect. JOSA 1969; 59: 950-954.
29. Ghosh G. Dispersion-equation coefficients for the refractive index and birefringence of calcite and quartz crystals. Opt. Com. 1999; 163: 95-102.

30. Malitson IH, Interspecimen Comparison of the Refractive Index of Fused Silica. Journal of Optical Society of America 1965; 55: 1205-1208.
31. Collett, E. Polarized Light: Fundamentals and Applications, 1st Edition. New York: Marcel Dekker, Inc. 1993.
32. Hipps KW, Crosby GA. Applications of the Photoelastic Modulator to Polarization Spectroscopy. J. Phys. Chem. 1979; 83: 555-562.
33. Johnson Jr. WC. Protein Secondary Structure and Circular Dichroism: A Practical Guide Proteins: Structure, Function, and Genetics 1990; 7: 205-214.
34. Chen GC, Yang JT. Two-Point Calibration of Circular Dichroism with d-10-Camphorsulfonic Acid. Analytical Letters 1977; 10: 1195-1207.
35. Gillen MF, Williams RE. The Use of the n-Propylammonium and n-Butylammonium Salts of d-10-Camphorsulfonic Acid for the Calibration of Spectropolarimeters: Circular Dichrometer Calibration. Canadian Journal of Chemistry 1975; 53: 2351-2352.
36. Schippers PH, Dekkers HPJM. Direct Determination of Absolute Circular Dichroism Data and Calibration of Commercial Instruments. American Chemical Society 1981; 53: 778-782.
37. Nguyen DD, Jones NC, Hoffmann SV, Spanget-Larsen J. Synchrotron radiation linear dichroism (SRLD) investigation of the electronic transitions of quinizarin, chrysazin, and anthrarufin. Spectrochimica Acta Part A 2010; 77: 279-286
38. Nguyen DD. Synchrotron radiation linear dichroism (SRLD) investigations of the electronic transitions of samples aligned in stretched low-density polyethylene. PhD dissertation; Roskilde University Denmark, 2010.

APPENDIX A: CHAPTER 2 SUPPLIMENTAL DATA

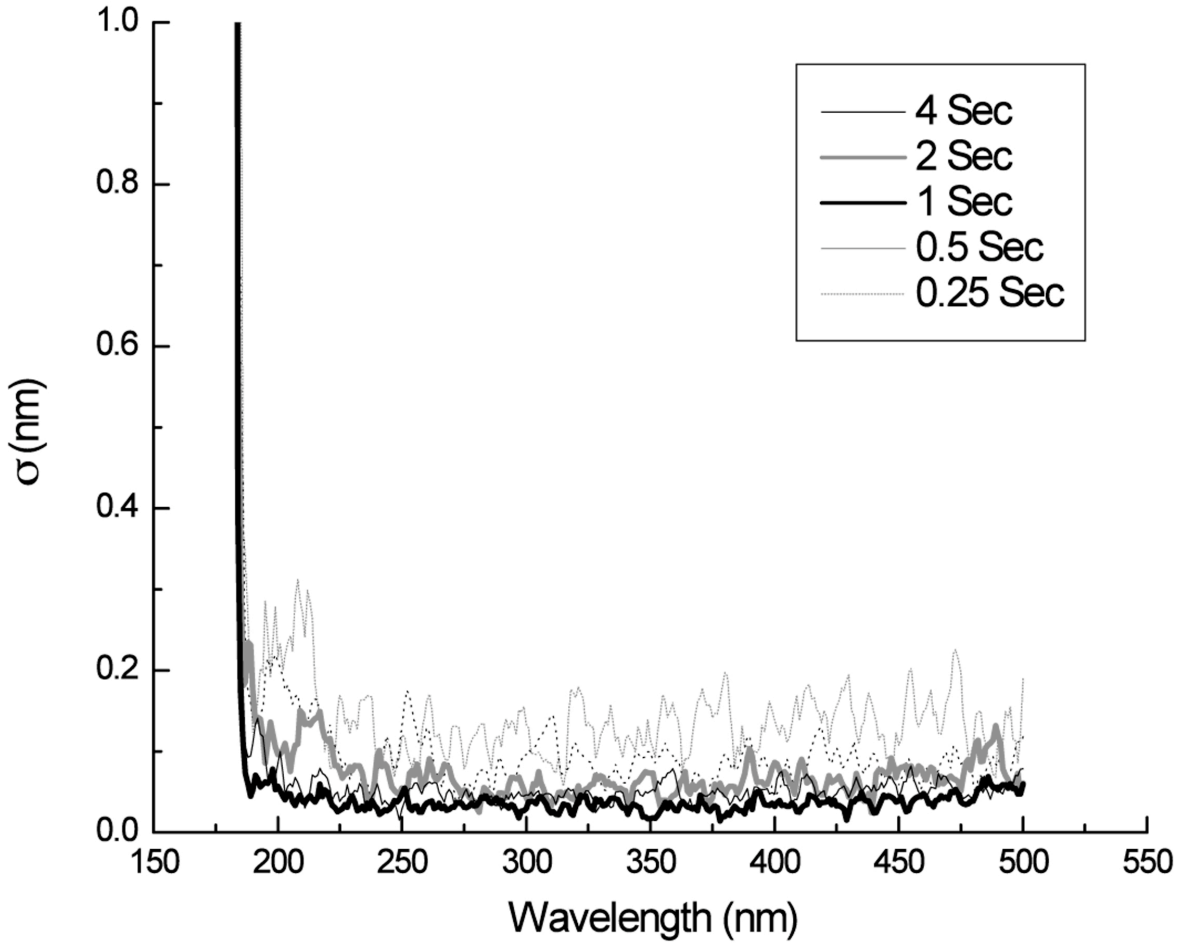

Figure 34: σ vs. wavelength for response time for max settings of scan speed from 180-500 nm.

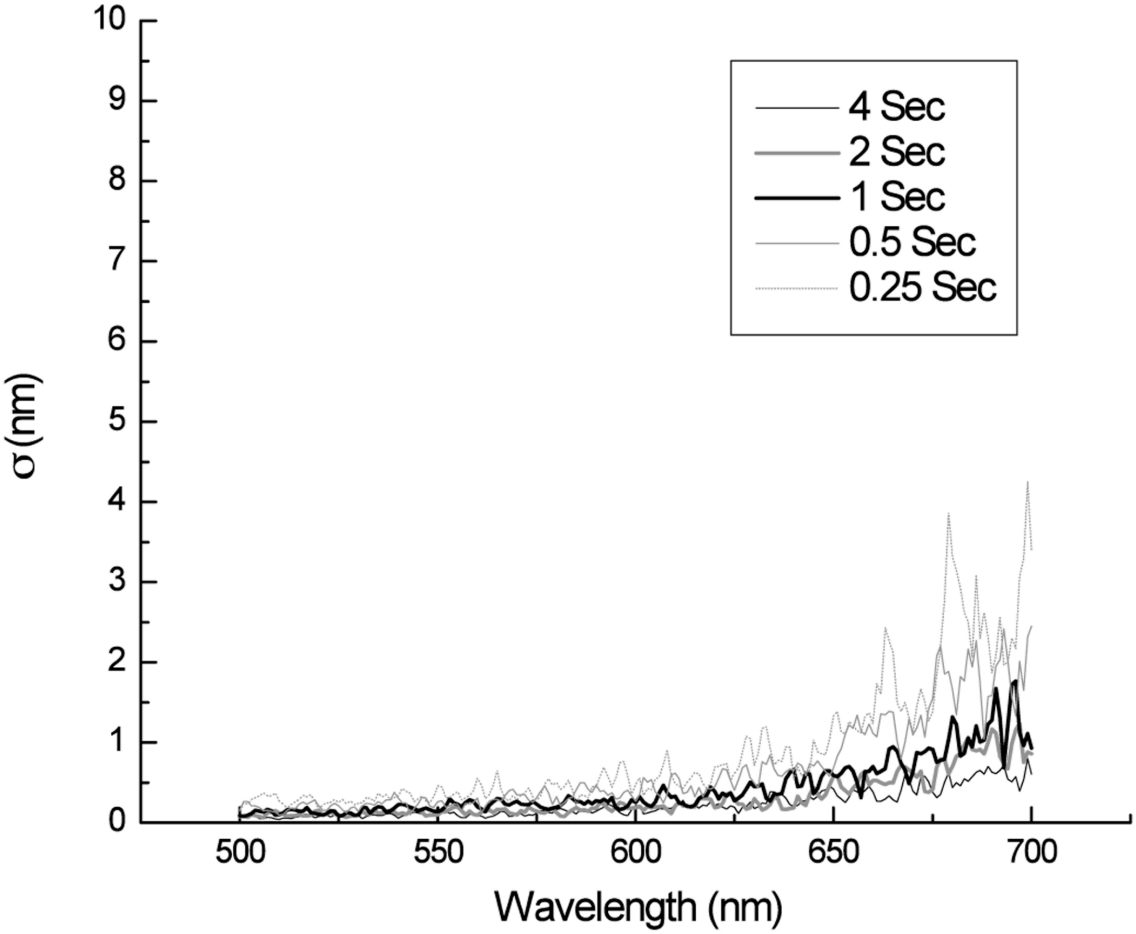

Figure 35: σ vs. wavelength for response time for max settings of scan speed.

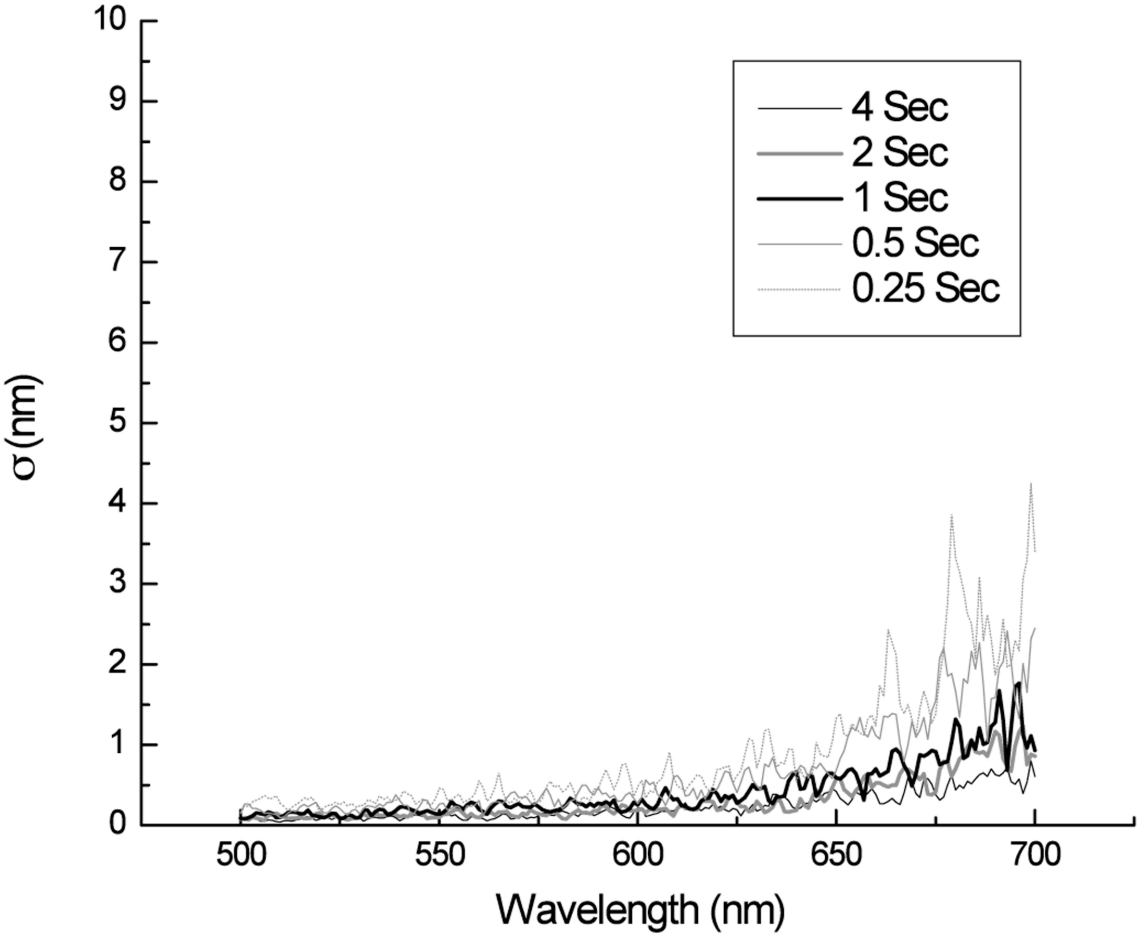

Figure 36: σ vs. wavelength for response time between 500 and 700 nm.

APPENDIX B: SCHEMATICS CHANGES ON JASCO J810 PEM DRIVER

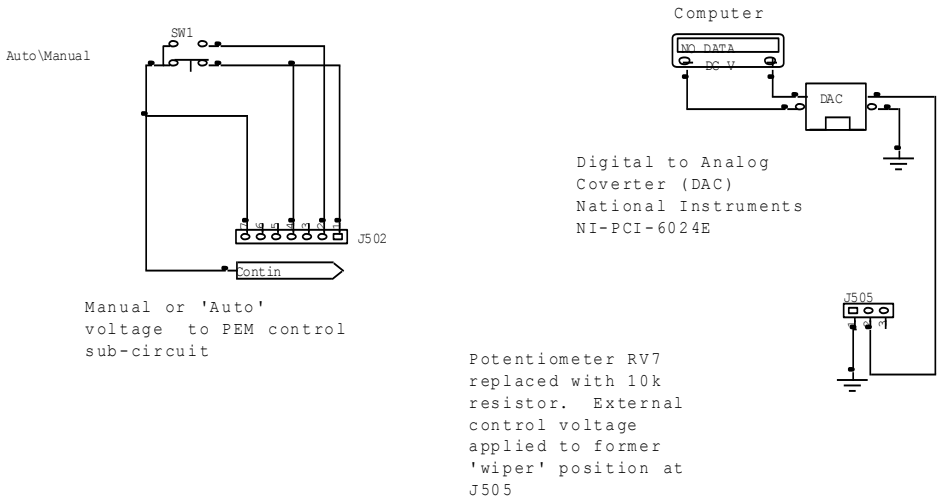

Figure 37: Schematics for external voltage application to PEM

APPENDIX C: LABVIEW SCHEMATICS

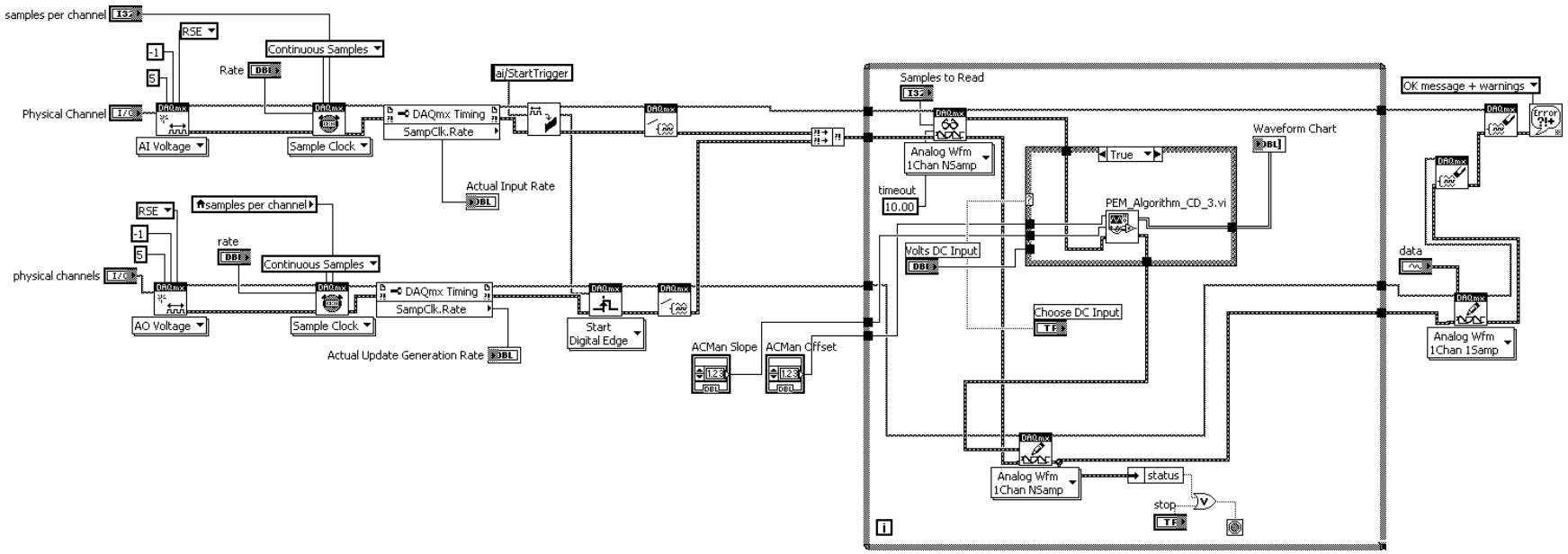

Figure 38: LabVIEW schematic for applying scanable voltage to photoelastic modulator

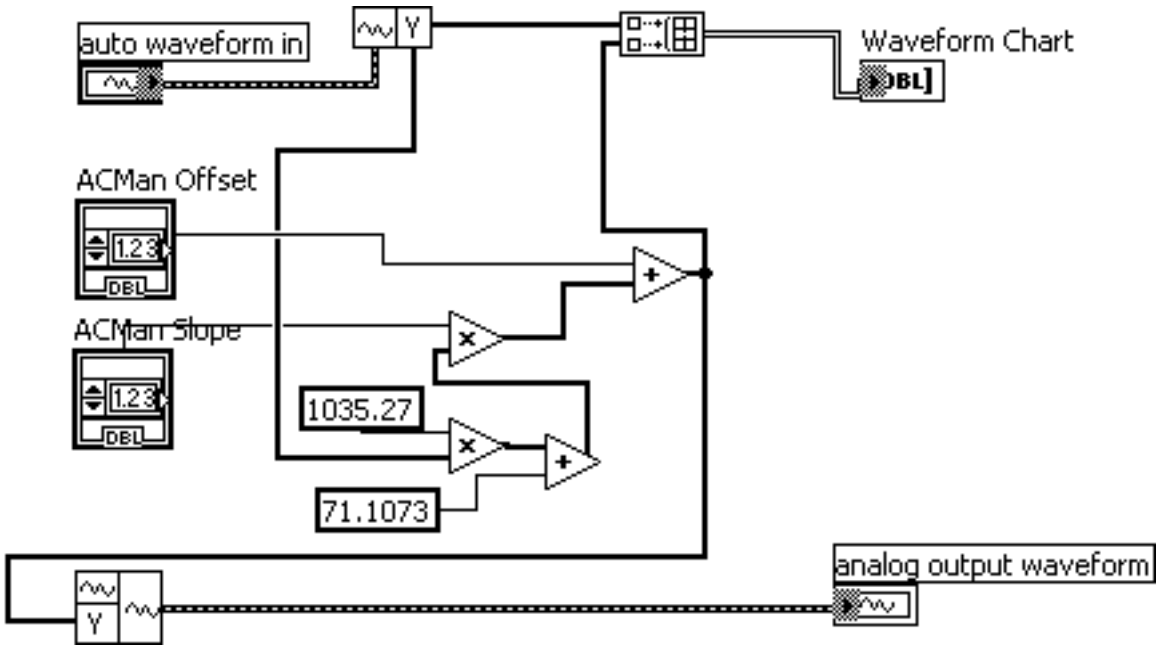

Figure 39: LabVIEW schematic for PEM_Algorithum_CD_3.vi.

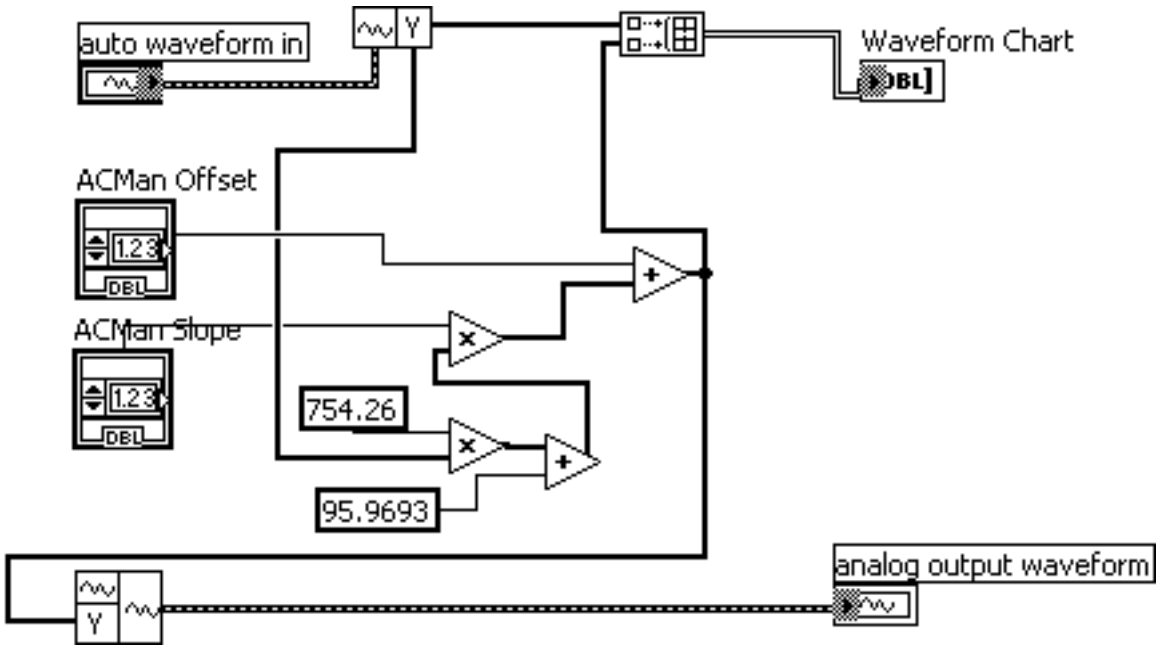

Figure 40: LabVIEW schematic for PEM_Algorithum_LD_3.vi

APPENDIX D: TOTAL INTESITY DERIVATION

The actual intensity that is being measured after the sample chamber is the total transmitted intensity, and therefore the intensity is defined as

$$I_{total} = I_{+}e^{-a_{+}} + I_{-}e^{-a_{-}} \tag{C.1}$$

where a_+ and a_- are the corresponding absorption factors for each intensity and are equal to

$$\begin{aligned} a_{+} &= \frac{a_{+} + a_{-}}{2} + \frac{a_{+} - a_{-}}{2} = \overline{a} + \frac{\Delta a}{2} \\ a_{-} &= \frac{a_{+} + a_{-}}{2} - \frac{a_{+} - a_{-}}{2} = \overline{a} - \frac{\Delta a}{2} \end{aligned} \tag{C.2}$$

where $\overline{a}$ is the averaged absorption and Δa is the difference in absorption.

APPENDIX E: WAVEPLATE MULLER MATRIX DERIVATION

Consider an incident beam on the PEM that is defined a

$$E_x(t) = E_{x_0} e^{i(\omega t + \delta_x)} \tag{D.1a}$$

$$E_y(t) = E_{y_0} e^{i(\omega t + \delta_y)} \tag{D.1b}$$

where E_{i_0} is the amplitude of the electric field component, ω is the angular frequency, and δ_i is the phase shift of the electric field[2].

The emerging electric field from the PEM is defined as

$$E'_x(t) = e^{i\frac{\delta}{2}} E_x(t) \tag{D.2a}$$

$$E'_y(t) = e^{-i\frac{\delta}{2}} E_y(t) \tag{D.2b}$$

where the magnitude of δ is the phase chance in the PEM ($\delta = \delta_y - \delta_x$). Stokes parameters are a combination of the electric field components that correspond to the intensity of the field. These parameters are defined as,

$$\begin{aligned} S_0 &= E_x E_x^* + E_y E_y^* \\ S_1 &= E_x E_x^* - E_y E_y^* \\ S_2 &= E_x E_y^* + E_y E_x^* \\ S_3 &= i(E_x E_y^* - E_y E_x^*) \end{aligned} \tag{D.3}$$

---

[2] Collett E. *Polarized Light: Fundamentals and Applications*. (Marcel Dekker, Inc. 1993)

$$
\begin{aligned}
S_0' &= E_x' E_x'^* + E_y' E_y'^* \\
S_1 &= E_x' E_x'^* - E_y' E_y'^* \\
S_2 &= E_x' E_y'^* + E_y' E_x'^* \\
S_3 &= i(E_x' E_y'^* - E_y' E_x'^*)
\end{aligned}
\tag{D.4}
$$

where S_0 corresponds to total intensity of the system, S_1 is the linearly polarized horizontal or vertical component, S_2 is the linearly polarized $\pm\pi/4$ component, and S_3 is the circularly polarized component of the total intensity. Applying (D.1) to (D.3), (D.3) becomes

$$
\begin{aligned}
S_0 &= E_{x_0}^2 + E_{y_0}^2 \\
S_1 &= E_{x_0}^2 - E_{y_0}^2 \\
S_2 &= 2E_{x_0} E_{y_0} \cos(\delta_y - \delta_x) \\
S_3 &= 2E_{x_0} E_{y_0} \sin(\delta_y - \delta_x)
\end{aligned}
\tag{D.5}
$$

and applying (D.2) to (D.4), (D.4) becomes

$$
\begin{aligned}
S_0 &= E_{x_0}^2 + E_{y_0}^2 \\
S_1 &= E_{x_0}^2 - E_{y_0}^2 \\
S_2 &= 2E_{x_0} E_{y_0} \cos(\delta - (\delta_y - \delta_x)) \\
S_3 &= -2E_{x_0} E_{y_0} \sin(\delta - (\delta_y - \delta_x))
\end{aligned}
\tag{D.6}
$$

and therefore S and S' become

$$
S = \begin{bmatrix}
E_{x_0}^2 + E_{y_0}^2 \\
E_{x_0}^2 - E_{y_0}^2 \\
2E_{x_0} E_{y_0} \cos(\delta_y - \delta_x) \\
2E_{x_0} E_{y_0} \sin(\delta_y - \delta_x)
\end{bmatrix}
\tag{D.7}
$$

$$S' = \begin{bmatrix} E_{x_0}^2 + E_{y_0}^2 \\ E_{x_0}^2 - E_{y_0}^2 \\ 2E_{x_0}E_{y_0}\cos(\delta - (\delta_y - \delta_x)) \\ -2E_{x_0}E_{y_0}\sin(\delta - (\delta_y - \delta_x)) \end{bmatrix} \tag{D.8}$$

where the difference between S and S' are shown below.

$$\begin{aligned} S_0' &= S_0 \\ S_1' &= S_1 \\ S_2' &\propto S_2 \\ S_3' &\propto S_3 \end{aligned} \tag{D.9}$$

Next it must be determined how S_2' and S_3' are related to S_2 and S_3 respectively. This is done by using (D.2) and (D.4). Plugging in (D.2) into (D.4), results with

$$\begin{aligned} S_0' &= E_x E_x^* + E_y E_y^* \\ S_1' &= E_x E_x^* - E_y E_y^* \\ S_2' &= e^{i\delta} E_x E_y^* + e^{-i\delta} E_y E_x^* \\ S_3' &= -i(e^{i\delta} E_x E_y^* - e^{-i\delta} E_y E_x^*) \end{aligned} \tag{D.10}$$

now using the relationship $e^{\pm i\delta} = \cos(\delta) \pm i\sin(\delta)$, (D.10) simplifies to

$$\begin{aligned} S_0' &= E_x E_x^* + E_y E_y^* \\ S_1' &= E_x E_x^* - E_y E_y^* \\ S_2' &= (\cos(\delta) + i\sin(\delta))E_x E_y^* + (\cos(\delta) - i\sin(\delta))E_y E_x^* \\ S_3' &= -i((\cos(\delta) + i\sin(\delta))E_x E_y^* - (\cos(\delta) - i\sin(\delta))E_y E_x^*) \end{aligned}$$

rearranging

$$
\begin{aligned}
S_0' &= E_x E_x^* + E_y E_y^* \\
S_1' &= E_x E_x^* - E_y E_y^* \\
S_2' &= \cos(\delta)(E_x E_y^* + E_y E_x^*) + i\sin(\delta)(E_x E_y^* - E_y E_x^*) \\
S_3' &= -i\cos(\delta)(E_x E_y^* - E_y E_x^*) - \sin(\delta)(E_x E_y^* + E_y E_x^*)
\end{aligned}
$$

using (D.3), the above simplifies to

$$
\begin{aligned}
S_0' &= S_0 \\
S_1' &= S_1 \\
S_2' &= \cos(\delta)S_2 + \sin(\delta)S_3 \\
S_3' &= -\sin(\delta)S_2 + \cos(\delta)S_3
\end{aligned}
\qquad \text{(D.11)}
$$

and the relationship between the initial and final state is determined in (D.11). Now, here is where Muller matrices are introduced. In order to go from the initial state to the final state of the light, the light must undergo a matrix transformation. In general, lets define the system as

$$
\begin{bmatrix} S_0' \\ S_1' \\ S_2' \\ S_3' \end{bmatrix} = \begin{bmatrix} m_{00} & m_{01} & m_{02} & m_{03} \\ m_{10} & m_{11} & m_{12} & m_{13} \\ m_{20} & m_{21} & m_{22} & m_{23} \\ m_{30} & m_{31} & m_{32} & m_{33} \end{bmatrix} \begin{bmatrix} S_0 \\ S_1 \\ S_2 \\ S_3 \end{bmatrix} \qquad \text{(D.12)}
$$

or in equation form

$$
\begin{aligned}
S_0' &= m_{00}S_0 + m_{01}S_1 + m_{02}S_2 + m_{03}S_3 \\
S_1' &= m_{10}S_0 + m_{11}S_1 + m_{12}S_2 + m_{13}S_3 \\
S_2' &= m_{20}S_0 + m_{21}S_1 + m_{22}S_2 + m_{23}S_3 \\
S_3' &= m_{30}S_0 + m_{31}S_1 + m_{32}S_2 + m_{33}S_3
\end{aligned}
\qquad \text{(D.13)}
$$

now using (D.11) and (D.13), (D.13) simplifies to

$$
\begin{aligned}
S_0' &= m_{00}S_0 \\
S_1' &= m_{11}S_1 \\
S_2' &= m_{22}S_2 + m_{23}S_3 \\
S_3' &= m_{32}S_2 + m_{33}S_3
\end{aligned}
\tag{D.14}
$$

where $m_{00} = 1$, $m_{11} = 1$, $m_{22} = \cos(\delta)$, $m_{23} = \sin(\delta)$, $m_{32} = -\sin(\delta)$, and $m_{33} = \cos(\delta)$,

$$
M_{WP} = \begin{bmatrix} 1 & 0 & 0 & 0 \\ 0 & 1 & 0 & 0 \\ 0 & 0 & \cos(\delta) & \sin(\delta) \\ 0 & 0 & -\sin(\delta) & \cos(\delta) \end{bmatrix}
\tag{D.15}
$$

In CD Spectroscopy, a PEM is rotated to 45° from the axis of the machine, therefore (D.15) must be rotated in order to be correct for a CD system. This is done by a series of rotations as defined below

$$
M_{PEM}(\theta) = M_R(-\theta)M_{WP}(\theta)M_R(\theta)
\tag{D.16}
$$

where $M_R(\theta)$ is the Muller matrix a rotator. Lets determine our rotating matrix by first defining the electric field (See Figure 41).

$$
E_x = E\cos(\beta)
\tag{D.17a}
$$

$$
E_y = E\sin(\beta)
\tag{D.17b}
$$

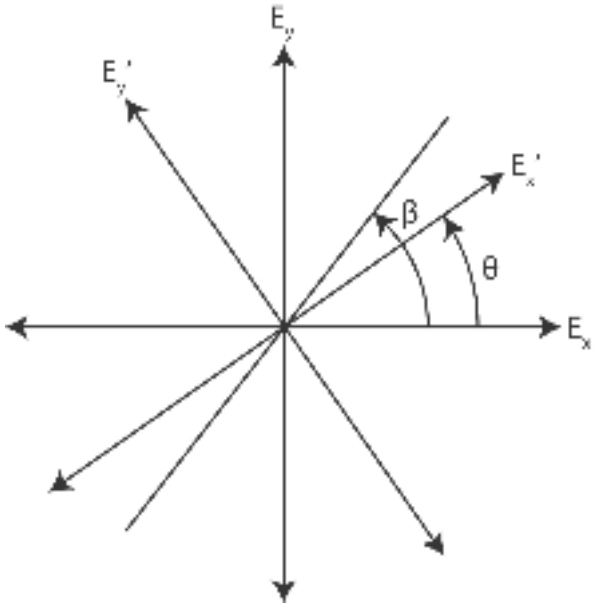

Figure 41: Vector representation of a rotatable electric field. θ is the angle between E_x and E_x' and β is the angle between E and E_x'.

Now rotating the plane of polarization (where E doe not move) by θ, the new angle between E_x' and E is now

$$E_x' = E\cos(\beta - \theta) \qquad \text{(D.18a)}$$

$$E_y' = E\sin(\beta - \theta) \qquad \text{(D.18b)}$$

expands to

$$E_x' = E(\cos(\beta)\cos(\theta) + \sin(\beta)\sin(\theta))$$

$$E_y' = E(\sin(\beta)\cos(\theta) - \cos(\beta)\sin(\theta))$$

simplifies to

$$E'_x = E_x \cos(\theta) + E_y \sin(\theta) \tag{D.19a}$$

$$E'_y = E_y \cos(\theta) - E_x \sin(\theta) \tag{D.19b}$$

Applying (D.19a) and (D.19b) to (D.4),

$$\begin{aligned} S'_0 &= E_x E_x^* + E_y E_y^* \\ S'_1 &= \cos(2\theta)(E_x E_x^* - E_y E_y^*) + \sin(2\theta)(E_x E_y^* + E_y E_x^*) \\ S'_2 &= \cos(2\theta)(E_x E_y^* + E_y E_x^*) - \sin(2\theta)(E_x E_x^* - E_y E_y^*) \\ S'_3 &= -i(E_x E_y^* - E_y E_x^*) \end{aligned} \tag{D.20}$$

by using (D.3), the above simplifies to

$$\begin{aligned} S'_0 &= S_0 \\ S'_1 &= \cos(2\theta) S_1 + \sin(2\theta) S_2 \\ S'_2 &= \cos(2\theta) S_2 - \sin(2\theta) S_1 \\ S'_3 &= S_3 \end{aligned} \tag{D.21}$$

Applying (D.13) to (D.21)

$$\begin{aligned} S'_0 &= m_{00} S_0 \\ S'_1 &= m_{11} S_1 + m_{12} S_2 \\ S'_2 &= m_{21} S_1 + m_{22} S_2 \\ S'_3 &= m_{33} S_3 \end{aligned}$$

implies that $m_{00} = 1$, $m_{11} = \cos(2\theta)$, $m_{12} = \sin(2\theta)$, $m_{21} = -\sin(2\theta)$, $m_{22} = \cos(2\theta)$, $m_{33} = 1$, giving the Muller matrix of a rotator to be

$$M_R(\theta)=\begin{bmatrix} 1 & 0 & 0 & 0 \\ 0 & \cos(2\theta) & \sin(2\theta) & 0 \\ 0 & -\sin(2\theta) & \cos(2\theta) & 0 \\ 0 & 0 & 0 & 1 \end{bmatrix} \tag{D.22}$$

where θ is the angle of rotation. Now applying (D.22) to (D.15), $M_{PEM}(\theta)$ becomes

$$M_{PEM}(\theta,\delta)=\begin{bmatrix} 1 & 0 & 0 & 0 \\ 0 & \cos^2(2\theta)+\cos(\delta)\sin^2(2\theta) & (1-\cos(\delta))\cos(2\theta)\sin(2\theta) & -\sin(\delta)\sin(2\theta) \\ 0 & (1-\cos(\delta))\cos(2\theta)\sin(2\theta) & \sin^2(2\theta)+\cos(\delta)\cos^2(2\theta) & \cos(2\theta)\sin(\delta) \\ 0 & \sin(\delta)\sin(2\theta) & -\cos(2\theta)\sin(\delta) & \cos(\delta) \end{bmatrix}$$

which defines a rotated PEM in CD system. $M_{PEM}(\theta,\delta)$ can be simplified because theta is always set at $\pi/4$ radians, and thus becomes

$$M_{PEM}(\frac{\pi}{4},\delta)=\begin{bmatrix} 1 & 0 & 0 & 0 \\ 0 & \cos(\delta) & 0 & -\sin(\delta) \\ 0 & 0 & 1 & 0 \\ 0 & \sin(\delta) & 0 & \cos(\delta) \end{bmatrix} \tag{D.23}$$

In CD Spectroscopy the incident beam is horizontally polarized before it enters the PEM and can be defined in terms of stokes parameters as

$$I_H = I_0\begin{bmatrix} 1 \\ 1 \\ 0 \\ 0 \end{bmatrix} \tag{D.24}$$

where I_0 is the initial intensity of the light beam. Multiplying (D.23) and (D.24) gives an output from the PEM as

$$I'_H = I_0 \begin{bmatrix} 1 \\ \cos(\delta(t)) \\ 0 \\ \sin(\delta(t)) \end{bmatrix} \tag{D.25}$$

where again $\delta(t)$ is the phase change in the PEM, I_0 is the initial intensity of the light beam, and assumed to have not lost any intensity in the process.

APPENDIX F: LINEAR POLARIZER MULLER MATRIX DERIVATION

In this appendix, the linear polarizer Muller matrix will be determined. The Muller Matrix for the linear polarizer is derived as follows. The incoming electric field is defined as

$$E_x(t) = E_{x_0} e^{i(\omega t + \delta_x)} \tag{E.1a}$$

$$E_y(t) = E_{y_0} e^{i(\omega t + \delta_y)} \tag{E.1b}$$

and the output electric field after passing through the linear polarizer is defined as

$$E'_x(t) = p_x E_x(t) \tag{E.2a}$$

$$E'_y(t) = p_y E_y(t) \tag{E.2b}$$

where p_i is the amplitude of the attenuation coefficients along the orthogonal transmission axes. (E.1) and (E.2) can be characterized in terms of stokes parameters by the following

$$\begin{aligned} S_0 &= E_x E_x^* + E_y E_y^* \\ S_1 &= E_x E_x^* - E_y E_y^* \\ S_2 &= E_x E_y^* + E_y E_x^* \\ S_3 &= i(E_x E_y^* - E_y E_x^*) \end{aligned} \tag{E.3}$$

and

$$\begin{aligned} S'_0 &= E'_x E'^*_x + E'_y E'^*_y \\ S_1 &= E'_x E'^*_x - E'_y E'^*_y \\ S_2 &= E'_x E'^*_y + E'_y E'^*_x \\ S_3 &= i(E'_x E'^*_y - E'_y E'^*_x) \end{aligned} \tag{E.4}$$

The next step is to define a Muller matrix that will transform the initial electric field to the final electric field. By applying (E.2) to (E.4) and using (E.3), the relationship between the two is

$$S_0' = p_x^2 E_x E_x^* + p_y^2 E_y E_y^* \tag{E.5a}$$

$$S_1' = p_x^2 E_x E_x^* - p_y^2 E_y E_y^* \tag{E.5b}$$

$$S_2' = p_x p_y (E_x E_y^* + E_y E_x^*) \tag{E.5c}$$

$$S_3' = p_x p_y i (E_x E_y^* - E_y E_x^*) \tag{E.5d}$$

To get (E.5) in term of initial Stokes parameters, one must first multiply S_0 and S_1 by 2 and add and subtracting $p_x^2 E_y E_y^*$ and $p_y^2 E_x E_x^*$, (E.5) becomes

$$S_0' = \frac{1}{2}(p_x^2 + p_y^2) S_0 + \frac{1}{2}(p_x^2 - p_y^2) S_1 \tag{E.6a}$$

$$S_1' = \frac{1}{2}(p_x^2 - p_y^2) S_0 + \frac{1}{2}(p_x^2 + p_y^2) S_1 \tag{E.6b}$$

$$S_2' = p_x p_y S_2 \tag{E.6c}$$

$$S_3' = p_x p_y S_3 \tag{E.6d}$$

Now applying (D.12) to simplify (E.6), the Muller matrix describing a linear polarizer is as follows.

$$M = \frac{1}{2}\begin{bmatrix} p_x^2 + p_y^2 & p_x^2 - p_y^2 & 0 & 0 \\ p_x^2 - p_y^2 & p_x^2 + p_y^2 & 0 & 0 \\ 0 & 0 & 2p_x p_y & 0 \\ 0 & 0 & 0 & 2p_x p_y \end{bmatrix} \tag{E.7}$$

One more simplification is needed, because p_x and p_y are not measurable quantities, lets redefine them as follows

$$
\begin{aligned}
p^2 &= p_x^2 + p_y^2 \\
p_x &= p\cos(\alpha) \\
p_y &= p\sin(\alpha)
\end{aligned}
\tag{E.8}
$$

plugging in (E.8) into (E.7)

$$
M(\alpha) = \frac{1}{2}\begin{bmatrix}
p^2(\cos^2(\alpha)+\sin^2(\alpha)) & p^2(\cos^2(\alpha)-\sin^2(\alpha)) & 0 & 0 \\
p^2(\cos^2(\alpha)-\sin^2(\alpha)) & p^2(\cos^2(\alpha)+\sin^2(\alpha)) & 0 & 0 \\
0 & 0 & 2p^2\cos(\alpha)\sin(\alpha) & 0 \\
0 & 0 & 0 & 2p^2\cos(\alpha)\sin(\alpha)
\end{bmatrix}
$$

reducing to

$$
M(\alpha) = \frac{p^2}{2}\begin{bmatrix}
1 & \cos(2\alpha) & 0 & 0 \\
\cos(2\alpha) & 1 & 0 & 0 \\
0 & 0 & \sin(2\alpha) & 0 \\
0 & 0 & 0 & \sin(2\alpha)
\end{bmatrix}
\tag{E.9}
$$

where α is the angle of the linear polarized light. Note that when $\alpha = 0$, (E.9) creates linear horizontally polarized light. Likewise when $\alpha = \pi$, (E.9) creates linear vertically polarized light. In this case, assume linear horizontally polarized light (i.e. $\alpha = 0$).

If a linear polarizer is rotatable, the Muller matrix becomes

$$
M_{LP} = M_R(-\varphi)M(\alpha)M_R(\varphi)
\tag{E.10}
$$

where M_R is the rotating matrix (see Appendix D for more detail), and applying (E.9), with $\alpha = 0$, to (E.10) gives,

$$M_{LP} = \frac{p^2}{2}\begin{bmatrix} 1 & \cos(2\varphi) & \sin(2\varphi) & 0 \\ \cos(2\varphi) & \cos^2(2\varphi) & \sin(2\varphi)\cos(2\varphi) & 0 \\ -\sin(2\varphi) & -\sin(2\varphi)\cos(2\varphi) & -\sin^2(2\varphi) & 0 \\ 0 & 0 & 0 & 0 \end{bmatrix} \tag{E.11}$$

where φ is the angle at which the polarizer is set at.

APPENDIX G: MULLER MATRIX DERIVATION FOR ANALYZER

The Muller matrix of the analyzer is

$$M = M_{WP} M_{LP} \tag{F.1}$$

where M_{WP} is the Muller matrix of a waveplate and M_{LP} is the Muller matrix of a linear polarizer (Derived in Appendix D and Appendix E). Carrying out the matrix multiplication of (F.1),

$$M = \frac{1}{2}\begin{bmatrix} 1 & \cos(2\theta) & \sin(2\theta) & 0 \\ \cos(2\theta) & \cos^2(2\theta) & \cos(2\theta)\sin(2\theta) & 0 \\ \cos(\psi)\sin(2\theta) & \cos(\psi)\cos(2\theta)\sin(2\theta) & \cos(\psi)\sin^2(2\theta) & 0 \\ -\sin(\psi)\sin(2\theta) & -\sin(\psi)\cos(2\theta)\sin(2\theta) & -\sin(\psi)\sin^2(2\theta) & 0 \end{bmatrix} \tag{F.2}$$

where $p = 1$ is the attenuation coefficient amplitude. Then setting $\psi = \pi/2$ to give a quarter wave retardation and $\varphi = +\pi/4$,

$$M = \frac{1}{2}\begin{bmatrix} 1 & 0 & 1 & 0 \\ 0 & 0 & 0 & 0 \\ 0 & 0 & 0 & 0 \\ -1 & 0 & -1 & 0 \end{bmatrix} \tag{F.3}$$

where M is the Muller matrix describing the analyzer or circular polarizer to be incorporated into the CD spectrophotometer chamber. In order to get information about the linear components of the Stokes parameters, the analyzer is rotated by π, i.e. switching the position of the waveplate and linear polarizer to

$$M = M_{LP} M_{WP} \tag{F.4}.$$

Note that when the analyzer is rotated, the Muller matrix for the linear polarizer is transposed because now the light is entering the opposite side from the last configuration. The Muller matrix for the analyzer is

$$M = \frac{1}{2}\begin{bmatrix} 1 & 0 & 0 & 1 \\ 0 & 0 & 0 & 0 \\ 1 & 0 & 0 & 1 \\ 0 & 0 & 0 & 0 \end{bmatrix} \qquad \text{(F.5)}.$$

APPENDIX H: DERIVATION OF CD AND LD DETECTED SIGNAL

The light leaving the sample is defined as

$$I_{total_{CD}} = I_L e^{-a_L} + I_R e^{-a_R} \quad \text{(G.1a)}$$

$$I_{total_{LD}} = I_V e^{-a_V} + I_H e^{-a_H} \quad \text{(G.1b)}$$

where I_i is the intensity of left circularly polarized light, right circularly polarized light, vertical linearly polarized light, and horizontal linearly polarized light respectively

$$I_{L/R} = \frac{I_0}{2}(1 \pm \sin(\delta(t))) \quad \text{(G.2a)}$$

$$I_{H/V} = \frac{I_0}{2}(1 \pm \cos(\delta(t))) \quad \text{(G.2b)}$$

and a_i is the absorption of left circularly polarized light, right circularly polarized light, vertical linearly polarized light, and horizontal linearly polarized light respectively

$$a_{L/R} = \overline{a}_{CD} \pm \frac{\Delta a_{CD}}{2} \quad \text{(G.3a)}$$

$$a_{V/H} = \overline{a}_{LD} \pm \frac{\Delta a_{LD}}{2} \quad \text{(G.3b).}$$

Plugging in (G.2a), (G.2b), (G.3a), and (G.3b) into (G.1a) and (G.1b),

$$I_{total_{CD}} = \frac{I_0}{2}(1+\sin(\delta(t)))e^{-\left(\overline{a}_{CD}+\frac{\Delta a_{CD}}{2}\right)} + \frac{I_0}{2}(1-\sin(\delta(t)))e^{-\left(\overline{a}_{CD}-\frac{\Delta a_{CD}}{2}\right)} \quad \text{(G.4a)}$$

$$I_{total_{LD}} = \frac{I_0}{2}(1+\cos(\delta(t)))e^{-\left(\overline{a}_{LD}+\frac{\Delta a_{LD}}{2}\right)} + \frac{I_0}{2}(1-\cos(\delta(t)))e^{-\left(\overline{a}_{LD}-\frac{\Delta a_{LD}}{2}\right)} \quad \text{(G.4b).}$$

This simplifies to

$$I_{total_{CD}} = \frac{I_0}{2} e^{-\bar{a}_{CD}} \left((1+\sin(\delta(t))) e^{-\frac{\Delta a_{CD}}{2}} + (1-\sin(\delta(t))) e^{\frac{\Delta a_{CD}}{2}} \right)$$

$$I_{total_{CD}} = \frac{I_0}{2} e^{-\bar{a}_{CD}} \left(e^{-\frac{\Delta a_{CD}}{2}} + e^{\frac{\Delta a_{CD}}{2}} + \sin(\delta(t)) \left(e^{-\frac{\Delta a_{CD}}{2}} - e^{\frac{\Delta a_{CD}}{2}} \right) \right)$$

$$I_{total_{CD}} = \frac{I_0}{2} e^{-\bar{a}_{CD}} \left(e^{-\frac{\Delta a_{CD}}{2}} + e^{\frac{\Delta a_{CD}}{2}} \right) \left(1+\sin(\delta(t)) \left(\frac{e^{-\frac{\Delta a_{CD}}{2}} - e^{\frac{\Delta a_{CD}}{2}}}{e^{-\frac{\Delta a_{CD}}{2}} + e^{\frac{\Delta a_{CD}}{2}}} \right) \right)$$

$$I_{total_{CD}} = \frac{I_0}{2} e^{-\bar{a}_{CD}} \left(e^{-\frac{\Delta a_{CD}}{2}} + e^{\frac{\Delta a_{CD}}{2}} \right) \left(1-\tanh\left(\frac{\Delta a_{CD}}{2} \right) \sin(\delta(t)) \right) \qquad \text{(G.5a)}$$

and

$$I_{total_{LD}} = \frac{I_0}{2} e^{-\bar{a}_{LD}} \left((1+\cos(\delta(t))) e^{-\frac{\Delta a_{LD}}{2}} + (1-\cos(\delta(t))) e^{\frac{\Delta a_{LD}}{2}} \right)$$

$$I_{total_{LD}} = \frac{I_0}{2} e^{-\bar{a}_{LD}} \left(e^{-\frac{\Delta a_{LD}}{2}} + e^{\frac{\Delta a_{LD}}{2}} + \cos(\delta(t)) \left(e^{-\frac{\Delta a_{LD}}{2}} - e^{\frac{\Delta a_{LD}}{2}} \right) \right)$$

$$I_{total_{LD}} = \frac{I_0}{2} e^{-\bar{a}_{LD}} \left(e^{-\frac{\Delta a_{LD}}{2}} + e^{\frac{\Delta a_{LD}}{2}} \right) \left(1+\sin(\delta(t)) \left(\frac{e^{-\frac{\Delta a_{LD}}{2}} - e^{\frac{\Delta a_{LD}}{2}}}{e^{-\frac{\Delta a_{LD}}{2}} + e^{\frac{\Delta a_{LD}}{2}}} \right) \right)$$

$$I_{total_{LD}} = \frac{I_0}{2} e^{-\bar{a}_{LD}} \left(e^{-\frac{\Delta a_{LD}}{2}} + e^{\frac{\Delta a_{LD}}{2}} \right) \left(1-\tanh\left(\frac{\Delta a_{LD}}{2} \right) \cos(\delta(t)) \right) \qquad \text{(G.5b)}$$

plugging in $\delta(t) = \delta_0 \sin(\omega_0 t) + \delta_s$, (G.5a) and (G.5b) simplifies to

$$I_{total_{CD}} = \frac{I_0}{2} e^{-\bar{a}_{CD}} \left(e^{-\frac{\Delta a_{CD}}{2}} + e^{\frac{\Delta a_{CD}}{2}} \right) \left(1-\tanh\left(\frac{\Delta a_{CD}}{2} \right) \sin(\delta_0 \sin(\omega_0 t) + \delta_s) \right)$$

$$I_{total_{CD}} = \frac{I_0}{2} e^{-\bar{a}_{CD}} \left(e^{-\frac{\Delta a_{CD}}{2}} + e^{\frac{\Delta a_{CD}}{2}} \right) \left(1-\tanh\left(\frac{\Delta a_{CD}}{2} \right) (\cos(\delta_s)\sin(\delta_0 \sin(\omega_0 t)) + \sin(\delta_s)\cos(\delta_0 \sin(\omega_0 t))) \right)$$

$$I_{total_{CD}} = \frac{I_0}{2} e^{-\bar{a}_{CD}} \left(e^{-\frac{\Delta a_{CD}}{2}} + e^{\frac{\Delta a_{CD}}{2}} \right) \left(1 - \tanh\left(\frac{\Delta a_{CD}}{2} \right) (2\cos(\delta_s) J_1(\delta_0) \sin(\omega_0 t) + \sin(\delta_s)(J_0(\delta_0) + 2J_2(\delta_0)\cos(2\omega_0 t))) \right) \quad \text{(G.6a)}$$

and

$$I_{total_{LD}} = \frac{I_0}{2} e^{-\bar{a}_{LD}} \left(e^{-\frac{\Delta a_{LD}}{2}} + e^{\frac{\Delta a_{LD}}{2}} \right) \left(1 - \tanh\left(\frac{\Delta a_{LD}}{2} \right) \cos(\delta_0 \sin(\omega_0 t) + \delta_s) \right)$$

$$I_{total_{LD}} = \frac{I_0}{2} e^{-\bar{a}_{LD}} \left(e^{-\frac{\Delta a_{LD}}{2}} + e^{\frac{\Delta a_{LD}}{2}} \right) \left(1 - \tanh\left(\frac{\Delta a_{LD}}{2} \right) (\cos(\delta_s)\cos(\delta_0 \sin(\omega_0 t)) - 2\sin(\delta_s)\sin(\delta_0 \sin(\omega_0 t))) \right)$$

$$I_{total_{LD}} = \frac{I_0}{2} e^{-\bar{a}_{LD}} \left(e^{-\frac{\Delta a_{LD}}{2}} + e^{\frac{\Delta a_{LD}}{2}} \right) \left(1 - \tanh\left(\frac{\Delta a_{LD}}{2} \right) (\cos(\delta_s)(J_0(\delta_0) + 2J_2(\delta_0)\cos(2\omega_0 t)) - 2\sin(\delta_s) J_1(\delta_0)\sin(\omega_0 t)) \right) \quad \text{(G.6b),}$$

where the DC and AC components are pulled out for CD,

$$\bar{I}_{CD} = \frac{I_0}{2} e^{-\bar{a}_{CD}} \left(e^{-\frac{\Delta a_{CD}}{2}} + e^{\frac{\Delta a_{CD}}{2}} \right) \left(1 - \tanh\left(\frac{\Delta a_{CD}}{2} \right) \sin(\delta_s)(J_0(\delta_0)) \right) \quad \text{(G.7)}$$

$$\Delta I_{CD_\omega} = \frac{I_0}{2} e^{-\bar{a}_{CD}} \left(e^{-\frac{\Delta a_{CD}}{2}} + e^{\frac{\Delta a_{CD}}{2}} \right) \left(-2\tanh\left(\frac{\Delta a_{CD}}{2} \right) \cos(\delta_s) J_1(\delta_0) \right) \quad \text{(G.8)}$$

$$\Delta I_{CD_{2\omega}} = \frac{I_0}{2} e^{-\bar{a}_{CD}} \left(e^{-\frac{\Delta a_{CD}}{2}} + e^{\frac{\Delta a_{CD}}{2}} \right) \left(-2\tanh\left(\frac{\Delta a_{CD}}{2} \right) \sin(\delta_s) J_2(\delta_0) \right) \quad \text{(G.9)}$$

and for LD,

$$\bar{I}_{LD} = \frac{I_0}{2} e^{-\bar{a}_{LD}} \left(e^{-\frac{\Delta a_{LD}}{2}} + e^{\frac{\Delta a_{LD}}{2}} \right) \left(1 - \tanh\left(\frac{\Delta a_{LD}}{2} \right) \cos(\delta_s)(J_0(\delta_0)) \right) \quad \text{(G.10)}$$

$$\Delta I_{LD_\omega} = \frac{I_0}{2} e^{-\bar{a}_{LD}} \left(e^{-\frac{\Delta a_{LD}}{2}} + e^{\frac{\Delta a_{LD}}{2}} \right) \left(2\tanh\left(\frac{\Delta a_{LD}}{2} \right) \sin(\delta_s) J_1(\delta_0) \right) \quad \text{(G.11)}$$

$$\Delta I_{LD_{2\omega}} = \frac{I_0}{2} e^{-\bar{a}_{LD}} \left(e^{-\frac{\Delta a_{LD}}{2}} + e^{\frac{\Delta a_{LD}}{2}} \right) \left(-2\tanh\left(\frac{\Delta a_{LD}}{2} \right) \cos(\delta_s) J_2(\delta_0) \right) \quad \text{(G.12).}$$

The detected signals for CD and LD become,

$$\frac{\Delta I_{CD_\omega}}{\overline{I}_{CD}} = \frac{\frac{I_0}{2}e^{-\overline{a}_{CD}}\left(e^{-\frac{\Delta a_{CD}}{2}} + e^{\frac{\Delta a_{CD}}{2}}\right)\left(-2\tanh\left(\frac{\Delta a_{CD}}{2}\right)\cos(\delta_s)J_1(\delta_0)\right)}{\frac{I_0}{2}e^{-\overline{a}_{CD}}\left(e^{-\frac{\Delta a_{CD}}{2}} + e^{\frac{\Delta a_{CD}}{2}}\right)\left(1-\tanh\left(\frac{\Delta a_{CD}}{2}\right)\sin(\delta_s)(J_0(\delta_0)\right)} \tag{G.13}$$

$$\frac{\Delta I_{CD_{2\omega}}}{\overline{I}_{CD}} = \frac{\frac{I_0}{2}e^{-\overline{a}_{CD}}\left(e^{-\frac{\Delta a_{CD}}{2}} + e^{\frac{\Delta a_{CD}}{2}}\right)\left(-2\tanh\left(\frac{\Delta a_{CD}}{2}\right)\sin(\delta_s)J_2(\delta_0)\right)}{\frac{I_0}{2}e^{-\overline{a}_{CD}}\left(e^{-\frac{\Delta a_{CD}}{2}} + e^{\frac{\Delta a_{CD}}{2}}\right)\left(1-\tanh\left(\frac{\Delta a_{CD}}{2}\right)\sin(\delta_s)(J_0(\delta_0)\right)} \tag{G.14}$$

$$\frac{\Delta I_{LD_\omega}}{\overline{I}_{LD}} = \frac{\frac{I_0}{2}e^{-\overline{a}_{LD}}\left(e^{-\frac{\Delta a_{LD}}{2}} + e^{\frac{\Delta a_{LD}}{2}}\right)\left(2\tanh\left(\frac{\Delta a_{LD}}{2}\right)\sin(\delta_s)J_1(\delta_0)\right)}{\frac{I_0}{2}e^{-\overline{a}_{LD}}\left(e^{-\frac{\Delta a_{LD}}{2}} + e^{\frac{\Delta a_{LD}}{2}}\right)\left(1-\tanh\left(\frac{\Delta a_{LD}}{2}\right)\cos(\delta_s)(J_0(\delta_0)\right)} \tag{G.15}$$

$$\frac{\Delta I_{LD_{2\omega}}}{\overline{I}_{LD}} = \frac{\frac{I_0}{2}e^{-\overline{a}_{LD}}\left(e^{-\frac{\Delta a_{LD}}{2}} + e^{\frac{\Delta a_{LD}}{2}}\right)\left(-2\tanh\left(\frac{\Delta a_{LD}}{2}\right)\cos(\delta_s)J_2(\delta_0)\right)}{\frac{I_0}{2}e^{-\overline{a}_{LD}}\left(e^{-\frac{\Delta a_{LD}}{2}} + e^{\frac{\Delta a_{LD}}{2}}\right)\left(1-\tanh\left(\frac{\Delta a_{LD}}{2}\right)\cos(\delta_s)(J_0(\delta_0)\right)} \tag{G.16}$$

and simplifies to,

$$\frac{\Delta I_{CD_\omega}}{\overline{I}_{CD}} = \frac{-2\tanh\left(\frac{\Delta a_{CD}}{2}\right)\cos(\delta_s)J_1(\delta_0)}{1-\tanh\left(\frac{\Delta a_{CD}}{2}\right)\sin(\delta_s)(J_0(\delta_0)} \tag{G.17}$$

$$\frac{\Delta I_{CD_{2\omega}}}{\overline{I}_{CD}} = \frac{-2\tanh\left(\frac{\Delta a_{CD}}{2}\right)\sin(\delta_s)J_2(\delta_0)}{1-\tanh\left(\frac{\Delta a_{CD}}{2}\right)\sin(\delta_s)(J_0(\delta_0)} \tag{G.18}$$

$$\frac{\Delta I_{LD_\omega}}{\overline{I}_{LD}} = \frac{2\tanh\left(\frac{\Delta a_{LD}}{2}\right)\sin(\delta_s)J_1(\delta_0)}{1-\tanh\left(\frac{\Delta a_{LD}}{2}\right)\cos(\delta_s)(J_0(\delta_0)} \tag{G.19}$$

$$\frac{\Delta I_{LD_{2\omega}}}{\overline{I}_{LD}} = \frac{-2\tanh\left(\frac{\Delta a_{LD}}{2}\right)\cos(\delta_s)J_2(\delta_0)}{1-\tanh\left(\frac{\Delta a_{LD}}{2}\right)\cos(\delta_s)(J_0(\delta_0)} \tag{G.20}.$$